

CLIMATE TRADE COSTS: EXTREME WEATHER, TRANSPORTATION, AND SUPPLY CHAINS

Hubert Massoni*

Job Market Paper

[**Click here for latest version**](#)

October 2025

ABSTRACT

Transportation infrastructure is vulnerable to extreme weather events. Vulnerability is prominent at maritime ports, where tropical cyclones frequently halt operations and force firms to adapt to transportation disruptions. I quantify these responses by linking high-frequency maritime shipment data to tropical cyclone tracks. Exposure to tropical cyclones temporarily disrupts port activities ($\approx 1\text{--}2$ weeks), prompting firms to adjust route choices along transportation networks (rerouting), even after ports resume operations ($\approx 2\text{--}6$ months). To evaluate the general equilibrium implications of these weather disruptions, I develop a quantitative model of spatial production networks with endogenous routing. Structural estimation reveals that maritime transportation costs decrease with port capacity (scale), but increase with port traffic (congestion) and cyclone risk. Investigating future climate hazards to the transportation network, I find that rerouting is a key adaptation mechanism that prevents global welfare losses. To translate evidence into policy, I derive model-based sufficient statistics for evaluating and targeting future port investments in light of climate change. Allocation rules that ignore weather risk and firms' adaptive responses systematically misallocate investment.

*University of Bologna, Department of Economics. Email: hubert.massoni2@unibo.it. I am grateful to Emanuele Campiglio and Bruno Conte for their guidance and support. This paper benefited from conversations with Jeanne Astier, Clare Balboni, Johannes Boehm, Mathieu Couttenier, Pierre Coster, Alejandro Graziano, Vasily Korovkin, Isabelle Méjean, David Nagy, Giacomo Oppacher, Gianluca Orefice, Filippo Pavanello, Giulia Romani, Filippo Santi, Vincenzo Scrutinio, Edouard Schaal, Tommaso Sonno, Catherine Thomas, Guglielmo Zappalà, and from the comments of numerous seminar and conference participants. I am grateful to Alireza Naghavi for kindly sharing data.

1 INTRODUCTION

Transportation infrastructure is the backbone of international trade and attracts large investments to improve efficiency and resilience. Yet, infrastructure is particularly vulnerable to extreme weather. Maritime ports – channeling more than 80% of global trade volumes – exemplify this risk through their exposure to storm surge, high winds, and flooding. Weather hazards threaten not only the physical infrastructure of ports but also the trade flows that depend on them.¹ Escalating climate risk raises concerns about the resilience of transportation networks, and the trade they carry.

Weather-related disruptions expose firms to shipping bottlenecks, delays, and uncertainty ([Blaum et al., 2024](#)). Firms can reduce exposure to disrupted ports by diverting away from risky infrastructure or from suppliers that rely on it. However, these private responses can also amplify disruptions by inducing congestion spillovers along alternative routes ([Allen and Arkolakis, 2022](#); [Brancaccio et al., 2024](#)). Accounting for such endogenous rerouting is crucial for evaluating returns to port investment, given that transportation costs have general equilibrium effects on the spatial distribution of economic activity ([Allen et al., 2025](#); [Redding and Turner, 2015](#)).

In this paper, I study firms' adaptation margins to transport-related climate risks and their impacts on the economy. First, using shipment-level maritime trade data linked to port operations and tropical cyclone exposure, I show that weather shocks disrupt port activity and prompt firm-level rerouting that preserves supply relationships. Second, to quantify the general-equilibrium impacts of future climate risks to port infrastructure, I develop a novel model of spatial production networks that captures complex routing decisions and the congestion spillovers they induce across transportation networks. Third, to evaluate public investment in ports, I develop a normative, sufficient-statistics framework that links port improvements to welfare while accounting for firms' responses and weather risk.

I measure firms' responses to transportation shocks by combining Brazilian administrative maritime trade data (bills of lading) with detailed micro-spatial information on tropical cyclones and daily global port operations. The data cover the universe of

¹Studying 1,340 ports globally, [Verschuur et al. \(2023b\)](#) find that 86% of ports are exposed to more than three weather-related hazards. About one-third of this risk is attributable to tropical cyclones, exposing USD 63 billion in trade annually.

Brazilian imports from 2014 to 2023 at the shipment level. Bills of lading contain information on shipment characteristics, on each trading firm, and on the ports used to ship the goods. Tropical cyclones provide plausibly exogenous weather shocks to infer firm-level adaptation margins.² I investigate the effect of these weather shocks on port activity and the responses of Brazilian firms to foreign transportation disruptions – i.e., shocks to the shipment’s port of origin.³

I exploit a stacked difference-in-differences design ([Cengiz et al., 2019](#); [Deshpande and Li, 2019](#)) to provide novel empirical evidence that port exposure to tropical cyclones prompts rerouting decisions – a mechanism that dampens firm-to-firm trade disruptions. Using quasi-random variation in cyclone exposure across ports, I first show that tropical cyclones temporarily disrupt the operations of maritime ports, on average for 12 days around the cyclone’s landfall.⁴ Second, I use shipment-level data to examine private adaptation through rerouting. Leveraging variation in port exposure to cyclones across the set of ports used by a pair of firms, I find that these disruptions induce a two-month rerouting away from exposed ports, relative to unexposed ports. This response is magnified (up to six months of rerouting) when the treatment is the first experienced by the relationship, suggesting a learning behavior along the treatment history. Third, aggregating shipment data at the firm-to-firm level, I show that the cyclone events are not disruptive enough to sever buyer-supplier links: I observe only a short-lived decline in relationship activity. Overall, the evidence indicates that the principal adaptation margin is routing rather than sourcing.

To investigate the welfare impacts of these adaptation margins in the context of climate change, I develop a static model of spatial production networks with endogenous trade costs affected by weather disruptions. Informed by the empirical evidence, the model accounts for private decisions: firms reroute trade toward safer routes in response to weather risk. However, such routing responses can affect other parts of the transportation network if congestion spillovers raise the costs of using alterna-

²Although tropical cyclones are concentrated within well-defined storm seasons and broad geographic areas, the exact location, timing, and intensity of the events remain unpredictable ([Hsiang and Jina, 2014](#)).

³In the sample I consider, no Brazilian port is exposed to tropical cyclones. Brazil’s coastal regions lie near the equator, where sea surface temperatures are relatively stable and the Coriolis force is weak – tropical cyclones rarely form or intensify in this region.

⁴Since port authorities forecast cyclones’ trajectories and intensities, port downtime can precede landfall. I use precautionary thresholds from Coast Guard authorities to inform my definition of a port-level shock. See Section [3.1](#).

tive routes. In the model, firms located across regions require intermediate inputs to produce final goods. They make joint sourcing and routing decisions based on factory-gate and transportation costs to find the most cost-effective supplier and delivery route. Road transportation is allowed when regions are directly connected by land, and maritime transportation is allowed when both regions have port infrastructure. Shipping through ports entails additional transportation costs related to port traffic and weather risks, which are alleviated by port capacity.

To quantify how congestion, port capacity, and local weather shape firms' sourcing-routing decisions, I parametrize transportation costs and structurally estimate their components using Brazilian microdata linked to information on port operations and cyclone risk. I address endogeneity in port traffic and capacity using a novel set of geography-based instruments. For port traffic, I use global container throughput interacted with each port's 1950 coastal-population share – a predetermined demand shifter that scales common traffic shocks across ports while leaving local handling costs unchanged. For port capacity, I use mean terrain ruggedness around ports – a geologic supply determinant that raises inland evacuation costs and limits optimal capacity, yet remains exogenous to current trade flows. Estimation confirms three predictions of the model: (i) port-level traffic leads to congestion and increases transportation costs; (ii) this congestion is alleviated by port capacity; and (iii) transportation costs are affected by wind conditions around ports. A 1% increase in cyclone risk at the port level raises transportation costs by 0.01%.

I calibrate the model at the subnational level for the global economy and use probabilistic projections of tropical cyclones to infer future weather risk at ports under an unmitigated climate change scenario.⁵ The model quantifies the distributional impacts of these climate-related risks on maritime traffic and regional welfare. Aggregate welfare is virtually unaffected (+0.005 basis points) but masks stark spatial heterogeneity: the 5th and 95th percentiles of welfare changes are -0.47 and +0.12 basis points, respectively. Aggregate port traffic, however, declines by 0.26%, reflecting the combined effects of increased weather risks and congestion spillovers. I further show that rerouting is a key adaptation mechanism that prevents larger declines in global maritime

⁵I rely on model-based quantification and counterfactual exercises to address the impacts of climate change. While the reduced-form evidence I propose captures firms' responses to individual weather events, the maritime shipments data cover only ten years and therefore do not allow observing a distributional *shift* in weather risk – a key feature of climate change.

traffic and averts global welfare losses. When routing is held fixed at baseline, aggregate welfare declines by 0.04 basis points, while maritime traffic declines by 4.4%.

I finally explore infrastructure policy and how future climate risks can affect infrastructure investment patterns. To address the high dimensionality of an optimal infrastructure improvement problem, I propose a computationally tractable sufficient-statistics approach to recover first-order welfare gains from port capacity improvements. I express marginal welfare gains from port capacity as a function of general-equilibrium objects, accounting for adjustments in both production and transportation networks, and port-level weather risk. These sufficient statistics allow me to evaluate the desirability of capacity improvements at specific ports and to quantify how ignoring future climate-related risks may lead to misallocation of infrastructure investment. In the case of global port investments, when the allocation rule is proportional to port-level global welfare gains – a *first-order* allocation rule – I estimate that not accounting for future climate at ports can lead to a 2.3% misallocation of port-capacity investment.⁶

To further demonstrate the use of the sufficient-statistics approach for port investment allocation, I use evidence that EU27 ports plan roughly USD 93 billion in investments by 2034 ([ESPO, 2024](#)). I construct a counterfactual that allocates this aggregate budget across 110 EU ports in proportion to each port’s EU27 first-order welfare gains. Incorporating future climate shifts these gains, and thus the first-order investment allocation rule. To translate spending into capacity, I map investment dollars into port capacity using an elasticity estimated from World Bank PPI projects. Comparing an allocation guided by the current climate with one guided by an RCP8.5 climate yields a 0.5% misallocation of the USD 93 billion. This results in aggregate EU welfare losses of –0.04 basis points and leaves nearly all EU ports with lower traffic.

Related Literature. This paper connects three strands of research. First, it relates to the growing literature on how natural disasters and extreme weather affect production networks ([Barrot and Sauvagnat, 2016](#); [Boehm et al., 2019](#); [Carvalho et al., 2021](#); [Pankratz and Schiller, 2021](#); [Rabano and Rosas, 2024](#)). Both the empirical and theoretical exercises I undertake are most closely related to recent work studying firms’ responses to climate risks: [Balboni et al. \(2024\)](#) and [Castro-Vincenzi et al. \(2024\)](#) doc-

⁶Misallocation refers to the share of aggregate investment which should be reallocated from low-welfare-improving to high-welfare-improving ports.

ument flood impacts on domestic supply chains and firms' adaptive responses, while [Martinez \(2024\)](#), [Blaum et al. \(2024\)](#), and [Clark et al. \(2024\)](#) explicitly address weather disruptions to transportation and their effects on firms' sourcing choices.⁷ Building on the insight that firms incorporate climate risks when making sourcing decisions, I reinterpret private adaptation through the lens of transportation-linked disruptions. I foreground an additional margin – rerouting – and show how these private decisions generate congestion spillovers that justify a role for infrastructure policy.

Second, the paper contributes to the literature on transportation costs and infrastructure as determinants of economic activity. A subset of this literature studies the welfare consequences of traffic congestion ([Brancaccio et al., 2020](#); [Fajgelbaum and Schaal, 2020](#); [Allen and Arkolakis, 2022](#)). I draw on the framework of [Allen and Arkolakis \(2022\)](#) and incorporate an optimal transportation problem – where firms select bilateral least-cost routes – into a model of spatial production networks. Closely related, [Ganapati et al. \(2024\)](#) introduce increasing returns in maritime traffic, and [Wong and Fuchs \(2022\)](#) study multimodal networks. I extend this class of models by introducing infrastructure-level operating costs and capacity constraints that endogenously shape congestion ([Ducruet et al., 2024](#); [Brancaccio et al., 2024](#)). This modeling choice delivers precise traffic predictions at the *node* level (ports), rather than at the *link* level (shipping lanes). This distinction is particularly relevant for maritime trade, where bottlenecks arise primarily at terminals (and a few chokepoints), while open-sea lanes rarely bind. In addition, the sufficient-statistics approach I develop brings climate risk into the welfare analysis of infrastructure policy ([Allen et al., 2025](#)). This approach preserves the discipline of the routing structure, delivers transparent comparative statics for future climates, and scales to large transportation networks where full planner solutions are computationally prohibitive.

Finally, this study relates to the broader literature on the spatial consequences of climate change ([Bilal and Rossi-Hansberg, 2023](#); [Desmet and Rossi-Hansberg, 2015](#); [Cruz and Rossi-Hansberg, 2024](#); [Rudik et al., 2021](#)). Rather than viewing trade frictions as merely constraining climate-induced geographic reallocation, I highlight that climate damage can propagate across space through transportation networks, generating in-

⁷[Balboni et al. \(2024\)](#) also consider flood-induced road disruptions and subsequent firms' responses using GPS tracker data from commercial trucks. Their quantitative framework, however, does not model disaster-driven changes in transportation costs nor the spillovers those shocks generate across the broader transport network.

direct losses in otherwise less-exposed regions via rerouting and congestion. This has implications for infrastructure policy because local shocks can trigger network-wide externalities at critical nodes. Related work studies the spatial allocation of infrastructure under climate risk, including the costs of maintaining coastal cities (Desmet et al., 2021; Balboni, 2025). I propose a complementary perspective: assessments of where to expand infrastructure must internalize firms' routing responses. Rerouting can reshape the spatial propagation of local shocks by diverting trade flows, and infrastructure investments should be designed to support these adjustments while managing congestion externalities.

The rest of the paper proceeds as follows. Section 2 describes the data. Section 3 provides empirical evidence on firms' responses to weather-related transportation disruptions. Section 4 incorporates these responses into a theoretical model of production-network formation with traffic congestion and weather-dependent transportation costs. Section 5 details the model's parameterization and calibration. Section 6 presents quantitative results under climate-change scenarios. Section 7 studies infrastructure policy. Section 8 concludes.

2 DATA

In this section, I describe the main data sources used in the paper. In the empirical analysis, I study Brazilian firms' responses to global transportation shocks. I therefore combine *Brazilian* maritime trade data with *global* port-level information, historical tropical cyclone tracks, and tropical cyclone climate data. Appendix B provides a comprehensive review of data sources and processing – including additional data for model quantification at the global level.

Firm-to-firm shipments. I study firm-to-firm relationships and trading routes using bill of lading data assembled by S&P Panjiva.⁸ The dataset encompasses the universe of maritime import transactions conducted by Brazilian firms between June 2014 and December 2023. Each shipment entry includes the company names of both the Brazilian importer and the foreign exporter. Geographic details – such as street address, city, postal code, and country – are recorded for each trading party, allowing precise

⁸A bill of lading is a document issued by a carrier to acknowledge receipt or shipment of cargo. It typically contains information on the cargo's origin, destination, quantity, packaging, shipping details, and description.

geocoding of shipment origins and destinations. The data also record the maritime ports of loading (origin) and unloading (destination) for each shipment, enabling the reconstruction of trading routes. For each transaction, an indicator specifies whether the goods were containerized. The dataset includes the weight, volume, and current US dollar value of each shipment. It also reports whether the trading parties owned the cargo or acted as forwarders – i.e., third parties transporting the goods.

I perform a series of steps to clean the data and remove incomplete shipment information. I refer to geolocated establishments belonging to an identified parent company as *firms*.⁹ First, I remove all shipments with missing parent company names or port IDs, since I cannot identify the trading parties or routes. Second, I drop from the sample all firms that are not geolocated at the city or postal code level. Third, I restrict attention to shipments where both parties are declared the real owners of the cargo, thereby excluding warehouses and transportation companies.¹⁰ Fourth, I remove all importers not geolocated in Brazil and all exporters geolocated in Brazil.

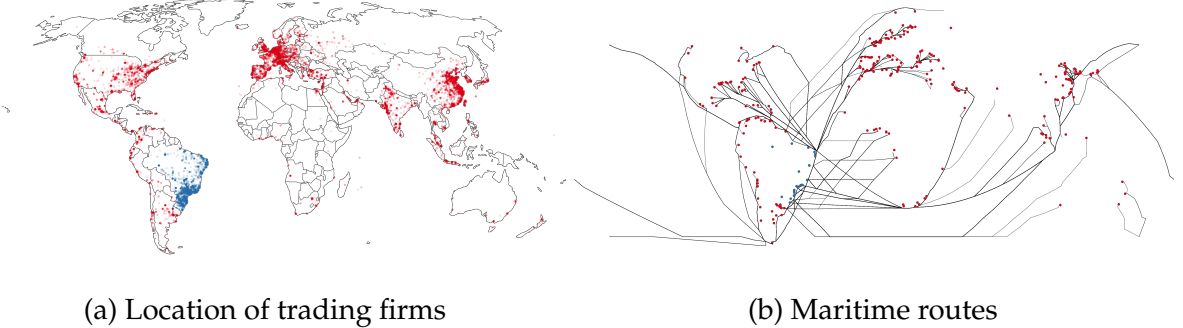
Throughout the empirical section, I denote Brazilian importers as *buyers* (indexed by b), foreign exporters as *suppliers* (indexed by s), and buyer-supplier pairs $\{b,s\}$ as *relationships*. Based on the geographic coordinates of establishments, I assign to each supplier and buyer their location at the subnational level (or *region* in Section 4), denoted n_o for the origin location and n_d for the destination location, respectively.¹¹ When shipments transit from a port of origin p_o to a port of destination p_d , I denote the quadruplet $\{n_o, n_d, p_o, p_d\}$ as a *route* (indexed by r). The set of routes used by relationship (b,s) is denoted \mathcal{R}_{bs} . The baseline sample contains 1,039,012 shipments from 23,291 suppliers to 17,692 buyers, across 1,822 routes. Appendix B.1 describes the sampling procedure and provides summary statistics on firm-to-firm trade. Figure 1a presents the geographic distribution of firms in the sample.

Global port-level traffic. To measure global port-level traffic, I use daily indicators of port activity provided by IMF PortWatch. The data include daily counts of port

⁹To address frequent typos in company names and geographic details, I clean the name strings and assign a single firm ID to all establishments sharing the same parent company name and geolocated within a 10 km radius.

¹⁰Although third parties are likely to influence traffic at ports through routing decisions, they are not relevant for studying firm-to-firm relationships, as the data do not link these shipments to the production-oriented firms trading the goods.

¹¹I map firms to the Global Administrative Unit Layers (GAUL), a set of administrative units with global coverage created by the Food and Agriculture Organization (FAO). I use GAUL1 administrative units – the first administrative layer within a country’s structure (e.g., states in the US).



(a) Location of trading firms

(b) Maritime routes

Notes: Panel 1a maps the locations of firms in the baseline sample. Each dot represents a firm: red dots denote foreign suppliers ($n = 23,291$), and blue dots denote Brazilian buyers ($n = 17,692$). Panel 1b maps the locations of ports and the corresponding active maritime routes in the sample. Each dot represents a port: red dots indicate foreign ports of origin ($n = 442$), and blue dots indicate Brazilian ports of destination ($n = 42$). Lines represent active routes ($n = 1,822$). I plot the shortest sea routes – computed using the Eurostat SeaRoute program – as a proxy for maritime routes, and exclude inland waterway routes.

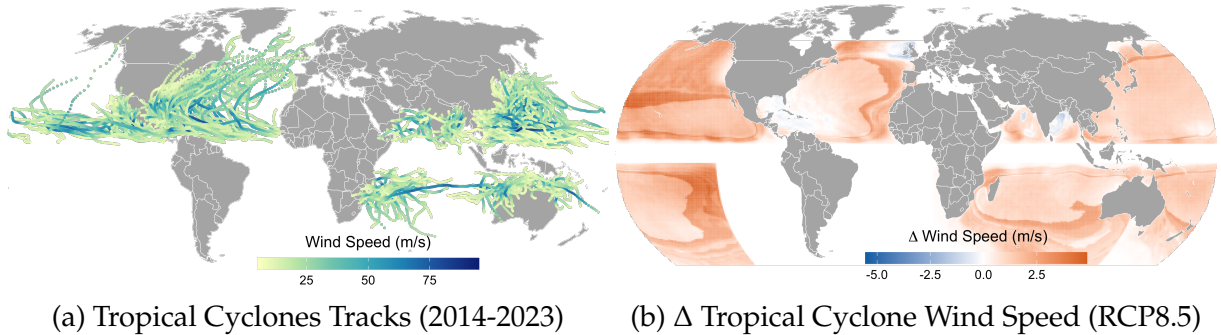
Figure 1: Firms, Ports, and Routes

calls and estimates of import and export volumes, disaggregated by ship type (e.g., container, dry bulk), for 1,666 global ports from 2019 to 2023.¹² I match 621 ports by name to those in the Brazilian bill of lading data and use the daily port-level aggregates of imported and exported volumes – expressed in *twenty-foot equivalent units* (TEU) – as a proxy for port traffic.¹³

Tropical cyclone tracks. I obtain information on tropical cyclones from the IBTrACS (International Best Track Archive for Climate Stewardship) database (Knapp et al., 2010). This database provides a comprehensive record of tropical storms and cyclones since 1841. It contains detailed characteristics of storm systems' positions and intensities, with a temporal resolution of 3 hours and a spatial resolution of 0.1° . I focus on all cyclones that occurred from 2014 to 2023 within a 200 km buffer zone around global coastlines. Figure 2a maps the tropical cyclone events in the sample, along with the sustained wind speeds (in meters per second) experienced along their paths. Appendix B.3 describes the data in detail and provides summary statistics on cyclone wind profiles at ports.

¹²The port-level data (2019–2023) do not cover the entire timeframe of the Brazilian bill of lading data (2014–2023). I therefore use them (i) to verify that tropical cyclones affect port operations (Section 3.2) and (ii) to calibrate transportation costs based on 2019–2023 data (Section 5.1).

¹³TEU (twenty-foot equivalent unit) is a standard measure of container capacity. Data are downloaded from IMF PortWatch. The data are based on raw AIS data from the United Nations Global Platform. Port-level daily estimates are calculated by the PortWatch team, following the methodology described in Arslanalp et al. (2021).



Notes: Panel 2a shows the paths of all tropical cyclones recorded from 2014 to 2023 within a 200 km buffer zone around global coastlines. Wind speeds (m/s) correspond to the storm center (eye) and are reported at a 3-hour temporal resolution (IBTrACS). Panel 2b shows the change in expected wind speed induced by tropical cyclones, comparing the present-day scenario (1980–2015) with the RCP8.5 future scenario (2015–2050). Estimates are based on 10,000 years of synthetic storm tracks from the STORM model, with wind speeds weighted by the inverse of their return periods.

Figure 2: Tropical Cyclones: Historical Tracks and Future RCP8.5 Projections

Tropical cyclone climate. I obtain port-level current and future tropical cyclone climate data from the STORM model (Bloemendaal et al., 2020a,b). The data report maximum wind speeds (meters per second) for a fixed set of return periods, derived from 10,000 years of synthetic tropical cyclone tracks under a present-day climate scenario (1980–2015) and a future climate scenario (2015–2050, RCP8.5/SSP5), at a spatial resolution of 10 km. I calculate the expected wind speed in each 2° grid cell as the sum of maximum sustained wind speeds weighted by the inverse of their return periods (i.e., their probabilities of occurrence over 10,000 years). Appendix B.4 describes the data in detail. Figure 2b maps the global change in expected wind speed from tropical cyclones. Figures B.2a and B.2b report the raw data.

3 EMPIRICAL EVIDENCE

In this section, I investigate the disruptions caused by port exposure to tropical cyclones at the port and firm-to-firm levels. I first show that tropical cyclones induce a short but severe disruption to port operations. I then document that firms reroute shipments to avoid ports' operational shutdowns. Such rerouting mechanisms prevent larger disruptions at the firm-to-firm level.

3.1 EMPIRICAL STRATEGY

Measuring port exposure to cyclones. Tropical cyclones may affect the operations of maritime ports in several ways ([Verschuur et al., 2023a](#)). Port infrastructure is at risk of damage from heavy rain, floods, and intense winds. To prevent the risk of infrastructure damage upon the arrival of a tropical cyclone, ports can suspend operations – i.e., restrict vessels from entering the port, partially or completely – as a means to ensure the safety of port infrastructure and prevent vessel damage.¹⁴ While the safety guidelines vary across ports and countries, most Coast Guard authorities restrict port operations around the threshold of 34–35 knots of expected wind speed (sustained *gale*), or approximately 18 meters per second.¹⁵ [Flynn \(2023\)](#) refers to this zone of precaution as the *34-knot ship avoidance area*.

Exhaustive information on the closure of ports exposed to tropical cyclones is not easily accessible, nor is data on the actual wind speeds experienced around ports during cyclone events. I therefore proxy disruptive tropical cyclone events by modeling the wind speed experienced around port locations.¹⁶ The input to this cyclone profile simulation method is the IBTrACS data described in Section 2. The output is a vector of cyclone characteristics at the port level, including the maximum sustained wind speed experienced at each port during the event. Figure B.1 provides an example of the cyclone profile modeling procedure across the US for Hurricane Harvey (August 2017).

For my baseline definition of a port-level shock, I use a threshold of 18 m/s for experienced maximum wind speed. Importantly, I use the time of the first-ever recorded information on the cyclone as the timing of the shock. This corresponds to the moment when the weather agency first detected the cyclone anomaly, thereby helping to avoid any anticipation by economic agents in a difference-in-differences setting. Table B.6

¹⁴The US Coast Guard, for instance, can issue a set of *port conditions* – i.e., measures restricting port operations – to guide ship operators in responding to tropical weather conditions. Importantly, these measures are issued upon the *projected* arrival of sustained gale-force winds (greater than 34 knots), leading ports to preemptively prepare for the arrival of a cyclone. When the cyclone is projected to reach the port within 12 hours, the port condition ZULU is issued, closing the port to all vessel traffic. Appendix A provides an example of a Maritime Bulletin Safety Information, issued upon the arrival of Hurricane Milton at the port of Key West (October 2024, Florida).

¹⁵The knot is a unit of speed corresponding to one nautical mile per hour. Sustained gale-force winds approximately correspond to wind speeds greater than 63 kilometers per hour, or 39 miles per hour.

¹⁶I use the parametric model of [Willoughby et al. \(2006\)](#), adjusted for asymmetry following [Chen \(1994\)](#)

reports summary statistics on tropical cyclones.

Identification. I leverage the quasi-random timing and location of tropical cyclones to examine how (i) port operations, (ii) firm-level route choices, and (iii) firm-to-firm trade are affected by weather shocks. The empirical setting I consider poses several challenges to estimation. First, the treatment is staggered, and the treatment effect is likely heterogeneous across groups and over time. Tropical cyclones may affect ports that differ in their preparedness and recovery capacity. Moreover, treated relationships may differ in unobservable factors that influence their duration and resilience to shocks, such as relationship age or input specificity. Recent work has shown that two-way fixed-effects difference-in-difference estimators are biased in such settings ([Borusyak et al., 2024](#)). Second, the treatment is non-absorbing: ports – and therefore relationships – can be treated multiple times while recovering in between. Third, the treatment is likely continuous, depending on the magnitude of the cyclone or the degree of exposure to weather-related disruptions.¹⁷ Fourth, to isolate the effects of cyclones on ports from those on firms, I need to control for a rich set of fixed effects.

I seek to address these concerns by using *stacked* dynamic difference-in-difference specifications, following [Cengiz et al. \(2019\)](#) and [Deshpande and Li \(2019\)](#). Conceptually, I define each time period during which at least one tropical cyclone occurs as a cyclone *event*, indexed by τ . For each event, I define a uniform event window, over which I observe the dynamics of port- and firm-level outcomes in the lead-up to and aftermath of the cyclone shock.¹⁸ I extend this framework to allow for non-absorbing treatments. That is, I only include units that either (i) are treated *once* within the event window (clean treated) or (ii) are not treated at all during the window (clean controls). Units may be treated multiple times (i.e., they may appear in several event windows), as long as subsequent treatments fall outside the relevant window.¹⁹ This approach allows me to control for a rich set of pre-shock unit characteristics and therefore strengthens the credibility of the common-trends assumption, while avoiding non-admissible comparisons inherent to staggered designs.²⁰

¹⁷Ports may rely on a set of critical infrastructure to operate, such as nearby power grids or entrepôts, with differing levels of exposure to weather disasters ([Verschuur et al., 2023a](#)). Firms also exhibit varying degrees of reliance on high-risk routes for the delivery of goods.

¹⁸To preserve compositional balance between treated and control groups, I restrict attention to cyclone events for which outcomes are fully observed within the event window.

¹⁹This implies an assumption of treatment-effect stabilization, as in [Dube et al. \(2023\)](#).

²⁰[Wing et al. \(2024\)](#) caution that stacked fixed-effects settings may introduce bias when averaging

3.2 PORT-LEVEL DISRUPTIONS

I first document that tropical cyclones temporarily affect the operations of ports. I construct daily measures of port activity from the IMF PortWatch data. The first outcome of interest – the extensive margin of port operations – is a binary variable that takes the value 1 if at least one vessel entered the port on day t , i.e., the port is *active*. The second outcome of interest – the intensive margin of port operations – is the log number of vessels that enter port p on day t , conditional on the port being active.

To construct the sample, I first restrict attention to ports that I can identify in the Brazilian bill of lading data and that therefore export at least once to Brazil. I then consider an event window of 15 days before and after each cyclone event τ , where τ refers to the day on which the first observation of a cyclone track is recorded at sea. Within each event window, I subsample all ports that are either (i) exposed only once to sustained winds of at least 18 m/s, or (ii) not exposed to sustained winds from tropical cyclones. The final sample consists of 594 ports, potentially exposed to 120 cyclone events from 2019 to 2023.²¹ I consider the following specification to estimate the effect of cyclones on port operations:

$$y_{p,t,\tau} = \sum_{h=-15}^{15} \beta_h E_{p,\tau} + \alpha_{p,\tau} + \alpha_{t,\tau} + \varepsilon_{p,t,\tau}, \quad (1)$$

where $y_{p,t,\tau}$ corresponds to the outcome of interest for port p on day t around cyclone event τ . In the baseline specification, the treatment variable $E_{p,\tau}$ is binary, taking the value 1 if port p was exposed to sustained winds of at least 18 m/s at event τ . The regression controls for port-event and time-event fixed effects. Standard errors are clustered at the port level.

Figure 3a shows the results of estimating Equation (1) on the extensive margin of port operations, for a 15-day window before and after the shocks. The effect of port exposure to cyclones is a 1- to 2-week decrease in the probability that the port is active, followed by a full recovery. The effect corresponds to an average 9% decrease in the probability of port activity across the post-event window (15 days).²² Figure 3b shows

ATT estimates across events if the share of treated units varies. However, the authors do not yet offer an extension of their framework for non-absorbing treatments.

²¹148 ports are treated at least once in the sample.

²²The unconditional probability of port activity in the pre-event window is 0.78. The duration of the

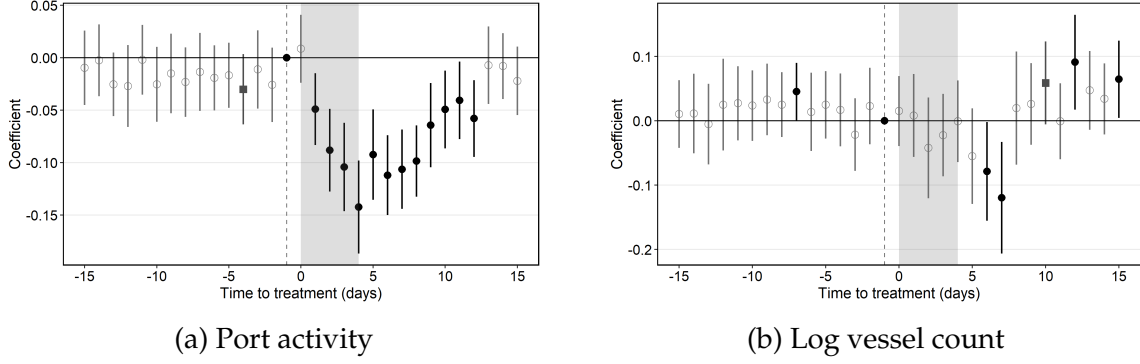


Figure 3: The impact of exposure to cyclones on port operations

Notes: These panels plot the effect of exposure to tropical cyclones on daily port-level outcomes, as specified by Equation (1). The outcome in Panel 3a is a binary variable taking the value 1 if at least one vessel entered the port on day t (port activity), and 0 otherwise. The outcome in Panel 3b is the log number of vessels that use the port on day t , conditional on the port being active. Standard errors are clustered at the port level. The bars correspond to 95% confidence intervals. Black dots are point estimates significant at the 5% level, gray squares at the 10% level, and empty dots are non-significant at the 10% level.

that, even when ports remain active, the number of vessels admitted to the port area may decrease, as ports reduce the intensity of operations. Immediately after the shock, port operations *recapture* – that is, port productivity increases briefly to reduce further shipment delays.

Heterogeneity and sensitivity. I first explore the sensitivity of the results to alternative treatment definitions. In Appendix C.1, I verify that exposure to weaker wind speeds (below the 18 m/s threshold) does not induce port disruptions. I also verify that stronger exposure induces larger disruptions in port activity. I estimate Equation (1) by splitting the treated group by the duration of exposure to at least 18 m/s. Hours of exposure proxy for both the port’s distance to the ship-avoidance area and the cyclone’s intensity. Figure C.2a confirms that the bulk of port-level disruptions are induced by long exposure (at least 12 hours) to sustained wind speeds.

Second, the data allow me to distinguish between ship types. I estimate Equation (1) using port–ship-type–specific outcomes: containerized vs. other ships (e.g., bulk). Container ships (or “liner” ships) typically operate along fixed, pre-planned lines, limiting real-time route adjustments, while owners/operators of other ship types have comparatively more flexibility in scheduling (Ksciuk et al., 2023). Figure C.2b shows that container ships are less responsive to port exposure to cyclones, consistent with

effect is consistent with the findings of Verschuur et al. (2020). Reviewing the effect of natural disasters on port operations using vessel tracking data, they find a median disruption duration of six days.

pre-scheduled shipping.

3.3 ROUTE CHOICE

I then examine how port exposure to cyclones affects firms' choice of shipping routes. I seek to understand whether route choice serves as a margin of adaptation after firm pairs are treated. I use monthly aggregates of the Brazilian shipment data at the buyer-supplier-route level (b, s, r) , where routes r are proxied by the pair of ports through which shipments are loaded (port of origin p_o) and unloaded (port of destination p_d).²³ The outcome of interest is a monthly measure of the extensive margin of route activity: a binary variable equal to 1 if there is a positive number of shipments between b and s using route r , and 0 otherwise. Route activity is conditioned on relationship-route *entry* – i.e., a route can be active for a relationship only after its first shipment on that route.²⁴ I also consider an intensive margin outcome – namely, the log of the total weight of shipments between b and s using route r , conditional on relationship-route activity.

To construct the sample, I aim to compare relationship-routes that are as similar as possible in frequency, volume, and timing of shipments. I define an event window of 5 months before and 10 months after each cyclone event τ , where τ refers to the month in which the first observation of a cyclone track is recorded at sea.²⁵ I sample relationship-routes that trade at least once within the 5-month pre-shock window, thereby restricting attention to relationship-routes active before the shock. Relationship-routes are treated if their port of origin is exposed to tropical cyclones at event τ . Importantly, ports of destination (i.e., Brazilian ports) in the sample are not exposed to tropical cyclones (see Figure 2a), allowing me to define treatment solely on the basis of origin ports. I consider the following specification to estimate the effect of cyclone-induced port disruptions on route choice:

$$y_{bsr,t,\tau} = \sum_{h=-5}^{10} [\beta_h E_{p_o \in r, \tau} + \delta_h X_{bsr,h,\tau} + \alpha_{h,\tau}] + \alpha_{bsr,\tau} + \alpha_{bs,t} + \varepsilon_{bsr,t,\tau}, \quad (2)$$

²³Formally, routes are also defined over the origin and destination regions of shipments: $\{n_o, n_d, p_o, p_d\}$. Conditional on (geolocated) firms fixed effects, route definition boils down to $\{p_o, p_d\}$.

²⁴This avoids comparing poorly defined *potential* routes – i.e., periods before a route's first recorded shipment. If a relationship's first shipment on a route occurs within the first year of the sample, I assume the relationship-route enters in the first month of the sample.

²⁵ τ refers to a month in which at least one cyclone forms and at least one port is exposed. A cyclone event may include multiple cyclones, and ports may be exposed several times within the same event.

where $y_{bsr,t,\tau}$ corresponds to the outcome of interest for relationship–route (b,s,r) at month t around cyclone event τ . In the baseline specification, the treatment variable $E_{p_o \in r,\tau}$ is binary, equal to 1 if the port of origin p_o in route r was exposed to at least 18 m/s of sustained wind speed at event τ . The regression includes time–event, relationship–route–event, and relationship–month fixed effects. This specification restricts comparisons to route choices within relationships and within events. Control variables $X_{bsr,h,\tau}$ are time dummies interacted with pre-treatment characteristics of each relationship–route.²⁶ Standard errors are clustered at the relationship level.

Figure 4a reports the estimation of Equation (2) on route activity, 5 months before and 10 months after the shock. Results indicate that port exposure to cyclones decreases trade through affected routes for about 2 months, relative to unaffected routes. At the time of exposure, the effect corresponds to a 12% decrease in the probability of using the affected route.²⁷ Figure 4b shows that firms do not adjust shipment size when they continue trading through the affected route. Because the specification includes relationship-level fixed effects, the estimated impact of rerouting reflects an additional adjustment margin beyond any direct disruption at the firm-to-firm level. In other words, the results isolate the role of route substitution as a distinct channel of adaptation, separate from the overall continuity of trade relationships between firms.

Heterogeneity and sensitivity. The short-lived treatment effect on route choice suggests that firms adapt ex ante to the possibility of increased transportation costs due to weather shocks.²⁸ Still, Equation (2) pools all treatments and does not capture heterogeneity in treatment effects based on a relationship's treatment history. I therefore decompose Equation (2) by including two treatment variables: $\mathbb{1}_{bs,\tau}^1 \times E_{p_o \in r,\tau}$, which equals 1 if the treatment at τ is the first experienced by relationship (b,s) , and $\mathbb{1}_{bs,\tau}^{1<} \times E_{p_o \in r,\tau}$, which equals 1 for any subsequent treatment. This allows me to examine whether firms learn or adapt following past events. Figure C.3a shows that the rerouting mechanism is much more pronounced for the first treatment than for subsequent ones. Route activity decreases for up to six months following the first port exposure to a cyclone – well after port operations resume. By contrast, subsequent

²⁶These include the number of shipments, the number of active months, and the month of the last shipment within the 5-month pre-treatment period.

²⁷The unconditional probability of route activity in the pre-shock window is 0.43.

²⁸This fact is consistent with the findings of [Castro-Vincenzi et al. \(2024\)](#), who observe mean reversion in supply chain composition following flood shocks to firm premises.

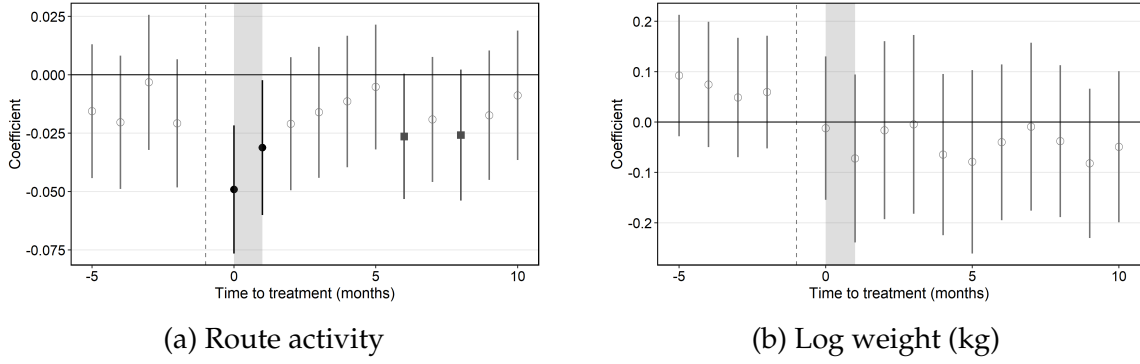


Figure 4: The impact of port exposure to cyclones on route choice

Notes: These panels plot the effect of port exposure to tropical cyclones on monthly firm-to-firm-route-level outcomes, as specified by Equation (2). The outcome in Panel 4a is a binary variable equal to 1 if at least one shipment is observed for the trading pair through route r in month t (active route), and 0 otherwise. The outcome in Panel 4b is the log of total weight (kg) shipped through route r in month t , conditional on the relationship-route being active. Regressions include relationship-month fixed effects, and control for time dummies interacted with relationship-routes' pre-treatment characteristics. Standard errors are clustered at the relationship level. The bars show 95% confidence intervals. Black dots indicate point estimates significant at the 5% level, gray squares at the 10% level, and empty dots denote estimates that are not significant at the 10% level.

treatments lead to only a one-month decline in route activity, likely reflecting the mechanical effect of port closures. This suggests that firms learn from experience and quickly converge toward ex ante adaptation in response to future shocks.

Route choice may also be constrained by which party schedules shipments. Containerized goods are typically carried by liner ships, operated by large companies along fixed, pre-planned services. While firms can switch operators, choices may be limited by compatibility between preferred ports and the ability of those ports to service container ships. Bulk shipping, by contrast, generally offers greater flexibility in scheduling vessels and ports. To assess the importance of these constraints, I decompose Equation (2) by allowing treatment effects to differ between containerized and non-containerized shipping. I define $\mathbb{1}_{bs,r,\tau}^c \times E_{p_o \in r,\tau}$ to equal 1 if the relationship traded only containerized goods in the 5-month pre-treatment window, and $\mathbb{1}_{bs,r,\tau}^{non-c} \times E_{p_o \in r,\tau}$ to equal 1 if at least one shipment was non-containerized. Figure C.4a shows that non-containerized shipping accounts for most of the treatment effect, consistent with greater scheduling flexibility outside containerized services.

3.4 FIRM-TO-FIRM DISRUPTIONS

I finally turn to the effect of port exposure to cyclones on firm-to-firm trade. I am mainly interested in the extensive margin of firm-to-firm trade – that is, in supply

chain composition. I use monthly aggregates of the Brazilian shipment data at the buyer–supplier level (b,s) . My first outcome of interest is a monthly measure of relationship activity, defined as a binary variable equal to 1 if a positive number of shipments occurs within the relationship (b,s) in month t , and 0 otherwise. Relationship activity is conditioned on the entry of both the buyer and the supplier, respectively defined as the month of the first recorded shipment received by b or sent by s .²⁹ I also consider an intensive-margin outcome, defined as the log of total shipment weight between b and s , conditional on relationship activity.

The sample is constructed analogously to that in Section 3.3, though selection criteria are defined at the relationship (b,s) level. Treated relationships are those that used at least one exposed *port of origin* during the pre-shock window. I consider the following specification to estimate the effect of cyclone-induced port disruptions on firm-to-firm trade:

$$y_{bs,t,\tau} = \sum_{h=-5}^{10} \left[\beta_h E_{p_o \in \mathcal{R}_{bs}^{\tau}, \tau} + \delta_h X_{bs,h,\tau} + \alpha_{h,\tau} \right] + \alpha_{bs,\tau} + \alpha_{b,t} + \alpha_{s,t} + \varepsilon_{bs,t,\tau}, \quad (3)$$

where $y_{bs,t,\tau}$ denotes the outcome of interest for buyer–supplier relationship (b,s) in month t around cyclone event τ . In the baseline specification, the treatment variable $E_{p_o \in \mathcal{R}_{bs}^{\tau}, \tau}$ is binary, equal to 1 if at least one port of origin p_o used by the relationship (i.e., in the set of routes \mathcal{R}_{bs}^{τ}) was exposed to sustained wind speeds of at least 18 m/s during event τ .³⁰ The regression includes buyer–month and supplier–month fixed effects, which absorb buyer- and supplier-specific shocks. This is important for isolating the effect of cyclones on the ports used by relationships while controlling for potential direct effects on suppliers themselves. Control variables $X_{bs,h,\tau}$ are time dummies interacted with pre-treatment characteristics of each relationship.³¹ Standard errors are clustered at the buyer level.

Figure 5a reports the estimation of Equation (3) on relationship activity, 5 months before and 10 months after the shock. Results suggest that port exposure to cyclones

²⁹Here, I follow Balboni et al. (2024). As for route activity, this avoids comparisons between poorly defined *potential* relationships – i.e., before the first recorded activity of the trading parties. When the first recorded shipment is observed within the first year of the sample, I assume that the firm enters during the first period of the sample.

³⁰The set of routes \mathcal{R}_{bs}^{τ} is time-dependent, as it is defined using the pre-shock window.

³¹As with relationship–routes, these include the number of shipments, the number of active months, and the month of the last shipment within the 5-month pre-treatment period, specified at the buyer–supplier level.

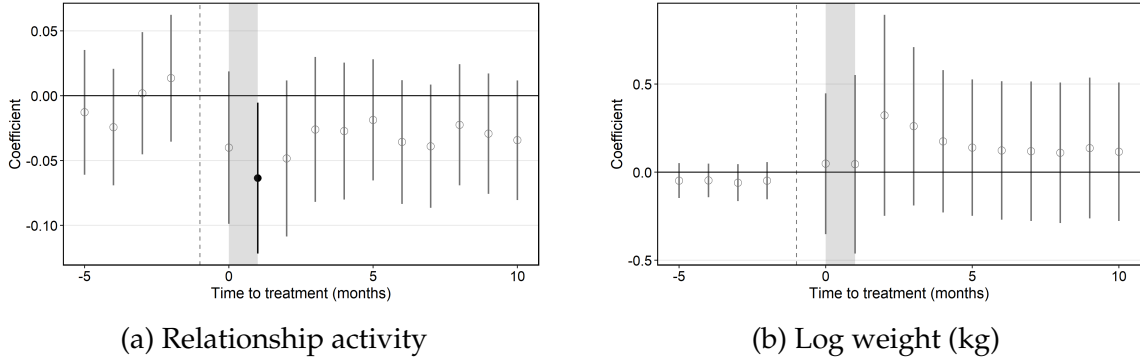


Figure 5: The impact of port exposure to cyclones on firm-to-firm relationship

Notes: These panels plot the effect of port exposure to tropical cyclones on monthly firm-to-firm-level outcomes, as specified by Equation (3). The outcome in Panel 5a is a binary variable equal to 1 if at least one shipment is observed for the trading pair in month t (active relationship), and 0 otherwise. The outcome in Panel 5b is the log total shipment weight for the relationship, conditional on the relationship being active. Regressions include buyer-time and supplier-time fixed effects, and control for time dummies interacted with relationships' pre-treatment characteristics. Standard errors are clustered at the buyer level. The bars denote 95% confidence intervals. Black dots indicate point estimates significant at the 5% level, gray squares at the 10% level, and empty dots denote non-significant estimates at the 10% level.

has a small, short-lived effect on the extensive margin of firm-to-firm trade, followed by a full recovery in the probability of activity. The effect is largest one month after cyclone onset, corresponding to a 17% decrease in the probability of trading for treated relationships compared to untreated relationships.³² Figure 5b suggests that firms do not adjust shipment size when they continue trading. Overall, results at the firm-to-firm level indicate that rerouting is a sufficient mechanism to prevent significant supply-chain recomposition.

Heterogeneity and sensitivity. I investigate the same heterogeneity dimensions as in Section 3.3, i.e., along the treatment history and by containerization status of shipments. Figure C.5a shows no significant differences between first and subsequent treatments of firm pairs, suggesting that most learning occurs along the route-choice margin. Trade in containerized goods, however, exhibits larger and more persistent disruptions in firm-to-firm activity – up to three months of reduced activity (see Figure C.6a). This pattern is consistent with constraints in containerized shipping: when scheduling limits route flexibility, higher transportation costs induce sourcing disruptions.

³²The unconditional probability of relationship activity in the pre-shock window is 0.42.

4 THEORY

In this section, I develop a theory of spatial production network formation with endogenous trade costs and weather shocks to trade infrastructure. The model rationalizes my empirical findings: (i) tropical cyclones affect the operations of maritime ports and induce firm-to-firm trade disruptions; (ii) firms adapt to these disruptions by rerouting trade; and (iii) so as to preserve sourcing relationships. I use the model to perform counterfactual simulations under a climate change scenario and to evaluate infrastructure-related adaptation policies.

To parsimoniously capture the empirical evidence on the impacts of trade infrastructure exposure to weather disasters on global supply chains, I assume that, in a production network environment similar to [Oberfield \(2018\)](#), firms make joint sourcing and routing decisions based on suppliers' factory-gate costs and transportation costs.³³ Transportation costs are endogenous to traffic congestion, as in [Allen and Arkolakis \(2022\)](#), and for maritime routes include the costs of using port infrastructure, which is potentially affected by weather disasters. Firms are perfectly informed about the underlying distribution of weather-related risks to port infrastructure.

The model can generate predictions that are not testable in the reduced-form empirical evidence in Section 3. First, the model incorporates traffic congestion, which is likely to affect transportation costs in the long run. Section 3 shows that firms adapt to weather shocks by redirecting trade through alternative routes. If traffic congestion increases the cost of using these alternatives, such adaptation may, in turn, distort the bilateral components of sourcing shares and affect the aggregate impact of infrastructure exposure to weather disasters. Second, while the empirical results describe reactions to single weather events, they do not address a local shift in the *distribution* of events – i.e., a shift in port-level climate conditions. The model accommodates such a counterfactual by assuming that a shift in the distribution of weather disasters is akin to a sequence of realized events through which firms update their information about the probability distribution of extreme weather events.³⁴

³³I draw from the model of endogenous production network formation under idiosyncratic and aggregate weather-disaster risks presented in [Balboni et al. \(2024\)](#). [Chen et al. \(2023\)](#) proposes a related model in which technology compatibility between firms shapes the marginal costs of inputs. I extend this class of models to include a geography, endogenous trade costs, and transportation-related weather risks.

³⁴Although static, the model can also describe the immediate aftermath of a weather disaster and

Environment. The economy consists of a discrete set \mathcal{N} of regions (indexed by n or n'), each populated by a unit measure of firms, $M_n = 1 \forall n \in \mathcal{N}$, and an exogenous measure of households $L_n \in \{L_n\}_{n \in \mathcal{N}} \equiv \mathcal{L}$. Each region is endowed with a fundamental productivity $a_n \in \{a_n\}_{n \in \mathcal{N}} \equiv \mathcal{A}$. Some regions contain port infrastructure, which enables trade across regions that are not directly connected by land.³⁵ The set of ports is denoted \mathcal{P} . Both regions and ports are connected through a *transportation network*, i.e., a set of bilateral trade frictions incurred when shipping directly from one location (a region or a port) to another. The transportation network depends on both endogenous variables (traffic) and exogenous ones (distance and capacity). Regions are distant from each other, with a bilateral measure of distance $\epsilon_{nn'} \in \{\epsilon_{nn'}\}_{n,n' \in \mathcal{N}^2} \equiv \mathcal{D}$. Each port has a capacity $K_p \in \{K_p\}_{p \in \mathcal{P}} \equiv \mathcal{K}$ (e.g., port berths). Regions are connected via a countable set of routes \mathcal{R} , which allow for trade in intermediate inputs.

Households. Households in region n inelastically supply labor l_i to local firms and consume a bundle of differentiated final goods supplied by local firms:

$$q_n = \left(\int_{i \in M_n} q_i^{\frac{\sigma-1}{\sigma}} di \right)^{\frac{\sigma}{\sigma-1}}, \quad (4)$$

where q_i is the quantity of final goods supplied by firm $i \in M_n$, and $\sigma > 1$ is the elasticity of substitution across varieties of final goods in region n . I assume no trade in final goods and no migration across regions.³⁶ Households face the budget constraint:

$$\int_{i \in M_n} q_i p_i di = w_n + \Pi_n, \quad (5)$$

where p_i is the price charged by firm i for final goods, w_n is the wage rate in region n , and Π_n denotes per-capita profits rebated from firms to households in region n .

Firms. Firms produce by combining local labor with perfectly substitutable intermediate inputs supplied by other firms along different routes. Each firm faces a mass of potential suppliers located in all regions (including its own) and a set of delivery routes. A specific combination of labor, input, and delivery route yields a *technique* of

therefore accommodate the dynamic – but short-lived – disruptions described in Section 3.

³⁵Regions may contain multiple ports.

³⁶These are restrictive assumptions, but they map directly to the evidence presented in Section 3, and to the fact that the bill of lading data only include firm-related transactions.

production, defined over a supplier–buyer match ϕ and a delivery route r :

$$y_i(\phi, r) = \chi a_{n(i)} l_i^{1-\alpha} (z(\phi) x_i(\phi, r))^\alpha, \quad (6)$$

where l_i is the amount of labor used by firm i , $x_i(\phi, r)$ is the amount of intermediate inputs supplied through route r , $z(\phi)$ is the match-specific input-augmenting productivity, and $a_{n(i)}$ is the productivity shifter of region $n(i)$.³⁷

Firms choose the technique that yields the minimum marginal cost of production, at which they sell their goods to other firms – i.e., buyers have full bargaining power (Oberfield, 2018). When selling final goods to local households, firms engage in monopolistic competition. Trade in intermediate inputs is subject to route-specific iceberg costs: for each unit required in production, $\tau_{n(j)n(i)}(r) \geq 1$ units must be shipped from supplier region $n(j)$ to buyer region $n(i)$ along route r . The factory-gate marginal cost of production using technique (ϕ, r) is therefore:

$$c_i(\phi, r) = \frac{w_{n(i)}^{1-\alpha}}{a_{n(i)}} \left(\tau_{n(j)n(i)}(r) \frac{c_j(\phi)}{z(\phi)} \right)^\alpha, \quad (7)$$

where $c_j(\phi)$ is the marginal cost of inputs from supplier j . I assume the following distributional form to obtain a tractable characterization of the equilibrium:

ASSUMPTION 1. *For any firm i in region n , the number of potential suppliers $j \in M_{n'}$ from which i can draw a match with productivity $z > \bar{z}$ follows a Poisson distribution with mean $a_{n'} \bar{z}^{-\xi}$, where $a_{n'}$ is the fundamental productivity of firms in region n' .*

Assumption 1 describes the distribution of match-specific productivity among the techniques available to a firm in region n . The parameter ξ governs the tail behavior of the distribution of productivity draws (Oberfield, 2018; Chen et al., 2023; Balboni et al., 2024). A higher value of ξ implies more similarity across draws, making buyers more willing to substitute toward alternative suppliers when route-level or factory-gate costs increase.

Shipping. Firms from region n can ship to any other region.³⁸ However, shipments

³⁷ χ is a normalizing constant equal to $\alpha^{-\alpha} (1 - \alpha)^{-(1-\alpha)}$.

³⁸With a slight abuse of terminology, *shipping* encompasses both road and maritime transportation. In this setting, transportation mode choice (e.g., road vs. maritime) is implied by route choice, with an elasticity equal to the dispersion of match-specific productivity ξ governing firm-to-firm matching (Fuchs and Wong, 2024).

may be indirect, as some regions are not directly connected (e.g., by a direct road or a maritime route). Shipping routes are composed of a countable set \mathcal{B}_r of legs, with $|\mathcal{B}_r| - 1$ stops from origin n ($k = 1$) to destination n' ($k = |\mathcal{B}_r|$). Each stop may be a port or a region. Each stop involves leg-specific iceberg transportation costs between locations, as well as port-level transportation costs. For a route r connecting n to n' through $|\mathcal{B}_r|$ legs, including $|\mathcal{P}_r|$ ports, the transportation costs are given by:

$$\tau_{n(j)n(i)}(r) = \prod_{k=1}^{|\mathcal{B}_r|} d_{r_{k-1}, r_k} \prod_{m=1}^{|\mathcal{P}_r|} t_{p(r)_m}. \quad (8)$$

Following Ganapati et al. (2024), I allow transportation costs to depend on both endogenous and exogenous variables:

$$d_{r_{k-1}, r_k} = d(\epsilon_{r_{k-1}, r_k}), \quad t_{p(r)_m} = t(\Xi, K_{p(r)_m}) \times \theta_{p(r)_m}, \quad (9)$$

where ϵ_{r_{k-1}, r_k} denotes exogenous transportation costs (i.e., distance), Ξ is a matrix of traffic flows, $K_{p(r)_m}$ denotes port-level infrastructure capacity, and $\theta_{p(r)_m}$ denotes port-level weather-related wedges, with the following assumption:

ASSUMPTION 2. *Port-level wedges are randomly drawn from a Pareto distribution with c.d.f. $F_{p(r)}(\theta) = 1 - \theta^{-\psi_{p(r)}}$ for $\theta_{p(r)} \geq 1$.*

Assumption 2 describes the distribution of port-level wedges. With a higher shape parameter $\psi_{p(r)}$, firms will on average draw lower transportation cost wedges, as the tail of the distribution becomes thinner. This assumption ensures that transportation costs in Equation (8) remain tractable. The set of shape parameters $\{\psi_p\}_{p \in \mathcal{P}}$ governing these weather-related wedges – i.e., climate trade costs – is denoted Ψ and summarizes the port-level tropical cyclone climate.

Sourcing and routing decisions. I first characterize the distribution of factory-gate costs:

PROPOSITION 1. *Under Assumption 1, the marginal cost of firms in $M_{n'}$ follows a Weibull distribution:*

$$P(c_i(\phi, r) > c) = \exp \left[- \left(a_{n'} w_{n'}^{\alpha-1} \right)^{\frac{\xi}{\alpha}} \left(\sum_n a_n \bar{c}_n^{-\xi} \sum_{r \in \mathcal{R}_{nn'}} \prod_{k=1}^{|\mathcal{B}_r|} d_{r_{k-1}, r_k}^{-\xi} \prod_{m=1}^{|\mathcal{P}_r|} \bar{t}_{p(r)_m}^{-\xi} \right) c^{\frac{\xi}{\alpha}} \right], \quad (10)$$

$$\text{where } \bar{c}_n^{-\xi} = a_n^{\xi} w_n^{(\alpha-1)\xi} \left(\sum_{\tilde{n}} a_{\tilde{n}} \bar{c}_{\tilde{n}}^{-\xi} \sum_{r \in \mathcal{R}_{\tilde{n}n}} \prod_{k=1}^{|\mathcal{B}_r|} d_{r_{k-1}, r_k}^{-\xi} \prod_{m=1}^{|\mathcal{P}_r|} \bar{t}_{p(r)_m}^{-\xi} \right)^{\alpha} \Gamma(1-\alpha), \quad (11)$$

$$\text{and } \bar{t}_{p(r)_m}^{-\xi} = t(\Xi, K_{p(r)_m})^{-\xi} \frac{\psi_{p(r)_m}}{\psi_{p(r)_m} + \xi}. \quad (12)$$

Proof. See Appendix D.1.

This result follows from the fact that, if the *effective* price of inputs for suppliers in all origin regions and delivering through any route follows a Weibull distribution, then the distribution of factory-gate prices for all firms i in destination n' also follows a Weibull distribution.³⁹ The production-network structure affects the distribution of marginal costs through the factory-gate costs of upstream suppliers, as shown in Equation (11), which specifies downstream cost indices as a fixed point. Transportation costs depart from related models of production-network formation (Chen et al., 2023; Balboni et al., 2024) by explicitly incorporating the set of links and transportation infrastructure that compose routes. I characterize the joint sourcing and routing decisions of firms as a corollary to Proposition 1.

COROLLARY 1. *The probability that firm i in n' sources from route r connecting n to n' is:*

$$\pi_{i,r} = \frac{a_n \bar{c}_n^{-\xi} \prod_{k=1}^{|\mathcal{B}_r|} d_{r_{k-1}, r_k}^{-\xi} \prod_{m=1}^{|\mathcal{P}_r|} \bar{t}_{p(r)_m}^{-\xi}}{\sum_{\tilde{n}} a_{\tilde{n}} \bar{c}_{\tilde{n}}^{-\xi} \sum_{r \in \mathcal{R}_{\tilde{n}n'}} \prod_{k=1}^{|\mathcal{B}_r|} d_{r_{k-1}, r_k}^{-\xi} \prod_{m=1}^{|\mathcal{P}_r|} \bar{t}_{p(r)_m}^{-\xi}}. \quad (13)$$

Proof. See Appendix D.1.

Equation (13) represents the unconditional probability of choosing route r to source goods. Given that route r links destination n' to origin n , Equation (13) jointly specifies the sourcing region and the delivery route. Because this probability is independent of firm i characteristics, $\pi_{i,r}$ is also the share of *expenditures* of region n' on region n through route r . Aggregating the sourcing–routing shares across routes yields region-to-region bilateral trade shares, as shown in Corollary 2:

³⁹I define the effective price of inputs delivered by supplier j through route r as

$$\lambda_j(\phi, r) = \frac{c_j}{z(\phi)} \prod_{k=1}^{|\mathcal{B}_r|} d_{r_{k-1}, r_k} \prod_{m=1}^{|\mathcal{P}_r|} t_{p(r)_m}.$$

COROLLARY 2. *The bilateral trade share between n' and n is:*

$$\pi_{nn'} = \frac{a_n \bar{c}_n^{-\xi} \tau_{nn'}^{-\xi}}{\sum_{\tilde{n}} a_{\tilde{n}} \bar{c}_{\tilde{n}}^{-\xi} \tau_{\tilde{n}n'}^{-\xi}}, \quad (14)$$

$$\text{where } \tau_{nn'} = \left(\sum_{r \in \mathcal{R}_{nn'}} \left(\prod_{k=1}^{|\mathcal{B}_r|} d_{r_{k-1}, r_k}^{-\xi} \right) \left(\prod_{m=1}^{|\mathcal{P}_r|} \bar{t}_{p(r)_m}^{-\xi} \right) \right)^{-\frac{1}{\xi}}. \quad (15)$$

Proof. See Appendix D.1.

Equation (14) resembles that of traditional trade models, with the addition of production network-affected marginal-cost indices \bar{c}_n and endogenous transportation costs. Equation (15) captures the departure from trade models with endogenous routing (Allen and Arkolakis, 2022; Ganapati et al., 2024; Fuchs and Wong, 2024) by explicitly incorporating infrastructure-level costs.

Equilibrium transportation costs. Define the auxiliary matrix of bilateral transportation resistance Δ as a $(|\mathcal{N}| + |\mathcal{P}|) \times (|\mathcal{N}| + |\mathcal{P}|)$ matrix. Each of the first $|\mathcal{N}|$ rows and columns of Δ corresponds to a region, while each of the last $|\mathcal{P}|$ rows and columns corresponds to a port. Denoting both regions and ports as *locations*, indexed by l or l' , the (l, l') entry $\delta_{ll'}$ of Δ is zero if l and l' are not directly connected. If the two locations are connected and l' is a port, then $\delta_{ll'} = d_{ll'}^{-\xi} \bar{t}_{l'}^{-\xi}$; if the two locations are connected and l' is not a port, then $\delta_{ll'} = d_{ll'}^{-\xi}$. It follows that the region-to-region transportation costs are given by the Leontief inverse of the auxiliary matrix Δ :

$$[\tau_{nn'}] = [(I - \Delta)^{-1}]^{\circ(-\frac{1}{\xi})}. \quad (16)$$

The conditional probability that a good passes through port p , given origin n and destination n' , is:⁴⁰

$$\Theta_{p|nn'} = \left(\frac{\tau_{np} \tau_{pn'}}{\tau_{nn'}} \right)^{-\xi}. \quad (17)$$

Using these port-level conditional probabilities, I characterize traffic as the total value of goods that transit through ports:

$$\Xi_p = \sum_n \sum_{n'} \Theta_{p|nn'} X_{nn'}, \quad (18)$$

⁴⁰Here, I follow Allen and Arkolakis (2022) and Ducruet et al. (2024).

where $X_{nn'}$ is the total trade value from n' to n . Equation (9) implies that port traffic affects transportation costs – a form of externality that firms do not internalize when making sourcing–routing decisions. I formalize this idea with the following parametrization of bilateral and port-level transportation frictions:

$$d_{nn'}^{-\xi} = \epsilon_{nn'}^{\lambda_1} \quad , \quad \bar{t}_p^{-\xi} = \Xi_p^{\lambda_2} K_p^{\lambda_3} \frac{\psi_p}{\psi_p + \xi}, \quad (19)$$

where λ_1 is the elasticity of link-level costs to distance, λ_2 is the elasticity of port-level costs to port traffic, and λ_3 is the elasticity of port-level costs to port capacity.⁴¹

Closing the model. Appendix D.2 completes the description of the model environment. The model closes with a goods market-clearing condition, which requires that trade in intermediate inputs be balanced.

Equilibrium. The economy is characterized by a set of parameters $\{\sigma, \alpha, \xi, \lambda_1, \lambda_2, \lambda_3\}$, a geography $\mathcal{G} = \{\mathcal{N}, \mathcal{P}, \mathcal{L}, \mathcal{M}, \mathcal{A}, \mathcal{D}, \mathcal{K}, \Psi\}$, and a distribution of wages and factory-gate prices $\{w_n, \bar{c}_n\}_{n \in \mathcal{N}}$, such that markets clear and the transportation network is in equilibrium. Appendix D.3 formally defines the general equilibrium of the model with traffic congestion and provides the system of equations that characterize it. Appendix D.4 describes the numerical algorithm implemented to recover counterfactual equilibria.

5 BRINGING THE MODEL TO THE DATA

The aim of this section is to quantify the model so that it matches global data at the subnational level in the early 21st century. To do so, I first estimate the key parameters of transportation costs using Brazilian bill of lading data.⁴² Other economy-wide parameters are drawn from the literature. I then use these parameters, together with a model inversion, to map the model’s geography \mathcal{G} onto global observables.

I recover the following parameters and fundamentals: the measure of labor (L_n); fundamental region-level productivity (a_n); port capacity (K_p); the elasticity of transportation costs with respect to distance (λ_1), traffic (λ_2), and port capacity (λ_3); port-level weather dispersion (ψ_p); the final-goods elasticity of substitution (σ); the inter-

⁴¹From Proposition 1, Assumption 2, and the definition of port-level trade costs in Equation (9), $\bar{t}_p^{-\xi} = t(\Xi, K_p)^{-\xi} \frac{\psi_p}{\psi_p + \xi}$. I parametrize $t(\Xi, K_p)^{-\xi} = \Xi_p^{\lambda_2} K_p^{\lambda_3}$.

⁴²A caveat of this exercise is that, due to data constraints, I calibrate a *global* model with *local* data from Brazil. An implicit assumption is that the estimated elasticities have external validity.

Table 1: Calibration of parameters and fundamentals

Parameters	Description	Source/Procedure
<i>Panel A: Parameters from related literature</i>		
$\sigma = 2$	Final goods CES	Castro-Vincenzi (2024)
$\alpha = 0.8$	Intermediate input share	Balboni et al. (2024)
$\xi = 8$	Trade elasticity	Allen and Arkolakis (2022)
<i>Panel B: Calibrated parameters</i>		
$\lambda_1 = -0.48$	Distance elasticity	Section 5.1
$\lambda_2 = -0.25$	Traffic elasticity	Section 5.1
$\lambda_3 = 0.42$	Capacity elasticity	Section 5.1
Fundamentals	Description	Source/Matched moments
<i>Panel C: Calibrated fundamentals</i>		
\mathcal{N}	Regions	Aggregation at GAUL1 level
\mathcal{P}	Ports	IMF PortWatch
\mathcal{L}	Population	Rossi-Hansberg and Zhang (2025)
\mathcal{A}	Region-level productivity	Matched to Rossi-Hansberg and Zhang (2025)
\mathcal{D}	Distance	Eurostat SeaRoute & Great-circle distance
\mathcal{K}	Port capacity	IMF PortWatch
$\{\psi_p\}_{p \in \mathcal{P}}$	Climate trade costs	Section 5.1

mediate input share (α); and the dispersion of match-specific productivity (ξ). Table 1 summarizes the provenance or procedure used to obtain the calibrated parameters and fundamentals. Section 5.3 describes validation tests of the baseline calibration.

5.1 ESTIMATING TRANSPORTATION COSTS

I aim to recover a set of transportation costs that accounts for the effects of traffic, port capacity, and weather risk. To estimate the parameters of transportation costs, I use a reduced-form analogue of route-level bilateral trade shares (Corollary 1):

$$\begin{aligned} \log(\pi_{n_d, r, t}^{value}) = & \alpha_{n_o, t} + \alpha_{n_d, t} + \alpha_{p_d, t} + \alpha_1 \log(Distance_r) + \alpha_2 \log(\Xi_{p_o, t}^{TEU}) \\ & + \alpha_3 \log(K_{p_o}^{TEU}) + \alpha_4 \log(CycloneRisk_{p_o}) + \varepsilon_{n_d, r, t}. \end{aligned} \quad (20)$$

I bring Equation (20) to the data by constructing a microdata analogue of the route-level bilateral trade share from Brazilian bill of lading data. That is, $\pi_{n_d, r, t}^{value}$ is defined as the weekly share of shipment value that destination location n_d sources through route r . In the data, locations refer to GAUL1 subnational units, while routes are approximated as the quadruplet $\{n_o, n_d, p_o, p_d\}$, where p_o and p_d are the ports of origin and destination, respectively. The distance component of transportation costs is approximated as the least-cost land–sea distance traveled by goods from supplier origin to buyer destination, passing through p_o and p_d . I use weekly estimates of total TEU

volumes transiting through ports from PortWatch to proxy port-level traffic. Port capacity is proxied by the 99th percentile of daily TEU traffic processed by each port over the sample period (2019–2023). I proxy cyclone risk using expected wind speed at the port, as reported in the STORM data (see Figure B.2a).⁴³ Origin-time and destination-time fixed effects control for any origin or destination general equilibrium terms in Equation (13).

Regressing route-level bilateral trade shares on port traffic and port capacity is vulnerable to simultaneity: both regressors are equilibrium-derived outcomes in the market for port throughput, so unobserved shocks that shift demand or supply curves also enter the error term. I address these endogeneity concerns by estimating Equation (20) with two-stage least squares (2SLS) and two orthogonal curve-shifters. Port traffic is instrumented with global container throughput interacted with each port’s 1950 coastal-population share – a predetermined demand shifter that scales worldwide traffic variations across ports while leaving local handling costs unchanged. Capacity is instrumented with mean terrain ruggedness within 20 km of the port, a geologic supply determinant that raises inland evacuation costs and therefore limits optimal port capacity, while remaining exogenous to current trade flows. Appendix E.1 details the construction of the instruments and documents robust first-stage relevance for both port traffic and capacity.

Table 2 reports the results. Conditional on port capacity, a 1% increase in port traffic reduces route-level bilateral trade shares by 1.78%. Assuming a trade elasticity of $\xi = 8$ ([Allen and Arkolakis, 2022](#)), this implies a 0.22% increase in port-level trade costs.⁴⁴ Conversely, a 1% increase in port capacity decreases port-level trade costs by 0.30%, indicating the presence of scale economies.⁴⁵ Furthermore, a 1% increase in cyclone risk lowers route-level bilateral trade shares by 0.08% – corresponding to a 0.01% increase in transportation costs.

⁴³Formally, I parameterize $\frac{\psi_p}{\psi_p + \xi} = CycloneRisk_p = \left(1 + windspeed_p^{(0)}\right)^{\lambda_w}$, where $windspeed_p^{(0)}$ is computed as the yearly mean expected wind speed in cells within a 50 km radius of the port under the current climate; λ_w is the elasticity of transportation costs with respect to expected wind speed.

⁴⁴By comparison, [Allen and Arkolakis \(2022\)](#) find an elasticity of traffic flow (per lane) with respect to transportation cost of 0.09 in the US highway system.

⁴⁵Given the high observed correlation between port-level traffic and capacity, this finding is consistent with [Ganapati et al. \(2024\)](#), who document scale economies in the maritime network, although they do not disentangle traffic from capacity.

Table 2: Estimation of transportation costs

	$\pi_{n_d, r, t}^{value}$	
	(1)	(2)
Log Port Origin Traffic	-0.01 (0.03)	-1.78 (0.25)
Log Port Origin Capacity	0.15 (0.04)	2.36 (0.31)
Log Distance	-0.36 (0.03)	-0.46 (0.04)
Log Cyclone Risk	-0.02 (0.01)	-0.08 (0.01)
Observations	90,504	90,504
Adjusted R ²	0.67	0.64
Wald-F, Log Port Origin Traffic	9,476.47	
Wald-F, Log Port Origin Capacity	9,453.84	
n_d -week fixed effects	✓	✓
n_o -week fixed effects	✓	✓
p_d -week fixed effects	✓	✓

Notes: This table presents the results of the estimation of transportation costs, as specified by Equation 20. The outcome is the log weekly share of shipment value that destination location n_d sources through route r . Port Origin traffic refers to weekly estimates of total TEU volumes transiting through ports of origin of shipments. Port Origin Capacity refers to the 99th percentile of daily TEU volume at ports. Distance refers to the total route distance (land and sea). Cyclone Risk refers to the expected windspeed at ports, as reported in the STORM data. Panel (1) reports the OLS estimation, while Panel (2) reports the 2SLS estimation. Robust standard errors are clustered at the $\{n_o, n_d, p_o, p_d\}$ -week level.

5.2 FUNDAMENTALS AND ECONOMY-WIDE PARAMETERS

Parameters from the literature. I follow [Castro-Vincenzi \(2024\)](#) by setting $\sigma = 2$, and [Allen and Arkolakis \(2022\)](#) by setting $\xi = 8$. I set the intermediate-input share to $\alpha = 0.8$ following [Balboni et al. \(2024\)](#).

Fundamentals. The model is calibrated at the GAUL1 level. I calibrate GAUL1-level population using [Rossi-Hansberg and Zhang \(2025\)](#), which provides population estimates at 1° spatial resolution. I assign the ports in PortWatch to each GAUL1 unit and use the 99th percentile of daily TEU traffic as a measure of port capacity. Distances between regions are approximated by great-circle distances between GAUL1 centroids. For computational sparsity in the transportation-network matrix, I retain centroid distances only for contiguous region pairs identified via polygon contiguity (first-order neighbors). I use Eurostat's SeaRoute program to calculate the shortest sea

routes between ports. As in Section 5.1, I parametrize $\frac{\psi_p}{\psi_p + \xi} = (1 + \text{windspeed}_p^{(0)})^{\lambda_w}$, where $\text{windspeed}_p^{(0)}$ is the yearly mean expected wind speed in cells within a 50 km radius of the port under the current climate (see Figure B.2a), and λ_w is the elasticity of transportation costs with respect to expected wind speed.

With the remaining model parameters calibrated, I recover region-level fundamental productivity by inverting the model so that it matches the local GDP-per-capita estimates reported by [Rossi-Hansberg and Zhang \(2025\)](#) at 1° spatial resolution. I compute the population-weighted mean GDP per capita within GAUL1 subnational units as a proxy for region-level wages. Using an inversion of the equilibrium conditions, I obtain the vector of fundamental productivities that rationalizes observed wages. The inversion procedure is described in Appendix E.2.

Geography sample. I subsample the geography data to reduce the dimensionality of the numerical problem and remove outliers. The raw geography comprises 2,381 GAUL1 subnational units (regions) and 1,666 ports from PortWatch. I first remove regions whose population and GDP-per-capita estimates are zero due to measurement error. I also remove ports whose port capacity is zero, due to very low and infrequent activity. A model requirement is that the transportation network be a complete graph – i.e., all locations (regions and ports) must be linked to every other location through at least one route. I retain all regions that are part of the largest connected graph the transportation network, resulting in 2,246 regions. I then truncate the port data to retain only the top 750 ports, ranked by total traffic volume across the sample (see Figure E.1). These ports account for 97% of total TEU volume and 86% of total vessel counts in the PortWatch data (2019–2023).

5.3 MODEL FIT

Before using the model to simulate future changes in port climates, I verify the plausibility of the quantification. I show that the model’s predictions align well with data moments for maritime traffic, local productivity, and trade. I also confirm that congestion in transportation networks – a novel feature in models of spatial production networks – is a key mechanism for fitting the data.

I first compare the model-based estimates for port traffic and fundamental productivity to their data counterparts. Figure 6a compares the model-derived port traffic

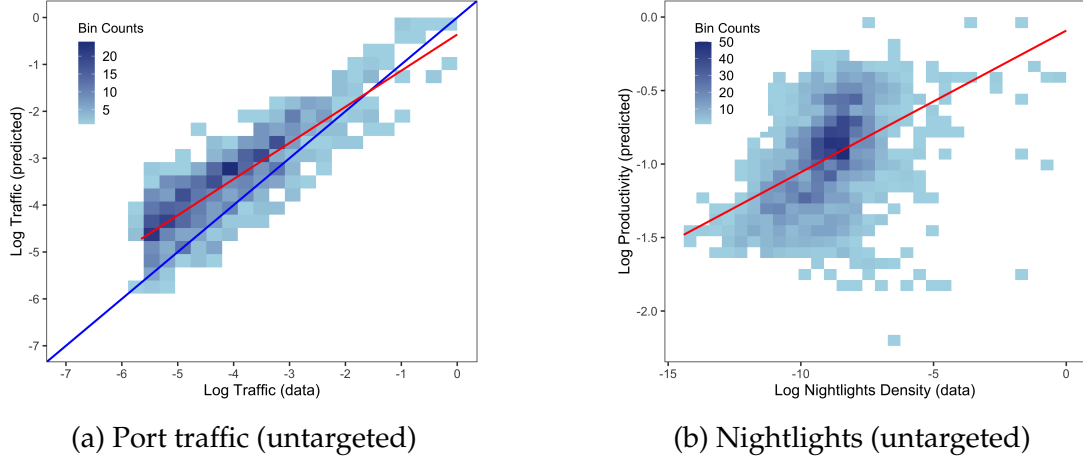


Figure 6: Model fit

Notes: These panels compare model-based moments to their (untargeted) data counterparts or proxies. Panel 6a plots log-normalized port traffic in the data – measured as average yearly total TEU volume – (x -axis) against log-normalized model-based estimates of port traffic (y -axis). Panel 6b plots per-capita nightlight intensity at the GAUL1 subnational level in the data (x -axis) against log-normalized model-based estimates of fundamental productivity (y -axis). Model-based moments are obtained from the inversion procedure described in Appendix E.2.

(normalized by the maximum) to the average yearly total TEU volume in the Port-Watch data (equally normalized), in logs. The model performs well in predicting port traffic, with a correlation of 0.86, despite port traffic being an untargeted moment. Figure 6b compares log fundamental productivity recovered from the model inversion with log per-capita nightlight intensity – a data-driven proxy for local productivity. Nightlight data are taken from Li et al. (2020) and aggregated at the GAUL1 level. While the comparison remains noisy, model-based fundamental productivity is positively correlated with per-capita nightlights (0.32).

I then verify the model fit with country-level bilateral trade shares. Figure E.3 compares log country-level trade shares – recovered from GLORIA input–output tables (IELab, 2025) – with their model-based counterparts. The model replicates the ranking of bilateral trade shares (correlation = 0.56), although it overestimates the level of domestic trade shares.⁴⁶ This discrepancy arises because the model does not explicitly account for domestic trade infrastructure – domestic trade costs are normalized to one.

Finally, to illustrate the role of port-level congestion in fitting the data, I solve for the equilibrium of the model with no congestion spillovers ($\lambda_2 = 0$). Figure E.2 compares the fit of model-based port traffic to the data with and without congestion

⁴⁶This implies that the counterfactual simulations provide lower bounds for welfare impacts from changes in transportation cost fundamentals.

spillovers. While the correlation with the data remains high (0.87), removing congestion significantly compresses the dispersion of port traffic estimates – highlighting that congestion spillovers are quantitatively important for explaining heterogeneity in port traffic.

6 QUANTITATIVE RESULTS

This section quantifies how firms' private responses shape the welfare effects of port-level climate change. I examine a counterfactual in which cyclone-related wind risk at ports rises under an unmitigated climate change scenario (RCP8.5). Comparing equilibria with and without rerouting isolates the adaptation margin and its implications for port traffic and regional welfare.

Climate change at ports and private rerouting. I first investigate the effect of a shift in the distribution of cyclone-related wind speed at ports on maritime traffic and global welfare. I infer the climate-change-induced increase in extreme wind events at the port level using the expected wind speed from the STORM data under an RCP8.5 scenario (see Figure B.2b). The change in predicted wind conditions around port locations provides my main counterfactual variable. In practice, I solve for the equilibrium at baseline (see Section 5.2), and compare model-based outcomes to alternative equilibria with changes in fundamentals.

Two main outcomes of interest are the change in port traffic and the change in region-level welfare. Port traffic is given by Equation (18). Welfare is defined as region-level real income, formally derived in the following proposition:

PROPOSITION 2. *Region-level welfare in this economy, measured as real income, is given by:*

$$V_n = L_n w_n \left[a_n w_n^{\alpha-1} \left(\sum_{n'} a_{n'} \bar{c}_{n'}^{-\xi} \tau_{n'n}^{-\xi} \right)^{\frac{\alpha}{\xi}} \right]^{\sigma-1} \Gamma \left(1 - \frac{\alpha(\sigma-1)}{\xi} \right) \quad (21)$$

Proof. See Appendix D.5.

Figure 7a plots regional welfare changes under a climate change scenario. While aggregate welfare is virtually unaffected (+0.005 basis points), substantial heterogeneity emerges. At the 5th percentile, welfare losses amount to -0.47 bp, while welfare gains at the 95th percentile reach 0.12 bp. Welfare losses are generally concentrated

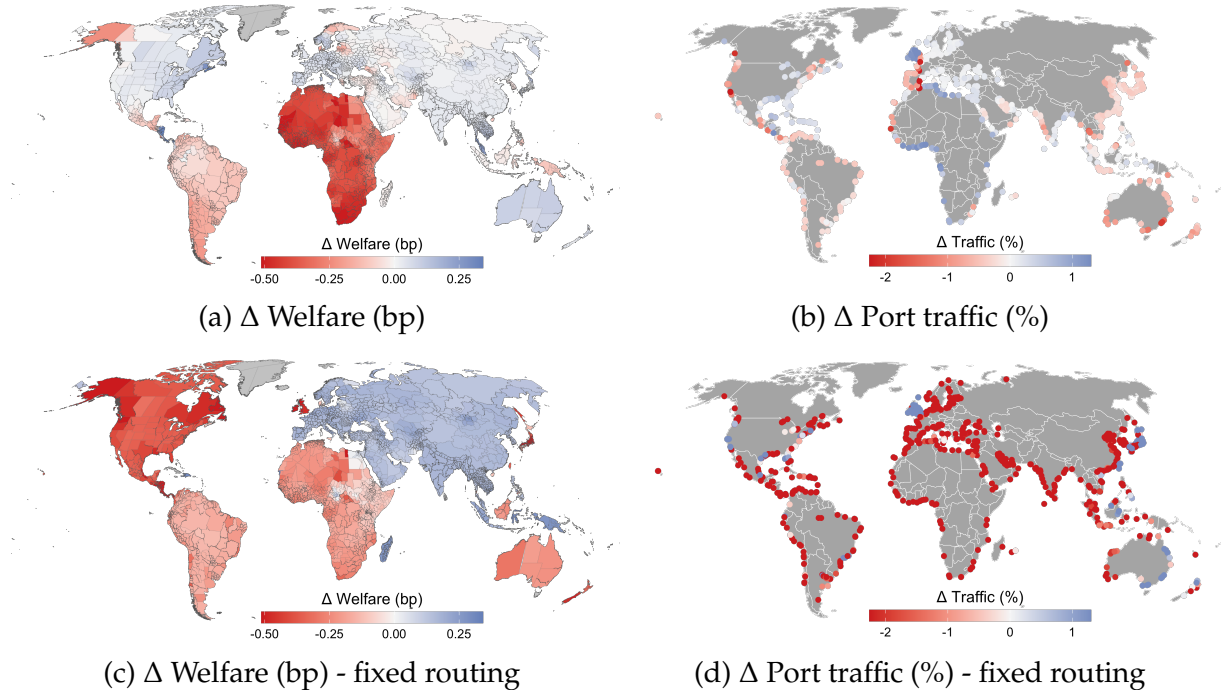


Figure 7: Quantitative results - Present to RCP8.5 (2020-2050)

Notes: These Panels present the change in port traffic and region-level welfare, in a scenario of increased climate risks at ports. In Panels (a) and (b), I allow firms to reroute optimally to avoid increased transportation costs. In Panels (c) and (d), the routing choice is fixed as baseline. All outcomes are generated using the algorithm described in Appendix D.4. The color scales of all Panels are truncated at the 1st and 99th percentiles.

in well-defined areas – e.g., Africa and South America – illustrating the presence of localized spillovers. Port traffic (Figure 7b) shows similar variation. At the 5th percentile, ports experience a -0.98% decrease in traffic, while at the 95th percentile traffic increases by 0.79%. Aggregate traffic decreases by 0.26%. Wind speed risk shifts trade toward less affected ports: Figure 8a shows a negative correlation between expected wind speed change and traffic change. The observed variance in port traffic change reflects the trade-off between increased weather risk at ports and congestion spillovers induced by rerouting.

Rerouting as adaptation. I seek to disentangle the role of rerouting, which induces spillovers in general equilibrium, from the increase in weather risks. To do so, I simulate an equilibrium with the same increase in weather risks as in the RCP8.5 counterfactual, but restrict route choice to baseline – that is, I shut down the rerouting margin. In practice, the probability that a good passes through port p conditional on origin n and destination n' is not given anymore by Equation (17), where $\tau_{nn'}$ encompasses

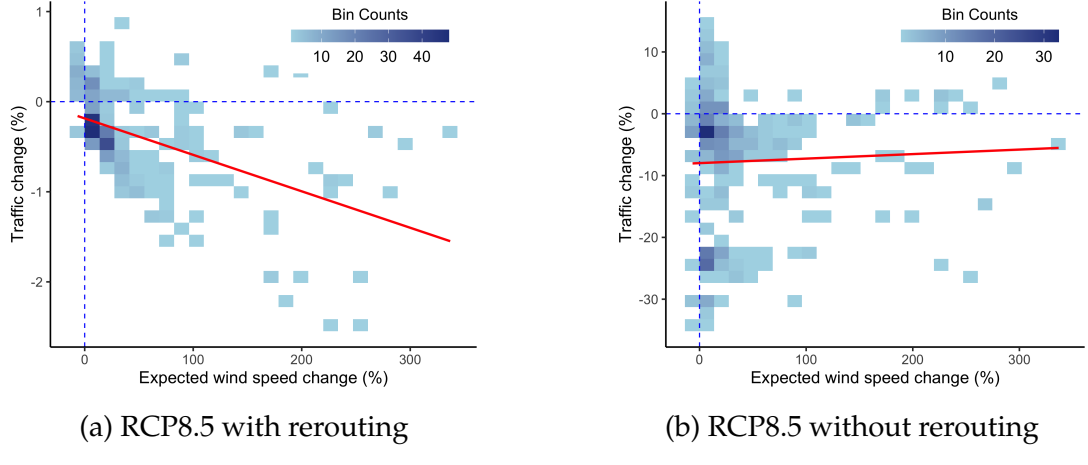


Figure 8: Port traffic and expected wind speed costs

Notes: These panels plot the change in port traffic against the change in expected wind speed from tropical cyclones. On the x-axis, I plot the change in yearly mean expected wind speed recovered from the STORM model, under both the current and future RCP8.5 climate. I remove port with zero expected windspeed at baseline, and truncate the data at the 5th and 95th percentile in expected wind-speed change. On the y-axis, I plot the change in port traffic, generated using the algorithm described in Appendix D.4. In Panel 8a, I allow firms to reroute optimally to avoid increased transportation costs. In Panel 8b, the routing choice is fixed as baseline.

increased weather risks. Rather, I fix

$$\pi_{p|nn'}^{(0)} = \left(\frac{\tau_{np}^{(0)} \tau_{pn'}^{(0)}}{\tau_{nn'}^{(0)}} \right)^{-\xi}, \quad (22)$$

where $\tau_{nn'}^{(0)}$ denotes the transportation costs estimated under the current climate. This amounts to not allowing private rerouting responses of firms.

Figure 7c plots regional welfare changes in a climate change scenario with fixed routing. In the absence of rerouting adaptation, aggregate welfare declines (-0.04 basis points). The distribution of welfare losses changes drastically – including concentrated losses in North America, the UK, and Japan. Aggregate port traffic, furthermore, decreases substantially (-4.4%, Figure 7d). Figure 8b shows that traffic change becomes de-correlated from increased weather risk, a consequence of fixed routing. In the absence of rerouting as an adaptation mechanism to weather risk, domestic trade substitutes for international trade, and demand for port traffic decreases globally. Figures E.4a and E.4b in Appendix E.4 show that the variance in welfare and traffic changes increases without rerouting, along with larger welfare and traffic losses.

7 INFRASTRUCTURE POLICY

This section studies the efficient allocation of scarce port investment under evolving port-level climate risk. I develop a sufficient-statistics, computationally tractable framework that maps port capacity expansions into welfare changes and delivers a ranking of investment priorities. I then quantify the misallocation that arises when investment decisions abstract from changing port-specific climate conditions and from firms' private responses – first globally, and then within the EU27.

7.1 A SOCIAL SAVINGS SUFFICIENT STATISTIC FOR PORT CAPACITY

I adopt a *social savings sufficient-statistics* approach, originating in [Fogel \(1962\)](#). This method entails expressing the elasticity of welfare to port capacity solely in terms of observable reduced-form objects, allowing to recover first-order welfare changes without solving the full general equilibrium of the model.⁴⁷ As in [Allen et al. \(2025\)](#), the sufficient statistics I derive account for general equilibrium economic adjustments and endogenous route choice.⁴⁸ I characterize the social savings sufficient statistics for port capacity as follows:

PROPOSITION 3. *The elasticity of region-level welfare V_n with respect to port capacity K_p is:*

$$\frac{\partial \log V_n}{\partial \log K_p} = \beta_w g_{n,p}^{(w)} + \beta_\tau \sum_{n'} \pi_{n'n} \left[-\xi g_{n',p}^{(c)} + \lambda_3 \Theta_{p|nn'} + \lambda_2 \sum_{p' \in \mathcal{P}} \Theta_{p'|nn'} g_{p',p}^{(\Xi)} \right], \quad (23)$$

where $g_{n,p}^{(w)} = \frac{\partial \log w_n}{\partial \log K_p}$, $g_{n,p}^{(c)} = \frac{\partial \log c_n}{\partial \log K_p}$, and $g_{p',p}^{(\Xi)} = \frac{\partial \log \Xi_{p'}}{\partial \log K_p}$, and β_w and β_τ are constants built from economy-wide parameters. The elasticities of wages, factory-gate costs, and port traffic to port capacity are the solution to the following set of equations:

$$\begin{bmatrix} \mathbf{A}_{ww} & \mathbf{A}_{w\Xi} & \mathbf{A}_{wc} \\ \mathbf{A}_{\Xi w} & \mathbf{A}_{\Xi\Xi} & \mathbf{A}_{\Xi c} \\ \mathbf{A}_{cw} & \mathbf{A}_{\Xi c} & \mathbf{A}_{cc} \end{bmatrix} \begin{bmatrix} g_{n,p}^{(w)} \\ g_{p',p}^{(\Xi)} \\ g_{n,p}^{(c)} \end{bmatrix} = \begin{bmatrix} b_w \\ b_\Xi \\ b_c \end{bmatrix}, \quad (24)$$

⁴⁷A full general equilibrium approach to evaluate the welfare effects of infrastructure improvements would involve sequentially increasing the capacity of each of the 750 ports by 1%, and computing welfare changes from baseline – as in [Brancaccio et al. \(2024\)](#). In my case, with a model calibrated at the subnational level, such an exercise is computationally burdensome – the estimated running time of the simulation is of 62 days.

⁴⁸I depart from [Allen et al. \(2025\)](#) in several ways. First, I consider infrastructure improvements to nodes (i.e., ports), rather than to links (e.g., rail segments). Second, I abstract from mode of transport choice. Third, I explicitly allow for trade in intermediate inputs via production networks.

where

$$\{\mathbf{A}_{ww}, \mathbf{A}_{w\Xi}, \mathbf{A}_{wc}, \mathbf{A}_{\Xi w}, \mathbf{A}_{\Xi\Xi}, \mathbf{A}_{\Xi c}, \mathbf{A}_{cw}, \mathbf{A}_{\Xi c}, \mathbf{A}_{cc}, b_w, b_\Xi, b_c\}$$

are constants built from equilibrium objects.

Proof. See Appendix D.6.

Although Proposition (3) characterizes *local* gains to port capacity improvements, aggregation can flexibly yield global (or larger-scale) gains. Global welfare elasticity to port capacity amounts to a welfare-weighted average of region-specific elasticities:

$$\frac{\partial \log \bar{V}}{\partial \log K_p} = \sum_{n \in \mathcal{N}} \frac{V_n}{\bar{V}} \frac{\partial \log V_n}{\partial \log K_p}. \quad (25)$$

Equation (23) highlights four channels that shape the welfare elasticity with respect to port capacity. The income channel, $g_{n,p}^{(w)}$, captures how a capacity shock at port p feeds through general equilibrium into local wages. The input cost channel, $g_{n',p}^{(c)}$, reflects the impact on factory-gate costs at every origin n' , weighted by the expenditure share $\pi_{n'n}$ of region n . The direct routing channel, $\lambda_3 \Theta_{p|nn'}$, captures the fact that increasing capacity at p lowers bilateral transport costs along any path that physically traverses p – in other words, the “shortcut” offered by expanding the port. Finally, the congestion spillover channel, $\lambda_2 \sum_{p'} \Theta_{p'|nn'} g_{p',p}^{(\Xi)}$, captures how capacity expansion at p affects traffic $\Xi_{p'}$ system-wide, thereby altering congestion even on routes that do not traverse p itself.

Importantly for policy analysis, the decomposition in Proposition (3) allows mapping welfare impacts of infrastructure improvements to observable quantities, at the sole cost of solving a system of linear equations. Armed with observed quantities $\{L_n, w_n, X_{nn'}, \pi_{nn'}, \Theta_{p|nn'}\}$ and economy-wide parameters $\{\sigma, \alpha, \xi, \lambda_1, \lambda_2, \lambda_3\}$, one can estimate welfare payoffs from port expansion without solving a large-scale general equilibrium model. These estimates account for first-order traffic congestion spillovers within transportation networks while preserving the income and input cost channels.⁴⁹

⁴⁹In the exercises below, I use model-based counterfactual outputs at the sub-national level. However, welfare impacts of port improvements can also be estimated at a higher level of aggregation using real data. Wages w_n , population L_n , trade flows $X_{nn'}$, and bilateral trade shares $\pi_{nn'}$ are readily available at the country level. The routing kernel $\Theta_{p|nn'}$ can be approximated using publicly available bilateral resistance data and port traffic volumes – requiring only the assumption of a functional form for bilateral transportation costs.

7.2 INFRASTRUCTURE POLICY UNDER CLIMATE CHANGE

The social-savings sufficient-statistics approach provides a framework to identify which nodes of the transportation network yield the highest welfare gains from marginal investment. I implement this approach using the general equilibrium results from Section 6, comparing the baseline and the RCP8.5 climate scenarios. Figure 9a reports the port-level global welfare elasticities for all 750 ports in the sample under the RCP8.5 scenario. On average, a 1% increase in port capacity raises global welfare by 0.02%.⁵⁰ This average conceals substantial heterogeneity across ports: the elasticity ranges from 0.004 at the 5th percentile to 0.06 at the 95th percentile, suggesting that uniform investment across ports would be highly inefficient.

How does the exposure of ports to future climate conditions alter these returns to investment? In line with Balboni (2025), I show that accounting for environmental damage is essential for the efficient allocation of infrastructure spending. Figure 9b illustrates that neglecting future climate impacts (“policy myopia”) can redirect resources toward ports with relatively low welfare payoffs. Under the RCP8.5 scenario, welfare gains from expanding port capacity fall by 15% at the 5th percentile of the elasticity distribution, while they rise by 12% at the 95th percentile. These results highlight the importance of incorporating forward-looking climate considerations into infrastructure investment decisions.

To quantify the extent of potential misallocation in port capacity investments, I construct an allocation rule in which the share of investment g_p^* received by each port is proportional to its global welfare elasticity under the RCP8.5 scenario.⁵¹ This *first-order* allocation rule ranks ports by their welfare-improving potential once future climate risks and firms’ adaptation margins are accounted for. I then compare this benchmark to alternative investment rules i , denoted $g_p^{(i)}$, using the following measure of misallocation:

$$\text{Misallocation}(\%) = \frac{1}{2} \sum_p |g_p^* - g_p^{(i)}|. \quad (26)$$

This metric answers the question: “what share of total port investment would need to be reallocated to match the climate-adjusted first-order allocation?” When comparing

⁵⁰For comparison, Brancaccio et al. (2024) estimate that a 1% increase in total U.S. port capacity raises aggregate welfare by 0.5%.

⁵¹Formally, $g_p^* = \frac{\partial \log \bar{V}}{\partial \log K_p} / \sum_{p'} \frac{\partial \log \bar{V}}{\partial \log K_{p'}}$, evaluated under the RCP8.5 scenario.

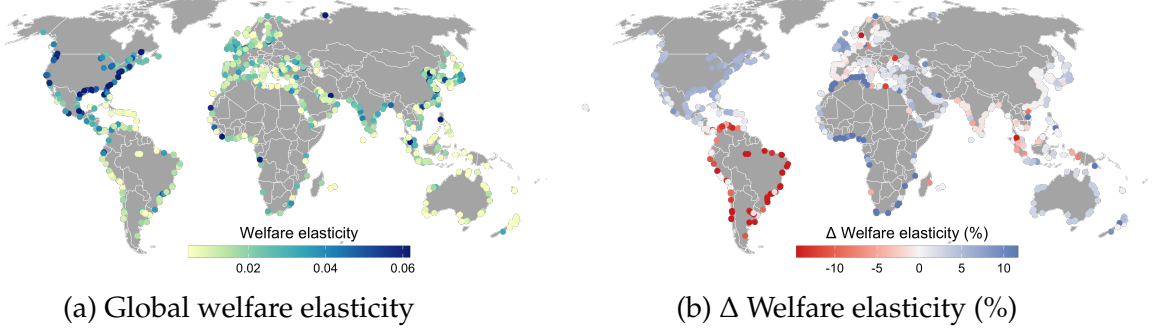


Figure 9: Welfare elasticity to port capacity

Notes: These panels plot the social savings sufficient statistics of port capacity under a RCP8.5 scenario. In Panel 9a, I plot the port-level elasticity of welfare to port capacity. In Panel 9b, I plot the change in port-level welfare elasticities from the baseline scenario to the RCP8.5 one. Welfare elasticities are computed from the counterfactual outputs of Section 6, using the solution method described in Appendix D.6. The color scales of both panels are truncated at the 5th and 95th percentiles.

the climate-aware first-order rule to a myopic one (based on present climate conditions), the results imply that policy myopia would misallocate 2.3% of total global port investment. For reference, a purely capacity-based rule misallocates 33.3%, while an equal-share rule misallocates 30.5%.⁵²

7.3 INVESTMENT INTO PORTS: THE CASE OF THE EU

I then illustrate how the social-savings sufficient-statistics framework can inform spatial investment decisions and how accounting for future climate conditions affects their allocation. I focus on the case of EU27 ports. Based on port-level surveys and investment pipeline data, [ESPO \(2024\)](#) estimates that EU ports plan approximately EUR 84 billion (around USD 93 billion) of investment by 2034. I construct a counterfactual scenario in which this aggregate amount is allocated across EU ports using the first-order allocation rule – computed for EU27 welfare gains – as the guiding criterion. The analysis assesses how future climate conditions may alter the spatial pattern of welfare-improving investment.

The first step is to derive the investment allocation rule. Using the social-savings sufficient-statistics framework, I compute the shares of total investment implied by the first-order allocation rule. The EU27 welfare elasticity of European ports is obtained by aggregating Equation (23) over regions belonging to EU27 countries. Investment

⁵²The “present-climate” rule allocates investment shares proportional to welfare elasticities computed under current climate conditions, while the other two rules allocate based on current port capacity or equal weights across ports.

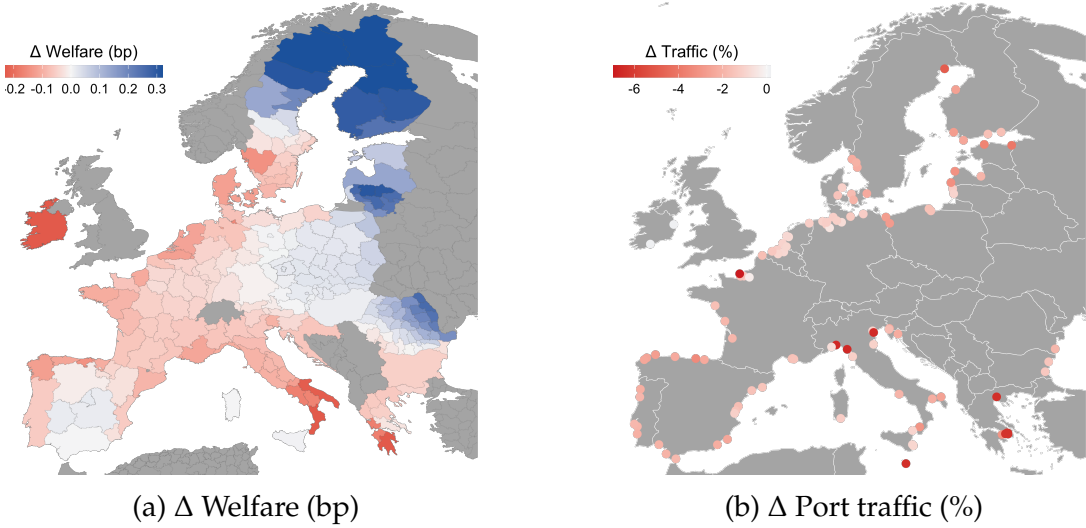


Figure 10: Port investments and RCP8.5 – the EU case

Notes: These panels display changes in region-level welfare (Panel 10a) and port traffic (Panel 10b) for the EU27 under a scenario of increased climate risks with port investment. Each panel compares an equilibrium in which investment follows a myopic first-order rule (evaluated under baseline climate) to one that accounts for future climate conditions at ports. All results are generated using the algorithm in Appendix D.4. Sufficient statistics for investment allocation are computed from the counterfactual outputs of Section 6, following the procedure in Appendix D.6. Color scales are truncated at the 1st and 99th percentiles.

shares are then constructed in proportion to each port’s welfare elasticity (Figure E.6a). As in the global analysis, future climate conditions modify the relative ranking of ports (Figure E.6b): welfare gains from additional port capacity decline by 2% at the 5th percentile and rise by 3% at the 95th percentile.

The second step is to translate the aggregate investment amount into port capacity changes. To do so, I use data on port investments collected by the World Bank in low- and middle-income countries (LMICs) and study the resulting increases in port capacity at the recipient ports (World Bank, 2025). The dataset is described in Appendix B.5. In a staggered difference-in-differences design (Appendix E.5.1), I estimate that USD 1 billion of investment increases port capacity by 3,649 TEU-days on average – equivalent to a 27% increase in unconditional port capacity in LMICs. This elasticity is used to translate the allocated investments into implied capacity expansions for EU27 ports.

Finally, I compare two counterfactuals in which the same USD 93 billion is distributed across 110 EU27 ports according to (i) the first-order allocation rule computed under baseline climate conditions (myopic), and (ii) the same rule computed under

the RCP8.5 scenario (climate-aware). The misallocation metric indicates that ignoring future climate conditions would misallocate 0.5% of total EU27 port investment, resulting in aggregate welfare losses of -0.04 basis points (Figure 10a). Nearly all EU27 ports experience a decline in traffic (Figure 10b), with total EU port traffic falling by 1.6%. These findings highlight that future climate conditions can meaningfully reshape the spatial pattern of welfare-improving investments. Incorporating climate-adjusted welfare improvements into investment planning is therefore essential for ensuring that long-term infrastructure policy remains both efficient and resilient.

8 CONCLUSION

This paper investigates the impacts of climate-induced disruptions on global supply chains, focusing on the role of disruptions to maritime transportation infrastructure. Leveraging high-frequency data on firm-to-firm shipments and detailed cyclone activity, I provide empirical evidence on how extreme weather events affect port operations and reshape trade routes. My findings show that, while firm-to-firm relationships are only temporarily affected due to the mechanical effect of port shutdowns, routing decisions across transportation networks adapt significantly and dampen the trade disruptions induced by weather at ports.

I further develop a quantitative model of spatial production networks incorporating endogenous transportation costs and congestion spillovers, offering a framework to evaluate the broader economic implications of climate-induced transportation disruptions. The model reveals spatial and welfare implications of climate risks to trade infrastructure for global trade, emphasizing the critical role of private adaptive strategies in mitigating adverse effects.

Finally, I explore infrastructure policy in a context of climate change. Using a sufficient-statistics approach, I develop a method to evaluate welfare gains from port capacity improvements and show how they are affected by climate change at ports. Failing to account for future environmental damage can lead to a misallocation of port infrastructure investments.

These findings have clear policy relevance. Investments in climate-resilient transportation networks can not only reduce the direct costs of disruptions but also alleviate secondary congestion effects on unaffected regions. Policymakers should prioritize

adaptive strategies that account for dynamic firm behaviors, transportation network spillovers, and future climate at ports. While I only focus on maritime trade, future research could extend this analysis by incorporating additional modes of transport and leveraging the rich set of climate data currently available to study a wider array of extreme weather events, offering a more comprehensive picture of global supply chain vulnerability to climate risks affecting trade infrastructure.

REFERENCES

- T. Allen and C. Arkolakis. The Welfare Effects of Transportation Infrastructure Improvements. *The Review of Economic Studies*, 89(6):2911–2957, 2022. ISSN 0034-6527, 1467-937X. doi: 10.1093/restud/rdac001. URL <https://academic.oup.com/restud/article/89/6/2911/6519332>.
- T. Allen, S. Fuchs, and W. F. Wong. Evaluating Transportation Improvements Quantitatively: A Primer. *Working Paper*, 2025.
- G. Amatulli, S. Domisch, M.-N. Tuanmu, B. Parmentier, A. Ranipeta, J. Malczyk, and W. Jetz. A suite of global, cross-scale topographic variables for environmental and biodiversity modeling. *Scientific Data*, 5(1):180040, Mar. 2018. ISSN 2052-4463. doi: 10.1038/sdata.2018.40. URL <https://www.nature.com/articles/sdata201840>. Publisher: Nature Publishing Group.
- M. S. Arslanalp, M. R. Koepke, and J. Verschuur. Tracking Trade from Space: An Application to Pacific Island Countries. *IMF Working Papers*, Aug. 2021. URL <https://ideas.repec.org//p/imf/imfwpa/2021-225.html>. Number: 2021/225 Publisher: International Monetary Fund.
- C. Balboni. In Harm’s Way? Infrastructure Investments and the Persistence of Coastal Cities. *American Economic Review*, 115(1):77–116, Jan. 2025. ISSN 0002-8282. doi: 10.1257/aer.20191943. URL <https://www.aeaweb.org/articles?id=10.1257/aer.20191943>.
- C. Balboni, J. Boehm, and M. Waseem. Firm Adaptation in Production Networks: Evidence from Extreme Weather Events in Pakistan. 2024.

- J.-N. Barrot and J. Sauvagnat. Input Specificity and the Propagation of Idiosyncratic Shocks in Production Networks*. *The Quarterly Journal of Economics*, 131(3):1543–1592, Aug. 2016. ISSN 0033-5533, 1531-4650. doi: 10.1093/qje/qjw018. URL <https://academic.oup.com/qje/article/131/3/1543/2461213>.
- A. Bilal and E. Rossi-Hansberg. Anticipating Climate Change Across the United States, June 2023. URL <https://www.nber.org/papers/w31323>.
- J. Blaum, F. Esposito, and S. Heise. Input Sourcing under Supply Chain Risk:. *Working paper*, 2024.
- N. Bloemendaal, H. de Moel, S. Muis, I. D. Haigh, and J. C. J. H. Aerts. Estimation of global tropical cyclone wind speed probabilities using the STORM dataset. *Scientific Data*, 7(1):377, Nov. 2020a. ISSN 2052-4463. doi: 10.1038/s41597-020-00720-x. URL <https://www.nature.com/articles/s41597-020-00720-x>. Publisher: Nature Publishing Group.
- N. Bloemendaal, I. D. Haigh, H. de Moel, S. Muis, R. J. Haarsma, and J. C. J. H. Aerts. Generation of a global synthetic tropical cyclone hazard dataset using STORM. *Scientific Data*, 7(1):40, Feb. 2020b. ISSN 2052-4463. doi: 10.1038/s41597-020-0381-2. URL <https://www.nature.com/articles/s41597-020-0381-2>. Publisher: Nature Publishing Group.
- C. E. Boehm, A. Flaaen, and N. Pandalai-Nayar. Input Linkages and the Transmission of Shocks: Firm-Level Evidence from the 2011 Tōhoku Earthquake. *The Review of Economics and Statistics*, 101(1):60–75, Mar. 2019. ISSN 0034-6535. doi: 10.1162/rest_a_00750. URL https://doi.org/10.1162/rest_a_00750.
- K. Borusyak, X. Jaravel, and J. Spiess. Revisiting Event-Study Designs: Robust and Efficient Estimation. *Review of Economic Studies*, 91(6):3253–3285, Nov. 2024. ISSN 0034-6527, 1467-937X. doi: 10.1093/restud/rdae007. URL <https://academic.oup.com/restud/article/91/6/3253/7601390>.
- G. Brancaccio, M. Kalouptsidi, and T. Papageorgiou. Geography, Transportation, and Endogenous Trade Costs. *Econometrica*, 88(2):657–691, 2020. ISSN 1468-0262. doi: 10.3982/ECTA15455. URL <https://doi.org/10.3982/ECTA15455>.

//onlinelibrary.wiley.com/doi/abs/10.3982/ECTA15455. eprint:
<https://onlinelibrary.wiley.com/doi/pdf/10.3982/ECTA15455>.

G. Brancaccio, M. Kalouptsidi, and T. Papageorgiou. Investment in Infrastructure and Trade: The Case of Ports, May 2024. URL <https://papers.ssrn.com/abstract=4843062>.

V. M. Carvalho, M. Nirei, Y. U. Saito, and A. Tahbaz-Salehi. Supply Chain Disruptions: Evidence from the Great East Japan Earthquake*. *The Quarterly Journal of Economics*, 136(2):1255–1321, May 2021. ISSN 0033-5533. doi: 10.1093/qje/qjaa044. URL <https://doi.org/10.1093/qje/qjaa044>.

J. Castro-Vincenzi. Climate Hazards and Resilience in the Global Car Industry. 2024.

J. Castro-Vincenzi, G. Khanna, N. Morales, and N. Pandalai-Nayar. Weathering the Storm: Supply Chains and Climate Risk, Mar. 2024. URL <https://www.nber.org/papers/w32218>.

D. Cengiz, A. Dube, A. Lindner, and B. Zipperer. The Effect of Minimum Wages on Low-Wage Jobs*. *The Quarterly Journal of Economics*, 134(3):1405–1454, Aug. 2019. ISSN 0033-5533. doi: 10.1093/qje/qjz014. URL <https://doi.org/10.1093/qje/qjz014>.

K. Chen. A Computation Method for Typhoon Wind Field. *Tropic Oceanology*, 13(2): 41–48, 1994.

W. Chen, J. Fan, and W. Luo. Trade and Technology Compatibility in General Equilibrium. *SSRN Electronic Journal*, 2023. ISSN 1556-5068. doi: 10.2139/ssrn.4647210. URL <https://www.ssrn.com/abstract=4647210>.

D. P. Clark, V. Kozlova, and G. Schaur. Supply Chain Uncertainty in Ocean Transit as a Trade Barrier. 2024.

J.-L. Cruz and E. Rossi-Hansberg. The Economic Geography of Global Warming. *Review of Economic Studies*, 91(2):899–939, Mar. 2024. ISSN 0034-6527, 1467-937X. doi: 10.1093/restud/rdad042. URL <https://academic.oup.com/restud/article/91/2/899/7107009>.

- M. Deshpande and Y. Li. Who Is Screened Out? Application Costs and the Targeting of Disability Programs. *American Economic Journal: Economic Policy*, 11(4):213–248, Nov. 2019. ISSN 1945-7731, 1945-774X. doi: 10.1257/pol.20180076. URL <https://pubs.aeaweb.org/doi/10.1257/pol.20180076>.
- K. Desmet and E. Rossi-Hansberg. On the spatial economic impact of global warming. *Journal of Urban Economics*, 88:16–37, July 2015. ISSN 00941190. doi: 10.1016/j.jue.2015.04.004. URL <https://linkinghub.elsevier.com/retrieve/pii/S0094119015000339>.
- K. Desmet, R. E. Kopp, S. A. Kulp, D. K. Nagy, M. Oppenheimer, E. Rossi-Hansberg, and B. H. Strauss. Evaluating the Economic Cost of Coastal Flooding. *American Economic Journal: Macroeconomics*, 13(2):444–486, Apr. 2021. ISSN 1945-7707, 1945-7715. doi: 10.1257/mac.20180366. URL <https://pubs.aeaweb.org/doi/10.1257/mac.20180366>.
- A. Dube, D. Girardi, Jordà, and A. M. Taylor. A Local Projections Approach to Difference-in-Differences, 2023. URL <https://www.nber.org/papers/w31184>.
- C. Ducruet, R. Juhász, D. K. Nagy, and C. Steinwender. All aboard: The effects of port development. *Journal of International Economics*, 151:103963, Sept. 2024. ISSN 0022-1996. doi: 10.1016/j.inteco.2024.103963. URL <https://www.sciencedirect.com/science/article/pii/S0022199624000904>.
- ESPO. Port Investment Study 2024: The Investment Pipeline and Challenges of European Ports. Technical report, 2024. URL <https://www.espo.be/media/ESPOPortInvestmentsStudy2024.pdf>.
- P. D. Fajgelbaum and E. Schaal. Optimal Transport Networks in Spatial Equilibrium. *Econometrica*, 88(4):1411–1452, 2020. ISSN 1468-0262. doi: 10.3982/ECTA15213. URL <https://onlinelibrary.wiley.com/doi/abs/10.3982/ECTA15213>. eprint: <https://onlinelibrary.wiley.com/doi/pdf/10.3982/ECTA15213>.
- D. J. Flynn. Mariner’s Tropical Cyclone Guide. *National Weather Service*, 2023.

- R. W. Fogel. A Quantitative Approach to the Study of Railroads in American Economic Growth: A Report of Some Preliminary Findings. *The Journal of Economic History*, 22(2):163–197, June 1962. ISSN 1471-6372, 0022-0507. doi: 10.1017/S0022050700062719. URL <https://www.cambridge.org/core/journals/journal-of-economic-history/article/abs/quantitative-approach-to-the-study-of-railroads-in-american-economic-growth>.
- S. Fuchs and W. F. Wong. Multimodal Transport Networks. *SSRN Electronic Journal*, 2024. ISSN 1556-5068. doi: 10.2139/ssrn.4991910. URL <https://www.ssrn.com/abstract=4991910>.
- S. Ganapati, W. F. Wong, and O. Ziv. Entrepôt: Hubs, Scale, and Trade Costs. *American Economic Journal: Macroeconomics*, 16(4):239–278, 2024. ISSN 1945-7707. doi: 10.1257/mac.20220250. URL <https://www.aeaweb.org/articles?id=10.1257/mac.20220250>.
- S. M. Hsiang and A. S. Jina. The Causal Effect of Environmental Catastrophe on Long-Run Economic Growth: Evidence From 6,700 Cyclones, July 2014. URL <https://www.nber.org/papers/w20352>.
- IELab. Global Resource Input-Output Assessment, 2025. URL <https://ielab.info/labs/ielab-gloria>.
- K. Klein Goldewijk. History Database of the Global Environment 3.3, Mar. 2024. URL <https://public.yoda.uu.nl/geo/UU01/94FNH0.html>. Publisher: Utrecht University.
- K. R. Knapp, M. C. Kruk, D. H. Levinson, H. J. Diamond, and C. J. Neumann. The International Best Track Archive for Climate Stewardship (IBTrACS). Mar. 2010. doi: 10.1175/2009BAMS2755.1. URL https://journals.ametsoc.org/view/journals/bams/91/3/2009bams2755_1.xml. Section: Bulletin of the American Meteorological Society.
- J. Ksciuk, S. Kuhlemann, K. Tierney, and A. Koberstein. Uncertainty in maritime ship routing and scheduling: A Literature review. *European Journal of Operational Research*, 308(2):499–524, July 2023. ISSN 0377-2217. doi: 10.1016/j.ejor.2022.

- 08.006. URL <https://www.sciencedirect.com/science/article/pii/S037722172200649X>.
- X. Li, Y. Zhou, M. Zhao, and X. Zhao. A harmonized global nighttime light dataset 1992–2018. *Scientific Data*, 7(1):168, June 2020. ISSN 2052-4463. doi: 10.1038/s41597-020-0510-y. URL <https://www.nature.com/articles/s41597-020-0510-y>. Publisher: Nature Publishing Group.
- A. Martinez. Trade Relationships During and After a Crisis: Evidence from Road Disruptions in Colombian Flower Exports. *Working Paper*, 2024.
- E. Oberfield. A Theory of Input–Output Architecture. *Econometrica*, 86(2):559–589, 2018. ISSN 1468-0262. doi: 10.3982/ECTA10731. URL <https://onlinelibrary.wiley.com/doi/abs/10.3982/ECTA10731>. eprint: <https://onlinelibrary.wiley.com/doi/pdf/10.3982/ECTA10731>.
- N. M. C. Pankratz and C. Schiller. Climate Change and Adaptation in Global Supply-Chain Networks, June 2021. URL <https://papers.ssrn.com/abstract=3475416>.
- A. Rabano and J. N. Rosas. The Transmission of Climate Shocks: The Case of Floods in India. *Working Paper*, 2024.
- S. J. Redding and M. A. Turner. Chapter 20 - Transportation Costs and the Spatial Organization of Economic Activity. In G. Duranton, J. V. Henderson, and W. C. Strange, editors, *Handbook of Regional and Urban Economics*, volume 5 of *Handbook of Regional and Urban Economics*, pages 1339–1398. Elsevier, Jan. 2015. doi: 10.1016/B978-0-444-59531-7.00020-X. URL <https://www.sciencedirect.com/science/article/pii/B978044459531700020X>.
- E. Rossi-Hansberg and J. Zhang. Local GDP Estimates Around the World, Feb. 2025. URL <https://www.nber.org/papers/w33458>.
- I. Rudik, G. Lyn, W. Tan, and A. Ortiz-Bobea. The Economic Effects of Climate Change in Dynamic Spatial Equilibrium, June 2021. URL https://osf.io/usghb_v1.
- J. Verschuur, E. E. Koks, and J. W. Hall. Port disruptions due to natural disasters: Insights into port and logistics resilience. *Transportation Research Part D: Transport*

and Environment, 85:102393, Aug. 2020. ISSN 1361-9209. doi: 10.1016/j.trd.2020.102393. URL <https://www.sciencedirect.com/science/article/pii/S1361920920305800>.

J. Verschuur, E. E. Koks, and J. W. Hall. Systemic risks from climate-related disruptions at ports. *Nature Climate Change*, 13(8):804–806, Aug. 2023a. ISSN 1758-6798. doi: 10.1038/s41558-023-01754-w. URL <https://www.nature.com/articles/s41558-023-01754-w>. Publisher: Nature Publishing Group.

J. Verschuur, E. E. Koks, S. Li, and J. W. Hall. Multi-hazard risk to global port infrastructure and resulting trade and logistics losses. *Communications Earth & Environment*, 4(1):1–12, Jan. 2023b. ISSN 2662-4435. doi: 10.1038/s43247-022-00656-7. URL <https://www.nature.com/articles/s43247-022-00656-7>. Publisher: Nature Publishing Group.

H. E. Willoughby, R. W. R. Darling, and M. E. Rahn. Parametric Representation of the Primary Hurricane Vortex. Part II: A New Family of Sectionally Continuous Profiles. Apr. 2006. doi: 10.1175/MWR3106.1. URL <https://journals.ametsoc.org/view/journals/mwre/134/4/mwr3106.1.xml>. Section: Monthly Weather Review.

C. Wing, S. M. Freedman, and A. Hollingsworth. Stacked Difference-in-Differences, Jan. 2024. URL <https://www.nber.org/papers/w32054>.

W. F. Wong and S. Fuchs. Multimodal Transport Networks, Oct. 2022. URL <https://papers.ssrn.com/abstract=4277194>.

World Bank. Data on Private Participation in Infrastructure (PPI) - World Bank Group, 2025. URL <https://ppi.worldbank.org/en/ppidata>.

Appendix

A ANECDOTAL EVIDENCE

 **Marine Safety Information Bulletin** 

Commander
U.S. Coast Guard
Sector Key West
100 Trumbo Road
Key West, FL 33040-6655

MSIB Number: SKW-28-24
Date: Oct 7, 2024
Contact: LT Hailie Wilson
Phone: (305) 292-8768
Email: SKWWaterways@uscg.mil

U.S. COAST GUARD SECTOR KEY WEST PORT CONDITION ZULU

On October 8, 2024, at 0600 (6:00 AM), the Captain of the Port will set Port Condition (PORTCON) **ZULU** for the Port of Key West. The shift is based on the projected arrival of sustained gale force winds (greater than 34 knots/39mph) associated with Hurricane Milton. The table below summarizes COTP requirements for PORTCON Zulu in accordance with 33 CFR 165.707:

Hours Prior to Gales	Port Condition	Requirements (annotated from 33 CFR 165.707)
72	Whiskey	<ul style="list-style-type: none">Oceangoing vessels greater than 300 gross tons (GT) must make plans to depart no later than the setting of Port Condition Yankee unless authorized by the COTP. Vessels intending to remain in port must contact the COTP prior to setting PORTCON X-Ray.
48	X-Ray	<ul style="list-style-type: none">Vessels greater than 300 GT without an approval to remain in port must depart prior to the setting of PORTCON Yankee.All vessels, regulated facilities, and waterfront facilities must ensure that potential flying debris is removed or secured. HAZMAT/pollution hazards must be secured in a safe manner away from waterfront areas.
24	Yankee	<ul style="list-style-type: none">The port is closed to all inbound vessel traffic. All vessels greater than 300 GT must have departed the port, unless authorized by the COTP.
12	Zulu	<ul style="list-style-type: none">The port is closed to all vessel traffic except as specifically authorized by the COTP.Regulated facilities must cease all cargo operations, including bunkering and lightering.
After Storm's Passage	Four (All Clear)	<ul style="list-style-type: none">The port will be re-opened only after satisfactory assessments of the waterways, including critical aids to navigation verifications, have been conducted.

Mariners should be aware that no “safe havens” exist within the Florida Keys for vessels to safely survive hurricane force winds or storm surges without creating a threat to the safety of the port and public welfare. Owners/operators of vessels greater than 300 GT desiring to remain in port throughout hurricane season who have not already submitted heavy weather plans to the COTP for review should be prepared to depart no later than the setting of PORTCON Yankee. *Remain in Port Checklists* are available for review on the Sector Key West HOMEPAGE website: <https://homeport.uscg.mil/port-directory/key-west>. Regulated facilities are reminded to review and update their heavy weather response plans to safely weather any storm that may approach the Florida Keys.

Mariners navigating through the Islamorada Snake Creek Draw Bridge are reminded that the bridge may not operate on normally published schedules as early as 36 hours prior to forecasted storm’s arrival. The bridge will not open for maritime traffic upon arrival of gale force winds (34 knots or higher) or following a mandatory Monroe County evacuation order.

The official PORTCON and associated Marine Safety Information Bulletin (MSIB) will be set on Sector Key West’s Homeport website. As weather conditions may change rapidly, mariners are encouraged to monitor the National Weather Service’s forecasts and observations at <https://www.weather.gov/key> or on NOAA weather radios. For questions or additional information, call Coast Guard Sector Key West at (305) 292-8727 or email SKW@uscg.mil.

Sincerely,



J. D. INGRAM
Captain, U. S. Coast Guard
Captain of the Port

This Marine Safety Information Bulletin has been issued for public information and notification purposes.

Figure A.1: Example of port condition ZULU (US)

Notes: This document is the Marine Safety Information Bulletin issued on October 8, 2024, by the US Coast Guards of Port Key West (Florida), before the landfall of Hurricane Milton.

B DATA

In this appendix, I report all the data sources, and provide extensive details about data contents, manipulation, and summary statistics. Table B.1 provides a summary of all data used in the analysis.

Table B.1: Data sources and time coverage

Data type/variable	Time coverage	Source
Bills of lading (Brazil)	2014–2023	S&P Panjiva
Global port-level traffic	2019–2023	IMF PortWatch
Port capacity	2019–2023	IMF PortWatch
Tropical cyclone tracks	2014–2023	IBTrACS (Knapp et al., 2010)
Tropical cyclone climate	1980–2015/2025–2050	STORM (Bloemendaal et al., 2020a,b)
Regions	-	GAUL1
Distances (land)	-	Great-circle distance
Distances (sea)	-	Eurostat SeaRoute
Population	2012–2020	Rossi-Hansberg and Zhang (2025)
GDP per capita (2017 PPP)	2012–2020	Rossi-Hansberg and Zhang (2025)
Nightlights	2015	Li et al. (2020)
Historical population	1950	HYDE 3.3 (Klein Goldewijk, 2024)
Terrain Ruggedness Index	-	Amatulli et al. (2018)
PPI Wold Bank Port Investments	2019–2023	World Bank (2025)

Notes: This table reports all the data sources used in the analysis, by data type/variable. Appendices B.1 to B.5 provide additional information.

B.1 BILL OF LADING DATA – BRAZIL (2014–2023)

Source and coverage. I use firm-to-firm bills of lading assembled by S&P Panjiva for all maritime import transactions recorded as entering a Brazilian port between June 2014 and December 2023. The raw data contains shipment identifiers (`panjivaRecordId`), the date the shipment entered the first domestic port (`shpmtDate`), company names for the consignee/importer and shipper/exporter (`conName`, `shpName`), party address fields (street, city, state/region, postal code, country), party type (`shpType`, `conType`: *Real Cargo Owner* vs. *NVO/Forwarder*), maritime ports of lading/origin and unlading/destination (names and UNLOCODEs), transport mode, indicators for containerization, and physical/value measures (TEU volume, gross weight in kg, USD value).⁵³ The empirical analysis focuses on maritime shipments only; if non-maritime records are present in the extract, they are dropped.

Defining geocoded establishments (firms). Empty strings in Panjiva address fields are treated

⁵³The data also contains Panjiva-assigned establishment identifiers for the consignee and shipper (`conPanjivaId`, `shpPanjivaId`), but these are prone to errors. E.g., small variations in street names can lead to wrongly-assigned separate establishment identifiers. I address this issue by constructing new establishment identifiers, based on (cleaned) company names and addresses.

as missing. For both sides of the transaction I build full-address tokens by concatenating the available street, city, state/region, postal code, and country fields. These tokens are used for geocoding and as intermediate keys to define establishments. Company names are standardized prior to consolidation: I transliterate non-Latin scripts to Latin and then to ASCII, harmonize special characters, and remove legal-form affixes using a comprehensive cross-walk of entity-type abbreviations. The resulting sanitized parent names are then passed through a generic string-cleaning routine.

I geocode the full addresses via the ArcGIS service (through `tidygeocoder`). Minimum information for geolocalization is a city or postal code; street addresses are not required. I define a *firm* as the set of co-located establishments belonging to the same (cleaned) parent name. Concretely, within each parent, I cluster all geocoded points using single-linkage hierarchical clustering with a 10km cutoff and assign a unique establishment identifier to each cluster (constructed from the parent name and the cluster centroid). I then overlay cluster centroids onto GAUL1 polygons to assign a unique GAUL1 location identifier to each buyer and supplier. Observations without a city/postal code or without a successful GAUL1 assignment are excluded.

Defining geocoded ports. I parse Panjiva’s port names and countries, normalize them via the same transliteration/ASCII pipeline used for firm names, and remove unknown UNLOCODEs. For a limited set of ports with commonly used variants, I apply targeted name corrections (e.g., major Ukrainian, Chinese, and North African ports). I then construct port address strings (UNLOCODE, cleaned name, country) and geocode them via ArcGIS to obtain coordinates. When multiple geometries are observed under the same UNLOCODE, I retain only UNLOCODEs mapping to a single unique geometry. Finally, to facilitate linkage with global port-call data, I match cleaned port names within country to IMF PortWatch ports using fuzzy matching (Jaro–Winkler). I keep exact post-cleaning matches and store the PortWatch identifier for those ports.

Useful identifiers. I construct a set of unit identifiers used throughout the analysis. Let b denote a Brazilian buyer establishment and s a foreign supplier establishment. The buyer–supplier establishment pair is $\{b,s\}$. Each shipment lists a port of lading p_o and a port of unlading p_d , which define a sea route. The identifiers are:

- `BS.establishment.id`: buyer-supplier establishment pair;
- `route.id`: route (p_o, p_d) ;

- `BS.route.id`: buyer-supplier establishment pair \times route (p_o, p_d).

Calendar time is built from shipment dates by constructing a complete daily grid between the first and last observed shipment dates and then indexing months by their first day (`time.ym`). These normalized indices are merged back to shipments.

Aggregation and sample restrictions. I exclude records with missing parent party identifiers (`conPanjivaId` or `shpPanjivaId`), with poorly geocoded establishments, or transiting through poorly geocoded ports. I keep only shipments where (i) both parties are labeled as *Real Cargo Owner* (i.e., I exclude *NVO/Forwarder* on either side), and (ii) the buyer geocodes to Brazil and the supplier does not geocode to Brazil.

I build two main aggregated datasets, at the `BS.establishment.id` (relationship) level, and at the `BS.route.id` (relationship-route) level. For each relationship (relationship-route) identifier, I aggregate shipment quantities and values at the monthly level. I compute the sum of USD value, gross weight (kg), and TEU volume, the number of distinct shipments, and the number of containerized shipments. I finally drop infrequent relationships (relationship-routes), by keeping only `BS.establishment.id` (`BS.route.id`) identifiers that trade at least two months within the sample.

Table B.2 reports the effect of the data cleaning procedure on firm- and relationship-related variables. Table B.3 focuses on ports and routes. Table B.4 presents summary statistics on firm-to-firm trade when infrequent relationships are removed, while Table B.5 presents summary statistics on firm-to-firm trade when infrequent relationships or relationships-routes are removed.

Table B.2: Data Cleaning - Firms and Relationships

Desc.	Num. Shipments	Num. Importers	Num. Exporters	Num. Rel.
Full Sample				
(1) Raw Panjiva	9017154	44556	37973	185708
(2) Drop missing parent company ID	8950897	44509	37868	185355
(3) Drop poorly geolocalized firms	2205290	27136	31537	126811
(4) Drop poorly reported ports	2204392	27133	31526	126754
(5) Keep Brazilian imp., foreign exp.	2197635	26876	31027	125636
(6) Drop NVO/forwarders	1039012	17692	23291	73551
Estimation Sample				
(7) Drop infrequent rel.	994069	10787	13813	38665
(8) Drop infrequent rel.-routes	938570	9748	12500	33304

Note: This table reports the effect of the data cleaning procedure on firm-related variables. Firms refer to geolocalized establishments. "Num. Shipments" refers to the number of distinct shipments, as identified by the bill of lading ID. "Num. Importers" refers to the number of establishments importing goods. "Num. Exporters" refers to the number of establishments exporting goods. "Num. Rel." refers to the number of trading establishment pairs.

Table B.3: Data Cleaning - Maritime Ports and Routes

Desc.	Num. Exit Ports	Num. Entry Ports	Num. Routes	Num. Rel.-Routes
Full Sample				
(1) Raw Panjiva	1005	52	5877	576861
(2) Drop missing parent company ID	963	52	5430	572937
(3) Drop poorly geolocalized firms	483	44	2011	242377
(4) Drop poorly reported ports	474	43	1970	242005
(5) Keep Brazilian imp., foreign exp.	467	43	1950	240440
(6) Drop NVO/forwarders	442	42	1822	126684
Estimation Sample				
(7) Drop infrequent rel.	366	37	1493	91046
(8) Drop infrequent rel.-routes	247	35	1000	50932

Note: This table reports the effect of the data cleaning procedure on route-related variables. Routes refer to port of exit-port of entry pairs. "Num. Exit Ports" refers to the number of port of lading, as identified by the UN/LOCODE. "Num. Entry Ports" refers to the number of port of unlading, as identified by UN/LOCODE. "Num. Routes" refers to the number of observed port pairs. "Num. Rel.Routes" refers to the number of importer-exporter-route triplets.

Table B.4: Summary Statistics - Relationship Sample

Desc.	Mean	25%	50%	75%	90%	95%
Per Buyer - Month						
Num. transactions	6.20	1.00	2.00	4.00	10.00	19.00
Num. suppliers	1.71	1.00	1.00	2.00	3.00	4.00
Num. exit ports	1.73	1.00	1.00	2.00	3.00	5.00
Num. entry ports	1.13	1.00	1.00	1.00	1.00	2.00
Num. routes	1.78	1.00	1.00	2.00	3.00	5.00
Log weight (kg)	11.01	9.93	10.80	11.99	13.22	14.13
Log volume (TEU)	1.58	0.69	1.39	2.48	3.53	4.23
Log value (USD)	12.12	11.02	11.94	13.06	14.22	15.01
Per Supplier - Month						
Num. transactions	5.90	1.00	2.00	4.00	10.00	18.00
Num. buyers	1.63	1.00	1.00	1.00	3.00	4.00
Num. exit ports	1.34	1.00	1.00	1.00	2.00	3.00
Num. entry ports	1.28	1.00	1.00	1.00	2.00	3.00
Num. routes	1.55	1.00	1.00	2.00	3.00	4.00
Log weight (kg)	10.72	9.73	10.58	11.71	12.94	13.81
Log volume (TEU)	1.48	0.69	1.39	2.30	3.37	4.06
Log value (USD)	12.15	11.06	12.00	13.11	14.27	15.07
Per Relationship - Month						
Num. transactions	3.62	1.00	1.00	2.00	5.00	10.00
Num. exit ports	1.15	1.00	1.00	1.00	2.00	2.00
Num. entry ports	1.04	1.00	1.00	1.00	1.00	1.00
Num. routes	1.18	1.00	1.00	1.00	2.00	2.00
Log weight (kg)	10.57	9.77	10.34	11.46	12.55	13.34
Log volume (TEU)	1.23	0.69	0.69	1.95	2.94	3.58
Log value (USD)	11.79	10.85	11.63	12.61	13.68	14.42

Note: The table reports summary statistics of the relationship sample. "Num. Shipments" refers to the number of distinct shipments, as identified by the bill of lading ID. "Num. exit ports" refers to the number of ports of exit, as identified by the UN/LOCODE. "Num. entry ports" refers to the number of ports of entry, as identified by the UN/LOCODE. "Num. routes" refers to the number of pairs or ports of exit and entry. "Log weight (kg)" refers to the total weight of shipments, in kilograms. "Log volume (TEU)" refers to the total volume of shipments, in Twenty-foot Equivalent Units. "Log value (USD)" refers to the total value of shipments, in current USD.

Table B.5: Summary Statistics - Relationship-Route Sample

Desc.	Mean	25%	50%	75%	90%	95%
Per Buyer - Month						
Num. shipments	6.46	1.00	2.00	4.00	11.00	20.00
Num. suppliers	1.69	1.00	1.00	2.00	3.00	4.00
Num. exit ports	1.68	1.00	1.00	2.00	3.00	4.00
Num. entry ports	1.10	1.00	1.00	1.00	1.00	2.00
Num. routes	1.71	1.00	1.00	2.00	3.00	5.00
Log weight (kg)	11.02	9.93	10.81	12.00	13.22	14.10
Log volume (TEU)	1.61	0.69	1.39	2.48	3.53	4.26
Log value (USD)	12.13	11.02	11.96	13.07	14.24	15.04
Per Supplier - Month						
Num. shipments	6.11	1.00	2.00	4.00	10.00	18.00
Num. buyers	1.60	1.00	1.00	1.00	3.00	4.00
Num. exit ports	1.29	1.00	1.00	1.00	2.00	3.00
Num. entry ports	1.25	1.00	1.00	1.00	2.00	3.00
Num. routes	1.49	1.00	1.00	1.00	2.00	3.00
Log weight (kg)	10.72	9.73	10.59	11.72	12.94	13.80
Log volume (TEU)	1.50	0.69	1.39	2.30	3.40	4.09
Log value (USD)	12.16	11.07	12.01	13.13	14.29	15.09
Per Relationship - Month						
Num. shipments	3.82	1.00	1.00	3.00	6.00	10.00
Num. exit ports	1.14	1.00	1.00	1.00	1.00	2.00
Num. entry ports	1.03	1.00	1.00	1.00	1.00	1.00
Num. routes	1.15	1.00	1.00	1.00	2.00	2.00
Log weight (kg)	10.57	9.76	10.37	11.48	12.56	13.33
Log volume (TEU)	1.26	0.69	1.10	2.08	3.00	3.64
Log value (USD)	11.81	10.85	11.64	12.64	13.72	14.47

Note: The table reports summary statistics of the relationship-route sample. It contains only treated relationships. "Num. Shipments" refers to the number of distinct shipments, as identified by the bill of lading ID. "Num. exit ports" refers to the number of ports of exit, as identified by the UN/LOCODE. "Num. entry ports" refers to the number of ports of entry, as identified by the UN/LOCODE. "Num. routes" refers to the number of pairs or ports of exit and entry. "Log weight (kg)" refers to the total weight of shipments, in kilograms. "Log volume (TEU)" refers to the total volume of shipments, in Twenty-foot Equivalent Units. "Log value (USD)" refers to the total value of shipments, in current USD.

B.2 GLOBAL PORT-LEVEL TRAFFIC (2019–2023)

Source and coverage. I use the IMF PortWatch daily data on port activity and estimated trade flows for 1,666 global ports from 2019 to 2023. The data reports, at a daily \times port level, counts of port calls and estimated import/export trade flows (in metric tons) disaggregated by ship type (container, dry bulk, general cargo, tanker, and ro-ro).⁵⁴ These indicators are derived from raw AIS traces processed by the PortWatch team following the methodology in Arslanalp et al. (2021).⁵⁵ I link PortWatch ports to the Panjiva port universe using the fuzzy name matching described in Appendix B.1, which yields a stable mapping between PortWatch port IDs and UNLOCODEs. To avoid ambiguous joins, I retain only PortWatch IDs that map to a single UNLOCODE. The resulting linked sample contains 621 ports that can be used jointly with the Brazilian bill-of-lading data.

Construction of daily traffic measures. For each port-day (p,t), I compute (i) total vessel calls, (ii) container vessel calls, (iii) total traffic in TEU, and (iv) container traffic in TEU. To construct daily total vessel calls, I sum the PortWatch port-call counts across all ship types. To construct TEU traffic estimates, I sum import/export series across all ship types within port-day and rescale it by a factor of 1/10 so that the stored variables represent average TEU units.⁵⁶ Container vessel calls and TEU traffic estimates are constructed using the same logic, although they only account for container ships, and containerized import/export weights.

Unless noted, I use *total* daily TEU as the proxy for port traffic; container-specific TEU and vessel-call measures are used for robustness and by-ship-type checks. When higher-frequency noise is undesirable, I aggregate these series to the relevant time unit (e.g., week) by summation, as indicated in the empirical design.

Port capacity. I measure port capacity from PortWatch daily TEU flows. For each port, I compute the 99th percentile of daily total TEU (imports + exports) over 2019–2023, and I use this as the capacity proxy K_p . Unless noted, I use a normalized capacity measure (capacity divided by the global maximum).

⁵⁴Container ships carry standardized containers, mostly containing manufactured goods. Dry bulk carriers transport unpackaged commodities such as coal, iron ore, and grain in large holds. General cargo vessels move breakbulk items – often on pallets or in crates – using multipurpose ships with their own gear. Tankers carry liquid bulk – crude oil, refined products, chemicals, or liquefied gases – in segregated tanks. Ro-ro ships carry wheeled cargo such as cars and trucks that roll on and off via ramps.

⁵⁵Downloaded from [IMF PortWatch](#). Estimates are based on AIS data via the United Nations Global Platform; see Arslanalp et al. (2021) for details.

⁵⁶Twenty-foot equivalent units carry on average 10 tons of goods.

B.3 TROPICAL CYCLONE TRACKS (2014–2023)

Source and coverage. I use the International Best Track Archive for Climate Stewardship (IB-TrACS) global archive ([Knapp et al., 2010](#)). IBTrACS provides a harmonized record of tropical cyclones with 3-hourly observations and $\approx 0.1^\circ$ track coordinates. I extract all storms observed between 2014 and 2023 within 200km of global coastlines (measured by the distance between the coast, and the eye of the cyclone). The analysis centers on cyclones that affect ports. Operationally, I evaluate wind exposure at geocoded ports that export to Brazil (Appendix [B.1](#)) and retain, for 2014–2023, the set of storms whose modeled wind fields intersect at least one port. For descriptive figures (e.g., Figure [2a](#)), I display cyclone footprints within 200km of global coastlines to emphasize coastal exposure.

Wind fields and exposure surfaces. I use the `StormR` package to handle tropical cyclone tracks data. For each storm I compute gridded surfaces of (i) maximum sustained wind (MSW) and (ii) an exposure index conditional on winds exceeding 18m/s (hours of exposure). The 18m/s threshold (≈ 35 knots) aligns closely with the 34-knot operational threshold commonly used for port closure conditions (e.g., condition ZULU in the US).

Port-level extraction and variables. For each port–storm pair, I extract cell means at the port’s coordinates from the MSW and exposure rasters, yielding (i) the port’s expected sustained wind in m/s and (ii) the storm-specific exposure index above 18m/s. I also record the first observed timestamp of the storm, which serves as the shock time for this event to avoid anticipation from port authorities/firms. Ports with missing raster values are set to zero exposure for that storm.

Port-level shocks. The resulting dataset at the port \times storm level is later merged to the Port-Watch port data (Appendix [B.2](#)) at the daily level, and to the bill of lading data (Appendix [B.1](#)) at the monthly level. These joins yield the port-level treatment indicators used in the empirical analysis.

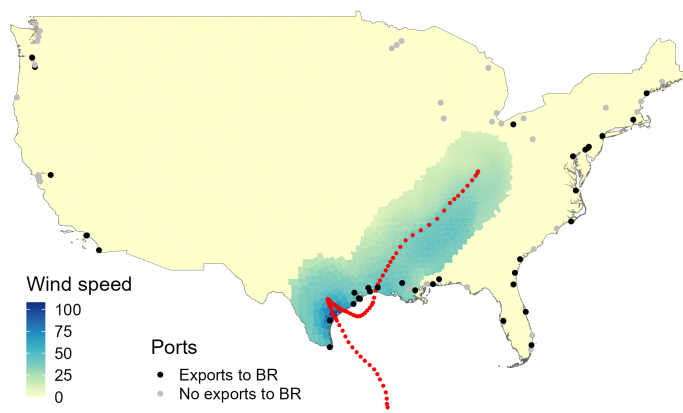


Figure B.1: Wind speed profile of hurricane Harvey

Notes: This map shows the maximum sustained wind speed experienced by US counties during Hurricane Harvey (23 August to 02 September 2017). The red dots represent the eye of the hurricane across its lifespan (IBTrACS). Wind speed is modeled using the method of [Willoughby et al. \(2006\)](#), adjusted for asymmetry using [Chen \(1994\)](#). Black dots indicate US ports that export to Brazil in the Brazilian bill of lading data. Grey dots represent US ports that do not export to Brazil.

Table B.6: Summary Statistics - Tropical Cyclones at Ports

Desc.	Mean	10%	25%	50%	75%	90%
(a) Panjiva sample						
Per Tropical Cyclone Event						
Num. ports of lading	7.17	1.00	1.00	4.00	10.00	17.00
Windspeed (m/s)	25.61	19.48	20.95	24.32	28.76	33.59
Exposure - 18m/s (hours)	10.94	4.60	6.55	9.32	13.56	19.63
Per Port - Year						
Num. cyclones	1.62	1.00	1.00	1.00	2.00	3.00
Windspeed (m/s)	26.77	19.51	21.76	25.26	30.04	36.05
Exposure - 18m/s (hours)	11.75	3.88	6.42	9.89	15.33	21.78
(b) Portwatch sample						
Per Tropical Cyclone Event						
Num. ports of lading	4.88	1.00	1.00	3.00	7.00	10.00
Windspeed (m/s)	26.37	19.55	20.74	25.23	29.75	34.60
Exposure - 18m/s (hours)	11.63	4.71	6.83	9.67	14.56	20.71
Per Port - Year						
Num. cyclones	1.61	1.00	1.00	1.00	2.00	3.00
Windspeed (m/s)	26.91	19.55	21.72	25.51	30.03	36.34
Exposure - 18m/s (hours)	11.87	4.00	7.08	9.90	15.33	21.57

Note: The table reports summary statistics for the exposure of ports to tropical cyclones. Panel (a) reports statistics for ports recorded in the Brazilian bill of lading data. Panel (b) reports statistics for ports recorded in IMF Portwatch data. "Per Tropical Cyclone Event: Num. ports of lading" refers to the number of ports exposed to at least 18m/s of wind speed, per cyclone event. "Per Tropical Cyclone Event: Windspeed (m/s)" refers to the mean maximum sustained wind speed experienced by ports, per cyclone event. "Per Tropical Cyclone Event: Exposure - 18m/s (hours)" refers to the mean exposure of ports, measured in hours of exposition to at least 18m/s of wind speeds, per cyclone event. "Per Port - Year: Num. cyclones" refers to the number of cyclones in which the port experiences at least 18m/s of maximum sustained wind speed, per port-year. "Per Port - Year: Windspeed (m/s)" refers to the mean maximum sustained wind speed from tropical cyclones experienced by ports, per port - year. "Per Port - Year: Exposure - 18m/s (hours)" refers to the mean exposure of ports during tropical cyclones, measured in hours of exposition to at least 18m/s of wind speeds, per port-year.

B.4 TROPICAL CYCLONES CLIMATE - STORM

Source and coverage. I use the STORM tropical cyclone hazard dataset (Bloemendaal et al., 2020a,b), which simulates 10,000 years of synthetic storm tracks to estimate wind hazards at $\approx 10\text{ km}$ resolution. In practice, I use the global-scale .tiff files derived by Russel (2022).⁵⁷ The data consists of gridded *fixed return period* rasters for (i) a present-day climate (1980–2015; hereafter *baseline*) and (ii) a future climate scenarios consistent with RCP8.5/SSP5 (2015–2050). The RCP8.5 scenarios correspond to the climate simulations of several climate models: CMCC-CM2-VHR4, CNRM-CM6-1-HR, EC-EARTH3P-HR, and HADGEM3-GC31-HM. For each scenario, STORM provides the maximum sustained wind speed (m/s) associated with a set of return periods $R = \{10, 20, \dots, 10,000\}$ years.

Defining expected wind speed. For each grid cell g and scenario s , I compute a simple expected (annual) windspeed proxy by weighting the return-period rasters by their annual probability:

$$\text{windspeed}_g^{(s)} = \sum_{r \in R} \frac{1}{r} V_{g,r}^{(s)},$$

where $V_{g,r}^{(s)}$ is the STORM raster of maximum sustained wind (m/s) for return period r . I implement this by dividing each raster by its return period and summing across $r \in R$; missing cells are treated as zeros. For display and merging, I spatially aggregate the resulting surface to $\approx 2^\circ$ resolution.

The baseline expected wind speed field $\text{windspeed}^{(0)}$ is built from the STORM “constant” (present-day) raster. The RCP8.5 expected wind speed field $\text{windspeed}^{(\text{RCP8.5})}$ is the mean of the climate models. I define the change in tropical cyclone climate as the grid-cell difference

$$\Delta \text{windspeed}_g = \text{windspeed}_g^{(\text{RCP8.5})} - \text{windspeed}_g^{(0)},$$

reported in (Figure 2b). Figures B.2a and B.2b report the respective baseline and RCP8.5 expected wind speed fields.

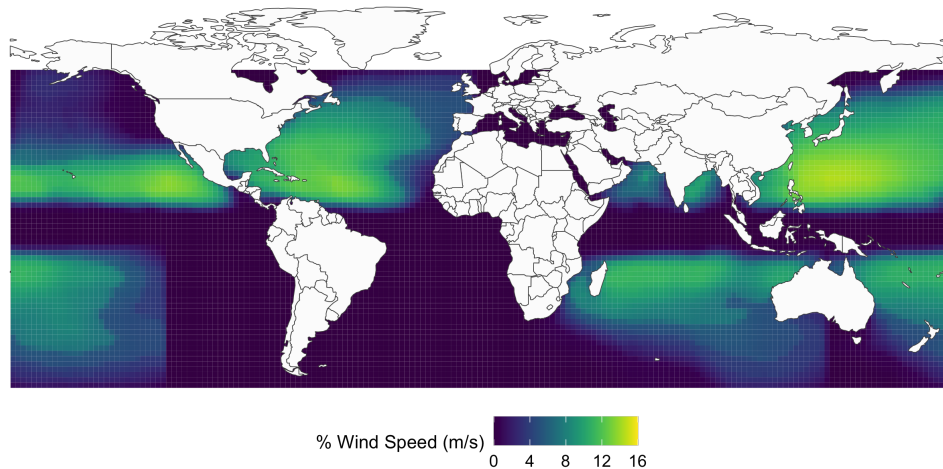
Port-level exposure (climate). To link climate hazards to ports, I buffer each port by 50km and extract the mean expected windspeed from the baseline and RCP8.5 rasters. I implement this both for the Panjiva-linked ports and for the IMF PortWatch global port set, yielding port-level measures of expected cyclone windspeed under baseline and future climates. Missing

⁵⁷The data is available [here](#).

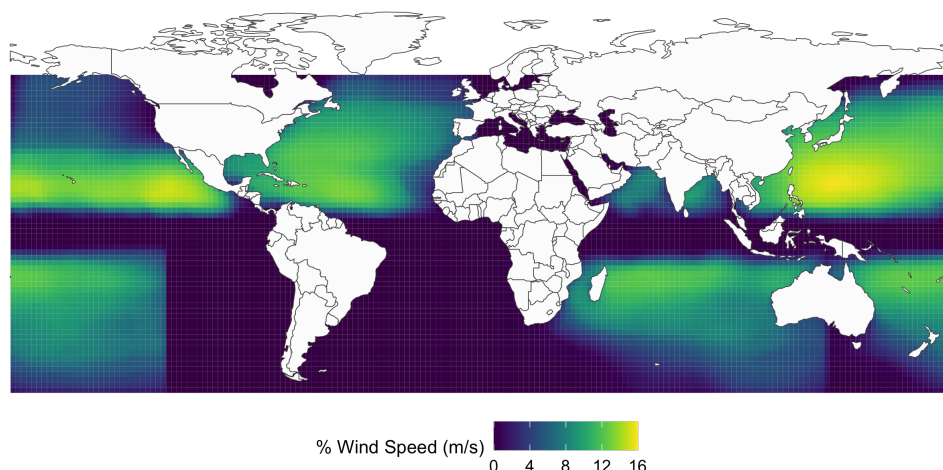
values in the baseline raster are set to zero before extraction; extraction uses area means over the buffer. The baseline and RCP8.5 expected wind speeds are treated as port fundamentals in both the estimation of transportation costs (Section 5.1), and the climate change counterfactuals (Section 5.2).

Figure B.2: Present and future (RCP8.5) tropical cyclone climates

(a) Present-day (1980-2015)



(b) RCP8.5 (2015-2050)



Notes: This map reports expected wind speeds (m/s) induced by tropical cyclones, in the present-day (Panel a) and the future RCP8.5 scenario (Panel b) of the STORM model.

B.5 ADDITIONAL DATA

Distances. Land route distances are approximated by great-circle distances between GAUL1 centroids. In the model calibration, I retain centroid distances only for contiguous region pairs identified via polygon contiguity (first-order neighbors). Shortest maritime distances between ports are computed with the Eurostat SeaRoute program; I build a directed port-to-port matrix with entries equal to the SeaRoute shortest-path length in kilometers, and zeros for unfeasible routes. I create a binary assignment matrix linking each port to the GAUL1 unit that contains it, and I record the (own) distance from the port to its region centroid. The full economy-wide distance matrix used in the model calibration stacks (i) the sparse region-to-region block, (ii) the port-to-region block (linking ports to their own region), and (iii) the maritime port-to-port block.

Population and GDP per capita (2012-2020). For fundamentals at the regional level, I use the global 1° grid from [Rossi-Hansberg and Zhang \(2025\)](#). I compute each GAUL1 unit's total population by rasterizing the gridded population field and summing over the polygon (averaging the raw population across 2012-2020). Regional GDP per capita is obtained as the population-weighted mean of the grid-cell GDP per capita (constant 2017 PPP, averaged across 2012-2020) over the GAUL1 polygon, using the population raster as weights; both population and GDP-per-capita aggregates are normalized by their global maxima for use in calibration and diagnostics.

Nightlights (2015). I use the data provided by [Li et al. \(2020\)](#). I aggregate the 2015 harmonized VIIRS nightlight raster to the GAUL1 polygons (sum of radiance), divide by regional population to obtain per-capita radiance, and normalize by the global maximum. These quantities are not used for calibration but provide an external check on the spatial allocation of activity.

Historical population (1950). To proxy historical coastal population at port, I use the HYDE 3.3 global gridded population for year 1950 at 5-arc-minute resolution ([Klein Goldewijk, 2024](#)). For each port p , I build a 100km radius buffer, and extract the sum of 1950 inhabitants within the buffer. I construct a share of 1950 coastal population by normalizing this count over total population around the 621 ports used in the estimation.

Terrain Ruggedness Index (TRI). To capture hinterland topography, I use the global Terrain Ruggedness Index based on GMTED at 30-arc-second resolution ([Amatulli et al., 2018](#)). For

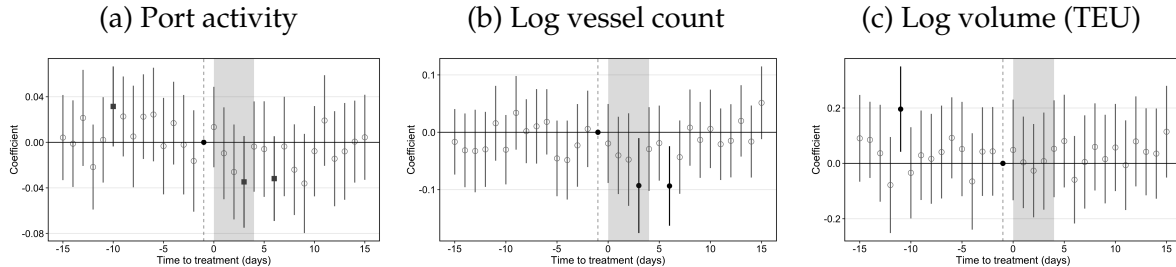
each port, I form a 20km radius buffer and extract the mean TRI over raster cells that fall within the buffer.

PPI World Bank - Ports (2019-2023). To recover a set of port investments, I use the World Bank PPI project data on port investments. I use all Ports projects from the World Bank's Private Participation in Infrastructure (PPI) database for 2019-2023 ([World Bank, 2025](#)). The data contains the port identifier, the investment year, and total committed investment (scaled in billions of USD) for all port infrastructure projects in which the World Bank participated. For ports with multiple projects in the same year, I sum investment amounts to obtain a port \times year aggregate. I manually assign PortWatch IDs to recipient ports, by port names.

C ROBUSTNESS AND ALTERNATIVE SPECIFICATIONS

C.1 PORT-LEVEL DISRUPTIONS

Figure C.1: Port exposure to weak cyclones



Notes: These panels plot the effect of exposure to tropical cyclones on daily port-level outcomes, as specified by Equation (1). The sample is constructed analogously to the one in Section 3.2, but treatment is defined as exposure to wind speed between 9 and 18 m/s (weak cyclones), removing any port treated by wind speed above 18 m/s. The outcome in Panel C.1a is a binary variable, taking value 1 if at least one vessel entered the port in period t (port activity), 0 otherwise. The outcome in Panel C.1b is the log number of vessels using the port in period t , conditioning on the port being active. The outcome of Panel C.1c is the log volume TEU transiting through the port in period t , conditioning on the port being active. Standard errors are clustered at the port level. The bars correspond to 95% confidence intervals. Black dots are point estimates significant at the 5% level, gray squares are point estimates significant at the 10% level, and empty dots are point estimates non-significant at the 10% level.

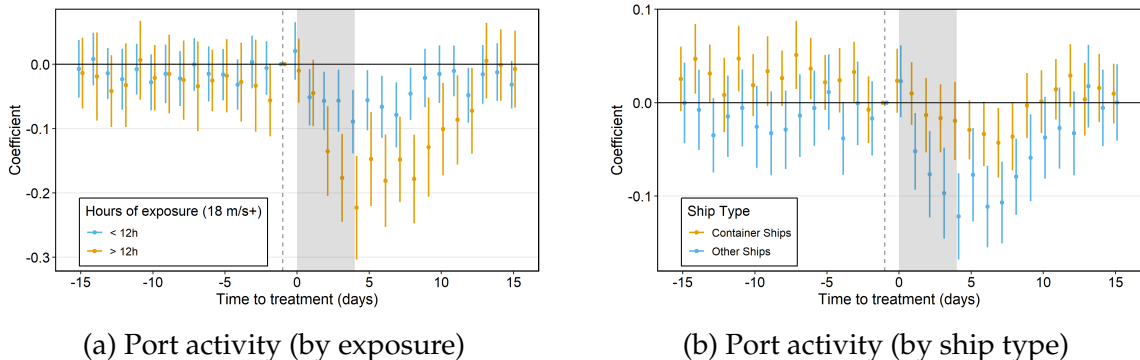


Figure C.2: The impact of exposure to cyclones on port operations

Notes: These panels plot the effect of exposure to tropical cyclones on daily port-level outcomes, as specified by Equation (1). The outcome of both panels is a binary variable, taking value 1 if at least one vessel entered the port in period t (port activity), 0 otherwise. In Panel C.2a, I estimate Equation (1) by splitting the treated group by the duration of exposure to at least 18 m/s: below and above 12 hours of exposure. In Panel C.2b, I estimate Equation (1) using port-ship-type-specific outcomes: containerized vs. other ships. Standard errors are clustered at the port level. The bars correspond to 95% confidence intervals. Black dots are point estimates significant at the 5% level, gray squares are point estimates significant at the 10% level, and empty dots are point estimates non-significant at the 10% level.

C.2 ROUTE CHOICE

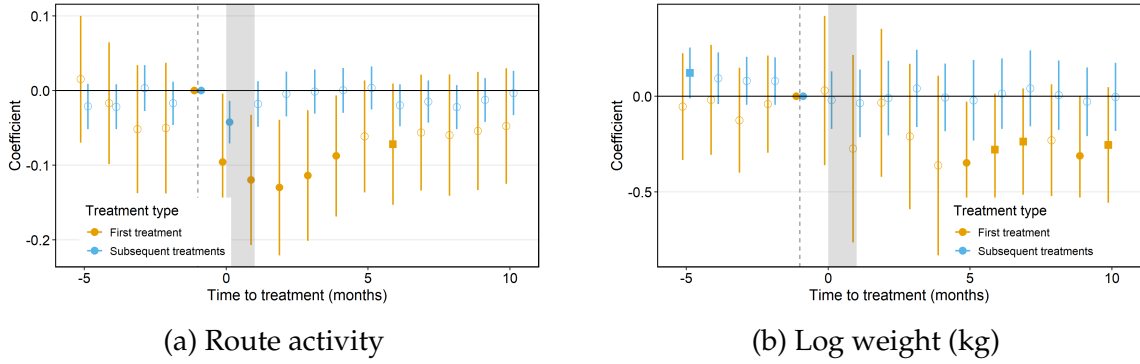


Figure C.3: Port exposure to cyclones & route choice (first vs. subsequent treatments)

Notes: These panels plot the effect of port exposure to tropical cyclones on monthly firm-to-firm-route-level outcomes, as specified by Equation (2). The treatment variable is interacted with two indicators variable, taking value 1 if the treatment is respectively (i) the first treatment experienced by the relationship (b, s), or (ii) subsequent treatments. The outcome in Panel C.3a is a binary variable, taking the value 1 if at least one shipment is observed for the trading pair through route r at month t (active route), and 0 otherwise. The outcome in Panel C.3b is the log total weight (kg) of shipments of the relationship using route r at month t , conditioned on the relationship-route being active. Regressions include relationship-month fixed effects, and control for time dummies interacted with relationship-routes' pre-treatment characteristics. Standard errors are clustered at the relationship level. The bars correspond to 95% confidence intervals. Black dots are point estimates significant at the 5% level, gray squares are point estimates significant at the 10% level, and empty dots are point estimates non-significant at the 10% level.

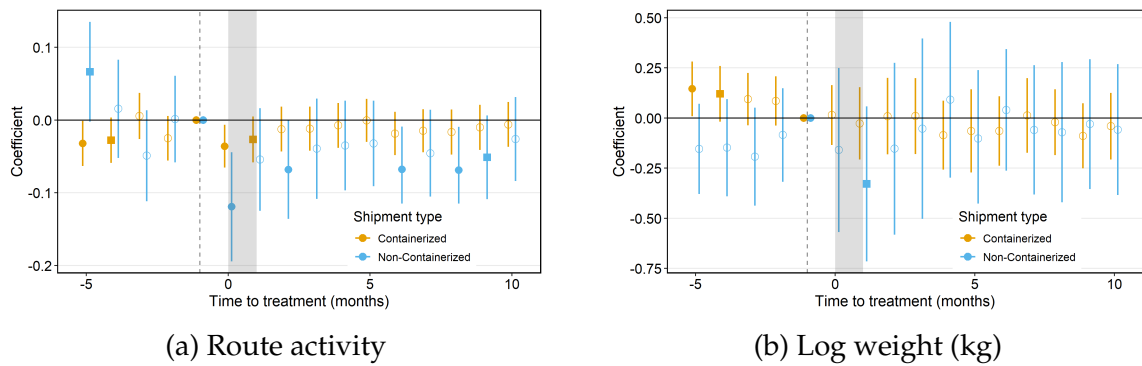


Figure C.4: Port exposure to cyclones & route choice (by good type)

Notes: These panels plot the effect of port exposure to tropical cyclones on monthly firm-to-firm-route-level outcomes, as specified by Equation (2). The treatment variable is interacted with two indicators variables, taking value 1 if the relationship-route traded respectively (i) only containerized goods, or (ii) at least one non-containerized good, in the 5-month period preceding the shock. The outcome in Panel C.4a is a binary variable, taking the value 1 if at least one shipment is observed for the trading pair through route r at month t (active route), and 0 otherwise. The outcome in Panel C.4b is the log total weight (kg) of shipments of the relationship using route r at month t , conditioned on the relationship-route being active. Regressions include relationship-month fixed effects, and control for time dummies interacted with relationship-routes' pre-treatment characteristics. Standard errors are clustered at the relationship level. The bars correspond to 95% confidence intervals. Black dots are point estimates significant at the 5% level, gray squares are point estimates significant at the 10% level, and empty dots are point estimates non-significant at the 10% level.

C.3 FIRM-TO-FIRM DISRUPTIONS

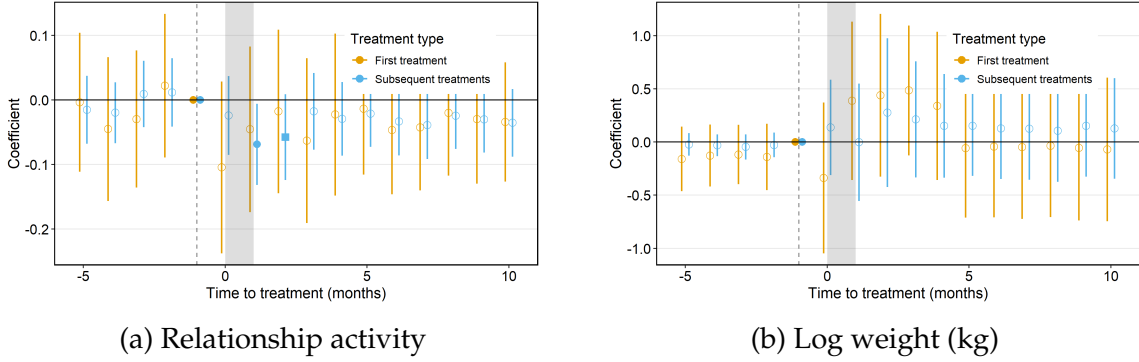


Figure C.5: Port exposure to cyclones & firm-to-firm relationship (first vs. subsequent treatments)

Notes: These panels plot the effect of port exposure to tropical cyclones on monthly firm-to-firm-level outcomes, as specified by Equation (3). The outcome in Panel C.5a is a binary variable, taking the value 1 if at least one shipment is observed for the trading pair at month t (active relationship), and 0 otherwise. Relationship activity is conditioned on the entry of both the buyer and the supplier. The outcome in Panel C.5b is the log total weight of shipments traded by the relationship, conditioning on activity. Regressions include buyer-time and supplier-time fixed effects, and control for time dummies interacted with relationships' pre-treatment characteristics. Standard errors are clustered at the buyer level. The bars correspond to 95% confidence intervals. Black dots are point estimates significant at the 5% level, gray squares are point estimates significant at the 10% level, and empty dots are point estimates non-significant at the 10% level.

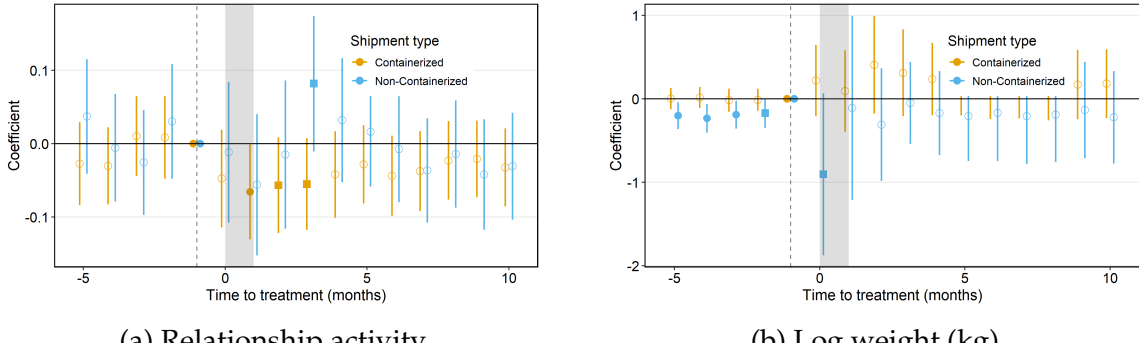


Figure C.6: Port exposure to cyclones & firm-to-firm relationship (by good type)

Notes: These Panels plot the effect of port exposure to tropical cyclones on monthly firm-to-firm-level outcomes, as specified by Equation (3). The outcome in Panel C.6a is a binary variable, taking the value 1 if at least one shipment is observed for the trading pair at month t (active relationship), and 0 otherwise. Relationship activity is conditioned on the entry of both the buyer and the supplier. The outcome in Panel C.6b is the log total weight of shipments traded by the relationship, conditioning on activity. Regressions include buyer-time and supplier-time fixed effects, and control for time dummies interacted with relationships' pre-treatment characteristics. Standard errors are clustered at the buyer level. The bars correspond to 95% confidence intervals. Black dots are point estimates significant at the 5% level, gray squares are point estimates significant at the 10% level, and empty dots are point estimates non-significant at the 10% level.

D THEORY

D.1 PROOFS

Proof: Proposition 1. Denote by $\lambda_j(\phi, r) = \frac{c_j}{z(\phi)} \prod_{k=1}^{|\mathcal{B}_r|} d_{r_{k-1}, r_k} \prod_{m=1}^{|\mathcal{P}_r|} t_{p(r)_m}$ the *effective* costs of using input from supplier j in technique ϕ , along route r . Consider the probability that the effective cost of supplier $j \in M_{n'}$ available to $i \in M_n$ through route r is strictly lower than a threshold λ ,

$$P(\lambda_j(\phi, r) \leq \lambda) = P\left(\frac{c_j}{z(\phi)} \prod_{k=1}^{|\mathcal{B}_r|} d_{r_{k-1}, r_k} \prod_{m=1}^{|\mathcal{P}_r|} t_{p(r)_m} \leq \lambda\right) = F_r(\lambda).$$

Integrating F_r over realizations of z and $t_{p(r)_1}, \dots, t_{p(r)_M}$, we obtain that the number of potential suppliers that deliver effective cost weakly less than λ through route r follows a Poisson distribution with mean

$$\begin{aligned} \Lambda_{jr} &= \int_0^\infty \left[\int_1^\infty \cdots \int_1^\infty F_r(\lambda) dF_{p(r)_1}(\theta) \cdots dF_{p(r)_M}(\theta) \right] dF_r(z) \\ &= \int_0^\infty \left[\int_1^\infty \cdots \int_1^\infty \left[\int_0^\infty \mathbb{1} \left(\frac{c_j}{z(\phi)} \prod_{k=1}^{|\mathcal{B}_r|} d_{r_{k-1}, r_k} \prod_{m=1}^{|\mathcal{P}_r|} t_{p(r)_m} \leq \lambda \right) dF_{n'}(c_j) \right] dF_{p(r)_1}(\theta) \cdots dF_{p(r)_M}(\theta) \right] \xi a_{n'} z^{-\xi-1} dz \\ &= a_{n'} \lambda^\xi \prod_{k=1}^{|\mathcal{B}_r|} d_{r_{k-1}, r_k}^{-\xi} \int_0^\infty \left[\int_1^\infty \cdots \int_1^\infty \left[\int_0^\infty \mathbb{1}(c_j \leq u) dF_{n'}(c_j) \right] \prod_{m=1}^{|\mathcal{P}_r|} t_{p(r)_m}^{-\xi} dF_{p(r)_1}(\theta) \cdots dF_{p(r)_M}(\theta) \right] \xi u^{-\xi-1} du \\ &= a_{n'} \lambda^\xi \prod_{k=1}^{|\mathcal{B}_r|} d_{r_{k-1}, r_k}^{-\xi} \left[\int_1^\infty \int_1^\infty \cdots \int_1^\infty \left[\int_0^\infty c_j^{-\xi} dF_{n'}(c_j) \right] \prod_{m=1}^{|\mathcal{P}_r|} t_{p(r)_m}^{-\xi} dF_{p(r)_1}(\theta) \cdots dF_{p(r)_M}(\theta) \right] \xi s^{-\xi-1} ds \\ &= a_{n'} \lambda^\xi \bar{c}_j^{-\xi} \prod_{k=1}^{|\mathcal{B}_r|} d_{r_{k-1}, r_k}^{-\xi} \prod_{m=1}^{|\mathcal{P}_r|} \bar{t}_{p(r)_m}^{-\xi}, \end{aligned} \tag{27}$$

where

$$\bar{c}_j^{-\xi} = \int_0^\infty c_j^{-\xi} dF_{n'}(c_j) \quad \text{and} \quad \bar{t}_{p(r)_m}^{-\xi} = \int_1^\infty t_{p(r)_m}^{-\xi} dF_{p(r)_m}(\theta) \tag{28}$$

The second equality follows when applying the transformation

$$z\lambda / \left(\prod_{k=1}^{|\mathcal{B}_r|} d_{r_{k-1}, r_k} \prod_{m=1}^{|\mathcal{P}_r|} t_{p(r)_m} \right) = u,$$

while the third equality follows when applying the transformation $u/c_j = s$. Therefore, number of potential suppliers along route r that deliver effective cost strictly greater than λ is such that:

$$P(\lambda_j(\phi, r) > \lambda) = e^{-\Lambda_{jr}} = e^{-a_{n'} \lambda^\xi \bar{c}_j^{-\xi} \prod_{k=1}^{|\mathcal{B}_r|} d_{r_{k-1}, r_k}^{-\xi} \prod_{m=1}^{|\mathcal{P}_r|} \bar{t}_{p(r)_m}^{-\xi}}. \tag{29}$$

Consider now the cost distribution of firm $i \in M_n$ with a supplier $j \in M_{n'}$ along route r . Using the marginal cost of firm i , one obtains

$$\begin{aligned} P(c_i(\phi, r) > c) &= P\left(\frac{w_n^{1-\alpha}}{a_n}\left(\tau_{n(i)n(j)}(r)\frac{c_j}{z(\phi)}\right)^\alpha > c\right) \\ &= P\left(\lambda_j(\phi, r) > \left(a_n w_n^{\alpha-1} c\right)^{\frac{1}{\alpha}}\right) \\ &= \exp\left[-\left(a_{n'} c^{\frac{\xi}{\alpha}} \left(a_n w_n^{\alpha-1}\right)^{\frac{\xi}{\alpha}} \prod_{k=1}^{|\mathcal{B}_r|} d_{r_{k-1}, r_k}^{-\xi} \prod_{m=1}^{|\mathcal{P}_r|} \bar{t}_{p(r)_m}^{-\xi} \bar{c}_j^{-\xi}\right)\right]. \end{aligned} \quad (30)$$

Then the probability that firm i 's minimal cost from sourcing from n' through route r is higher than a threshold, $P(c_i(\phi, r)_{\min, r} > c)$ is as follows:

$$\begin{aligned} P(c_i(\phi, r)_{\min, r} > c) &= P\left(\lambda_j(\phi, r)_{\min, r} > \left(a_n w_n^{\alpha-1} c\right)^{\frac{1}{\alpha}}\right) \\ &= \exp\left[-a_{n'} c^{\frac{\xi}{\alpha}} \left(a_n w_n^{\alpha-1}\right)^{\frac{\xi}{\alpha}} \prod_{k=1}^{|\mathcal{B}_r|} d_{r_{k-1}, r_k}^{-\xi} \prod_{m=1}^{|\mathcal{P}_r|} \bar{t}_{p(r)_m}^{-\xi} \bar{c}_{n'}^{-\xi}\right]. \end{aligned} \quad (31)$$

Consider finally the minimum cost at which firm i can produce (sourcing from any supplier through any route $r \in \mathcal{R}$), given realizations of a_n :

$$\begin{aligned} P(c_i(\phi, r)_{\min, r \in \mathcal{R}} > c) &= \prod_{r \in \mathcal{R}} P(c_i(\phi, r)_{\min, r} > c) \\ &= \prod_{r \in \mathcal{R}} \exp\left[-a_{n'} c^{\frac{\xi}{\alpha}} \left(a_n w_n^{\alpha-1}\right)^{\frac{\xi}{\alpha}} \prod_{k=1}^{|\mathcal{B}_r|} d_{r_{k-1}, r_k}^{-\xi} \prod_{m=1}^{|\mathcal{P}_r|} \bar{t}_{p(r)_m}^{-\xi} \bar{c}_{n'}^{-\xi}\right] \\ &= \exp\left[-\left(a_n w_n^{\alpha-1}\right)^{\frac{\xi}{\alpha}} \left(\sum_{n'} a_{n'} \bar{c}_{n'}^{-\xi} \sum_{r \in \mathcal{R}_{n'n}} \prod_{k=1}^{|\mathcal{B}_r|} d_{r_{k-1}, r_k}^{-\xi} \prod_{m=1}^{|\mathcal{P}_r|} \bar{t}_{p(r)_m}^{-\xi}\right) c^{\frac{\xi}{\alpha}}\right]. \end{aligned} \quad (32)$$

which is Weibull distributed. It remains to characterize \bar{c}_n and $\bar{\theta}_r$, both moments of the respective marginal cost and trade cost distributions. Consider first

$$\begin{aligned}
\bar{c}_n^{-\xi} &= \int_0^\infty c^{-\xi} d \left\{ 1 - \exp \left[- \left(a_n w_n^{\alpha-1} \right)^{\frac{\xi}{\alpha}} \left(\sum_{n'} a_{n'} \bar{c}_{n'}^{-\xi} \sum_{r \in \mathcal{R}_{n'n}} \prod_{k=1}^{|\mathcal{B}_r|} d_{r_{k-1}, r_k}^{-\xi} \prod_{m=1}^{|\mathcal{P}_r|} \bar{t}_{p(r)_m}^{-\xi} \right) c^{\frac{\xi}{\alpha}} \right] \right\} \\
&= a_n^\xi w_n^{(\alpha-1)\xi} \left(\sum_{n'} a_{n'} \bar{c}_{n'}^{-\xi} \sum_{r \in \mathcal{R}_{n'n}} \prod_{k=1}^{|\mathcal{B}_r|} d_{r_{k-1}, r_k}^{-\xi} \prod_{m=1}^{|\mathcal{P}_r|} \bar{t}_{p(r)_m}^{-\xi} \right) \int_0^\infty u^{-\xi} d \left\{ 1 - \exp \left[-u^{\frac{\xi}{\alpha}} \right] \right\} \\
&= a_n^\xi w_n^{(\alpha-1)\xi} \left(\sum_{n'} a_{n'} \bar{c}_{n'}^{-\xi} \sum_{r \in \mathcal{R}_{nn'}} \prod_{k=1}^{|\mathcal{B}_r|} d_{r_{k-1}, r_k}^{-\xi} \prod_{m=1}^{|\mathcal{P}_r|} \bar{t}_{p(r)_m}^{-\xi} \right) \int_0^\infty v^{-\alpha} d \left\{ 1 - e^{-v} \right\} \\
&= a_n^\xi w_n^{(\alpha-1)\xi} \left(\sum_{n'} a_{n'} \bar{c}_{n'}^{-\xi} \sum_{r \in \mathcal{R}_{n'n}} \prod_{k=1}^{|\mathcal{B}_r|} d_{r_{k-1}, r_k}^{-\xi} \prod_{m=1}^{|\mathcal{P}_r|} \bar{t}_{p(r)_m}^{-\xi} \right) \int_0^\infty v^{-\alpha} e^{-v} dv \\
&= a_n^\xi w_n^{(\alpha-1)\xi} \left(\sum_{n'} a_{n'} \bar{c}_{n'}^{-\xi} \sum_{r \in \mathcal{R}_{n'n}} \prod_{k=1}^{|\mathcal{B}_r|} d_{r_{k-1}, r_k}^{-\xi} \prod_{m=1}^{|\mathcal{P}_r|} \bar{t}_{p(r)_m}^{-\xi} \right)^\alpha \Gamma(1-\alpha).
\end{aligned} \tag{33}$$

The second equality follows from applying the transformation

$$a_n w_n^{\alpha-1} \left(\sum_{n'} a_{n'} \bar{c}_{n'}^{-\xi} \sum_{r \in \mathcal{R}_{n'n}} \prod_{k=1}^{|\mathcal{B}_r|} d_{r_{k-1}, r_k}^{-\xi} \prod_{m=1}^{|\mathcal{P}_r|} \bar{t}_{p(r)_m}^{-\xi} \right)^{\frac{\alpha}{\xi}} c = u.$$

The third equality follows from applying the transformation $v = u^{\frac{\xi}{\alpha}}$.

Moreover, $\bar{t}_{p(r)_m}^{-\xi}$ follows immediately from its definition and the Pareto assumptions on its distribution:

$$\begin{aligned}
\bar{t}_{p(r)_m}^{-\xi} &= \int_1^\infty t_{p(r)_m}^{-\xi} d F_{p(r)_m}(\theta) \\
&= \int_1^\infty t_{p(r)_m}^{-\xi} d \{1 - \theta^{-\psi_{p(r)_m}}\} \\
&= t(\Xi, K_p)^{-\xi} \frac{\psi_{p(r)_m}}{\psi_{p(r)_m} + \xi}.
\end{aligned} \tag{34}$$

Proof: Corollary 1. From the cost distribution of firm $i \in M_{n'}$ sourcing from route r , the number of suppliers located in n and using route r available to firm i in region n' , such that i achieves a cost below c is distributed Poisson with parameter

$$\rho_{i,r} = a_n c^{\frac{\xi}{\alpha}} \left(a_{n'} w_{n'}^{\alpha-1} \right)^{\frac{\xi}{\alpha}} \prod_{k=1}^{|\mathcal{B}_r|} d_{r_{k-1}, r_k}^{-\xi} \prod_{m=1}^{|\mathcal{P}_r|} \bar{t}_{p(r)_m}^{-\xi} \bar{c}_n^{-\xi}. \tag{35}$$

Moreover, from the cost distribution of firm $i \in M_{n'}$ sourcing from any route, the number of suppliers available to firm i from any route, such that i achieves a cost below c is distributed Poisson with parameter

$$\rho_i = \left(a_{n'} w_{n'}^{\alpha-1} \right)^{\frac{\xi}{\alpha}} \left(\sum_{\tilde{n}} a_{\tilde{n}} \bar{c}_{\tilde{n}}^{-\xi} \sum_{r \in \mathcal{R}_{\tilde{n}n'}} \prod_{k=1}^{|\mathcal{B}_r|} d_{r_{k-1}, r_k}^{-\xi} \prod_{m=1}^{|\mathcal{P}_r|} \bar{t}_{p(r)_m}^{-\xi} \right) c^{\frac{\xi}{\alpha}}. \quad (36)$$

The probability that a firm i in location n (able to deliver costs below c) supplies from location n' through route r is the ratio of $\rho_{i,r}$ and ρ_i :

$$\begin{aligned} \pi_{i,r} &= \frac{a_n c^{\frac{\xi}{\alpha}} \left(a_{n'} w_{n'}^{\alpha-1} \right)^{\frac{\xi}{\alpha}} \prod_{k=1}^{|\mathcal{B}_r|} d_{r_{k-1}, r_k}^{-\xi} \prod_{m=1}^{|\mathcal{P}_r|} \bar{t}_{p(r)_m}^{-\xi} \bar{c}_n^{-\xi}}{\left(a_{n'} w_{n'}^{\alpha-1} \right)^{\frac{\xi}{\alpha}} \left(\sum_{\tilde{n}} a_{\tilde{n}} \bar{c}_{\tilde{n}}^{-\xi} \sum_{r \in \mathcal{R}_{\tilde{n}n}} \prod_{k=1}^{|\mathcal{B}_r|} d_{r_{k-1}, r_k}^{-\xi} \prod_{m=1}^{|\mathcal{P}_r|} \bar{t}_{p(r)_m}^{-\xi} \right) c^{\frac{\xi}{\alpha}}} \\ &= \frac{a_n \bar{c}_n^{-\xi} \prod_{k=1}^{|\mathcal{B}_r|} d_{r_{k-1}, r_k}^{-\xi} \prod_{m=1}^{|\mathcal{P}_r|} \bar{t}_{p(r)_m}^{-\xi}}{\sum_{\tilde{n}} a_{\tilde{n}} \bar{c}_{\tilde{n}}^{-\xi} \sum_{r \in \mathcal{R}_{\tilde{n}n}} \prod_{k=1}^{|\mathcal{B}_r|} d_{r_{k-1}, r_k}^{-\xi} \prod_{m=1}^{|\mathcal{P}_r|} \bar{t}_{p(r)_m}^{-\xi}} \end{aligned} \quad (37)$$

Note that the probability of sourcing from r is the same for any firm in n' . Since there are a continuum of firms in n' , $\pi_{i,r}$ is also the *bilateral trade share* of route r in the total absorption of goods of destination n' , denoted $\pi_{n',r}$.

Proof: Corollary 2

$$\begin{aligned} \pi_{nn'} &= \sum_{r \in \mathcal{R}_{nn'}} \pi_{n',r} \\ &= \frac{a_n \bar{c}_n^{-\xi} \tau_{nn'}^{-\xi}}{\sum_{\tilde{n}} a_{\tilde{n}} \bar{c}_{\tilde{n}}^{-\xi} \tau_{n\tilde{n}}^{-\xi}} \end{aligned} \quad (38)$$

where

$$\tau_{nn'} = \left(\sum_{r \in \mathcal{R}_{nn'}} \left(\prod_{k=1}^{|\mathcal{B}_r|} d_{r_{k-1}, r_k}^{-\xi} \right) \left(\prod_{m=1}^{|\mathcal{P}_r|} \frac{\psi_{p(r)_m}}{\psi_{p(r)_m} + \xi} \right) \right)^{-\frac{1}{\xi}} \quad (39)$$

D.2 CLOSING THE MODEL

Labor market clearing: Labor demand for a firm i in location n is given by $l_i = (1 - \alpha)y_i c_i / w_n$. Plugging this condition into the labor market clearing gives:

$$L_n = \int_{i \in M_n} l_i di \Rightarrow \frac{w_n L_n}{1 - \alpha} = \int_{i \in M_n} y_i c_i di. \quad (40)$$

Good market clearing:

$$y_i = L_n q_i + \sum_{n'} \int_{j \in M_{n'}} \tau_{n(j)n(j)} x_{ij} dj, \quad x_{ij} = x_j \times \mathbf{1}\{i = i^*\} \quad (41)$$

Multiplying both sides by marginal costs c_j and aggregating over firms in $M_{n'}$:

$$\underbrace{\int_{i \in M_n} c_i y_i di}_{(1) \text{ Supply}} = \underbrace{L_n \int_{i \in M_n} c_i q_i di}_{(2) \text{ Final good demand}} + \underbrace{\int_{i \in M_n} c_i \left[\sum_{n'} \int_{j \in M_{n'}} \tau_{n(i)n(j)} (x_j \times \mathbf{1}\{i = i^*\}) dj \right] di}_{(3) \text{ Intermediate input demand}}. \quad (42)$$

Term (1) simplifies using the labor market clearing condition, $\int_{i \in M_n} c_i y_i di = w_n L_n / (1 - \alpha)$.

Term (2) simplifies as follows: With isoelastic preferences and monopolistic competition, households in region n demand $q_j = q_n p_n^\sigma p_j^{-\sigma}$, where $p_i = c_i^{\frac{\sigma}{\sigma-1}}$. Realizing that $q_n = (w_n + \Pi_n) / p_n$, where w_n is the wage rate and Π_n is the per-capita profits of firms in n rebated to labor, implies:

$$\begin{aligned} L_n \int_{i \in M_n} c_i q_i di &= L_n (w_n + \Pi_n) p_n^{\sigma-1} \left(\frac{\sigma}{\sigma-1} \right)^{-\sigma} \int_{i \in M_n} c_i^{1-\sigma} di \\ &= L_n (w_n + \Pi_n) \left(\left(\int_{i \in M_n} p_i^{1-\sigma} di \right)^{\frac{1}{1-\sigma}} \right)^{\sigma-1} \left(\frac{\sigma}{\sigma-1} \right)^{-\sigma} \int_{i \in M_n} c_i^{1-\sigma} di \\ &= L_n (w_n + \Pi_n) \left(\frac{\sigma}{\sigma-1} \right)^{-1} \left(\int_{i \in M_n} c_i^{1-\sigma} di \right)^{-1} \int_{i \in M_n} c_i^{1-\sigma} di \\ &= L_n (w_n + \Pi_n) \tilde{\sigma}^{-1}. \end{aligned} \quad (43)$$

[Note: term (2) simplifies also easily when considering that $q_n p_n = \int_{i \in M_n} \tilde{\sigma} c_i q_i di$, where $\tilde{\sigma} = \sigma / (\sigma - 1)$, and $q_n p_n = w_n + \Pi_n$.] It remains to characterize per-capita profit rebated to households in region n . Note that firms only gain profits from selling final goods to local households:

$$\text{Profit}_i = p_i q_i L_n - c_i q_i L_n. \quad (44)$$

Therefore, total profit per capita (aggregating over all firms in M_n) yields:

$$\begin{aligned} \Pi_n &= L_n^{-1} \int_{i \in M_n} L_n (p_i q_i - c_i q_i) di \\ &= \int_{i \in M_n} (\tilde{\sigma} c_i q_i - c_i q_i) di \\ &= (\tilde{\sigma} - 1) \int_{i \in M_n} c_i q_i di \\ &= (\tilde{\sigma} - 1) \tilde{\sigma}^{-1} q_n p_n \\ &= \frac{1}{\sigma} (w_n + \Pi_n). \end{aligned} \quad (45)$$

Solving for per-capita profits yields $\Pi_n = \frac{w_n}{\sigma-1}$. Therefore, term (2) simplifies to:

$$\begin{aligned} L_n \int_{i \in M_n} c_i q_i di &= L_n \left(w_n + \frac{w_n}{\sigma-1} \right) \tilde{\sigma}^{-1} \\ &= L_n w_n. \end{aligned} \quad (46)$$

Term (3) simplifies as follows: Firms demand $x_j = \frac{(1-\alpha)y_j c_j}{c_i \tau_{n(i)n(j)}}$ units of intermediate inputs. This implies:

$$\begin{aligned} \int_{i \in M_n} c_i \left(\sum_{n'} \int_{j \in M_{n'}} \tau_{nn'} (x_j \times \mathbf{1}\{i = i^*\}) dj \right) di &= \alpha \int_{i \in M_n} \left(\sum_{n'} \int_{j \in M_{n'}} \mathbf{1}\{i = i^*\} y_j c_j dj \right) di \\ &= \alpha \sum_{n'} \int_{j \in M_{n'}} \mathbf{1}\{i^* \in M_n\} y_j c_j dj \\ &= \alpha \sum_{n'} \pi_{nn'} \int_{j \in M_{n'}} y_j c_j dj \\ &= \alpha \sum_{n'} \pi_{nn'} \frac{w_{n'} L_{n'}}{1 - \alpha} \end{aligned} \quad (47)$$

Putting terms (1), (2) and (3) together yields the following system for region-level wages:

$$w_n L_n = \sum_{n'} \pi_{nn'} w_{n'} L_{n'}. \quad (48)$$

Finally, to obtain traffic, we recover the value of bilateral flows (i.e. the level of expenditures from firms in n' to firms in n):

$$\begin{aligned} X_{nn'} &= \int_{i \in M_n} \int_{j \in M_{n'}} c_i \tau_{nn'} (x_j \times \mathbf{1}\{i = i^*\}) dj di \\ &= \alpha \int_{i \in M_n} \int_{j \in M_{n'}} \mathbf{1}\{i = i^*\} y_j c_j dj di \\ &= \alpha \int_{j \in M_{n'}} \mathbf{1}\{i^* \in M_n\} y_j c_j dj \\ &= \alpha \pi_{nn'} \int_{j \in M_{n'}} y_j c_j dj \\ &= \alpha \pi_{nn'} \frac{w_{n'} L_{n'}}{1 - \alpha} \end{aligned} \quad (49)$$

D.3 GENERAL EQUILIBRIUM: DEFINITION

Given a geography $\mathcal{G} = \{\mathcal{N}, \mathcal{P}, \mathcal{L}, \mathcal{M}, \mathcal{A}, \mathcal{D}, \mathcal{K}, \Psi\}$ and a set of model parameters $\{\sigma, \alpha, \xi, \lambda_1, \lambda_2, \lambda_3\}$, an equilibrium is defined as a distribution of wages and factory-gate prices $\{w_n, \bar{c}_n\}_{n \in \mathcal{N}}$, such that:

- Given the equilibrium transportation network $\delta_{ll'} \in \{\delta_{ll'}\}_{l, l' \in \mathcal{N} \cup \mathcal{P} \times \mathcal{N} \cup \mathcal{P}}$, (i) consumers

maximize utility; (ii) firms choose the techniques and the routes that minimize costs, and markups that maximize profits; and (iii) market clears.⁵⁸

2. Given the transportation network fundamentals $\{\mathcal{D}, \mathcal{K}\}$ an equilibrium prices, the equilibrium transportation network $\delta_{ll'} \in \{\delta_{ll'}\}_{l,l' \in \mathcal{N} \cup \mathcal{P} \times \mathcal{N} \cup \mathcal{P}}$ is determined by the equilibrium levels of traffic $\{\Xi_p\}$.

This leads the equilibrium to be characterized by the following set of equations:⁵⁹

$$\begin{aligned}
w_n L_n &= \frac{1-\alpha}{\alpha} \sum_{n'} X_{nn'} \quad (\text{wage bill}) \\
\pi_{nn'} &= \frac{a_n \bar{c}_n^{-\xi} \tau_{nn'}^{-\xi}}{\sum_{\tilde{n}} a_{\tilde{n}} \bar{c}_{\tilde{n}}^{-\xi} \tau_{\tilde{n}n'}^{-\xi}} \quad (\text{bilateral trade shares}) \\
\bar{c}_n^{-\xi} &= a_n^\xi w_n^{(\alpha-1)\xi} \left(\sum_{\tilde{n}} a_{\tilde{n}} \bar{c}_{\tilde{n}}^{-\xi} \tau_{\tilde{n}n}^{-\xi} \right)^\alpha \Gamma(1-\alpha) \quad (\text{factory-gate cost indices}) \\
[\tau_{nn'}] &= \begin{cases} 1 & \text{if } n = n' \\ [(I - \Delta)^{-1}]^{\circ(-\frac{1}{\xi})} & \text{otherwise} \end{cases} \quad (\text{transportation costs}) \\
\Delta = [\delta_{ll'}], \quad \delta_{ij} &= \begin{cases} d_{ll'}^{-\xi} \bar{t}_{l'}^{-\xi} & \text{if } l' \in \mathcal{P} \\ d_{ll'}^{-\xi} & \text{otherwise} \end{cases} \quad (\text{transportation network}) \\
d_{ll'}^{-\xi} &= \epsilon_{ll'}^{\lambda_1}, \quad \bar{t}_{l'}^{-\xi} = \Xi_{l'}^{\lambda_2} K_{l'}^{\lambda_3} \frac{\psi_{l'}}{\psi_{l'} + \xi} \quad (\text{link- and port-level costs}) \\
\Xi_p &= \delta_{pp} \sum_n \sum_{n'} \left(\tau_{np} \tau_{pn'} \tau_{nn'}^{-1} \right)^{-\xi} X_{nn'} \quad (\text{link- and port-level traffic}) \\
X_{nn'} &= \alpha \pi_{nn'} \frac{w_{n'} L_{n'}}{1-\alpha} \quad (\text{bilateral trade})
\end{aligned}$$

D.4 GENERAL EQUILIBRIUM: NUMERICAL ALGORITHM

Given a geography $\mathcal{G} = \{\mathcal{N}, \mathcal{P}, \mathcal{L}, \mathcal{M}, \mathcal{A}, \mathcal{D}, \mathcal{K}, \Psi\}$ and a set of model parameters $\{\sigma, \alpha, \xi, \lambda_1, \lambda_2, \lambda_3\}$, the following algorithm solves for the equilibrium of the economy:

1. **Initialize** endogenous variables:

⁵⁸Formally, the economy admits ports as regions. However, I assume that ports have a 0 measure of households and firms, such that they do not consume or produce. It results that equilibrium prices have dimension $|\mathcal{N}|$, while the transportation network has dimensions $(|\mathcal{N} \cup \mathcal{P}|)^2$.

⁵⁹Up to a numeraire: $w_1 = 1$.

- (a) $\{w_n\}_{n \in \mathcal{N}}$ (wages)
- (b) $\{\bar{c}_n\}_{n \in \mathcal{N}}$ (factory-gate cost indices)
- (c) $\{\pi_{nn'}\}_{n,n' \in \mathcal{N}^2}$ (bilateral trade shares)
- (d) $\{\Xi_p\}_{p \in \mathcal{P}}$ (port traffic)

2. **Outer-loop** – While $distance_{wages} > tol$ or $distance_{traffic} > tol$:

- (a) Based on distances $\epsilon_{ll'}$, port capacity K_p and traffic Ξ_p , update Λ (*transportation network*)
- (b) Based on Λ , update transportation costs $\tau_{ll'}$ (*transportation costs*)
- (c) **Inner-loop (factory-gate costs)** – While $distance_{costs} > tol$:
 - i. Based on transportation costs $\tau_{nn'}$, region-level productivity a_n , factory-gate costs indices \bar{c}_n , and wages w_n , update \bar{c}_n (*factory-cost indices*)⁶⁰
 - ii. Compute $distance_{costs} = \sum_n [(\bar{c}_n)^{i_c} - (\bar{c}_n)^{i_c+1}]^2$, with i_c = iteration (inner-loop)
- (d) Based on transportation costs $\tau_{nn'}$, region-level productivity a_n , factory-gate costs indices \bar{c}_n , and wages w_n , update $\pi_{nn'}$ (*bilateral trade shares*)
- (e) Based on bilateral trade shares $\pi_{nn'}$ and wages bills $w_n L_n$, update $X_{nn'}$ (*bilateral trade*)
- (f) Based on the transportation network Λ and bilateral trade $X_{nn'}$, compute Ξ_p (*port-level traffic*)
- (g) Based on bilateral trade $X_{nn'}$, and households L_n compute wages w_n (*wage bills*), up to a normalization $w_1 = 1$
- (h) Compute $distance_{wages} = \sum_n [(w_n)^{i_{out}} - (w_n)^{i_{out}+1}]^2$ and $distance_{traffic} = \sum_p [(\Xi_p)^{i_{out}} - (\Xi_p)^{i_{out}+1}]^2$, with i_{out} = iteration (outer loop)

In practice, I dampen each wage and traffic iteration using a dampening factor of 0.1, and use the 'daarem' R package to optimize the resolution of the fixed point.

⁶⁰Note that transportation costs used in factory-gate cost indices and bilateral trade shares do not have the same dimension as transportation costs used for traffic. This is because ports have a measure 0 of labor, and therefore would not impact bilateral trade shares and costs indices. I use only the sub-matrix of τ_{ij} with dimensions $|N| \times |N|$.

D.5 WELFARE

Proof. Proposition 2. Define welfare in location d as:

$$\begin{aligned}
V_n &= \frac{L_n(w_n + \Pi_n)}{\left(\int_{i \in M_n} p_i^{1-\sigma} di\right)^{\frac{1}{1-\sigma}}} \\
&= \frac{L_n w_n \tilde{\sigma}}{\left(\int_{i \in M_n} (\tilde{\sigma} c_i)^{1-\sigma} di\right)^{\frac{1}{1-\sigma}}} \\
&= \frac{L_n w_n}{\left(M_n \int c^{1-\sigma} dF_i(c)\right)^{\frac{1}{1-\sigma}}}
\end{aligned} \tag{50}$$

It remains to characterize $\int c^{1-\sigma} dF_i(c)$:

$$\begin{aligned}
\int c^{1-\sigma} dF_i(c) &= \int_0^\infty c^{1-\sigma} d \left\{ 1 - \exp \left[- \left(a_n w_n^{\alpha-1} \right)^{\frac{\xi}{\alpha}} \left(\sum_{n'} a_{n'} \bar{c}_{n'}^{-\xi} \sum_{r \in \mathcal{R}_{n'n}} \prod_{k=1}^{|\mathcal{B}_r|} d_{r_{k-1}, r_k}^{-\xi} \prod_{m=1}^{|\mathcal{P}_r|} \bar{t}_{p(r)_m}^{-\xi} \right) c^{\frac{\xi}{\alpha}} \right] \right\} \\
&= \int_0^\infty c^{1-\sigma} d \left\{ 1 - \exp \left[- \left(a_n w_n^{\alpha-1} \right)^{\frac{\xi}{\alpha}} \left(\sum_{n'} a_{n'} \bar{c}_{n'}^{-\xi} \tau_{n'n}^{-\xi} \right) c^{\frac{\xi}{\alpha}} \right] \right\} \\
&= \left[a_n w_n^{\alpha-1} \left(\sum_{n'} a_{n'} \bar{c}_{n'}^{-\xi} \tau_{n'n}^{-\xi} \right)^{\frac{\alpha}{\xi}} \right]^{\sigma-1} \int_0^\infty u^{1-\sigma} d \left\{ 1 - \exp \left[-u^{\frac{\xi}{\alpha}} \right] \right\} \\
&= \left[a_n w_n^{\alpha-1} \left(\sum_{n'} a_{n'} \bar{c}_{n'}^{-\xi} \tau_{n'n}^{-\xi} \right)^{\frac{\alpha}{\xi}} \right]^{\sigma-1} \int_0^\infty v^{-\frac{\alpha(\sigma-1)}{\xi}} d \left\{ 1 - e^{-v} \right\} \\
&= \left[a_n w_n^{\alpha-1} \left(\sum_{n'} a_{n'} \bar{c}_{n'}^{-\xi} \tau_{n'n}^{-\xi} \right)^{\frac{\alpha}{\xi}} \right]^{\sigma-1} \int_0^\infty v^{-\frac{\alpha(\sigma-1)}{\xi}} e^{-v} dv \\
&= \left[a_n w_n^{\alpha-1} \left(\sum_{n'} a_{n'} \bar{c}_{n'}^{-\xi} \tau_{n'n}^{-\xi} \right)^{\frac{\alpha}{\xi}} \right]^{\sigma-1} \Gamma \left(1 - \frac{\alpha(\sigma-1)}{\xi} \right),
\end{aligned} \tag{51}$$

The third equality follows from applying the transformation $a_n w_n^{\alpha-1} \left(\sum_{n'} a_{n'} \bar{c}_{n'}^{-\xi} \tau_{n'n}^{-\xi} \right)^{\frac{\alpha}{\xi}} c = u$. The fourth equality follows from applying the transformation $v = u^{\frac{\xi}{\alpha}}$. The sixth equality follows from the definition of the Gamma function $\Gamma(z) = \int_0^\infty t^{z-1} e^{-t} dt$. Therefore, assuming a unit measure of firms in each region, welfare writes:

$$V_n = L_n w_n \left[a_n w_n^{\alpha-1} \left(\sum_{n'} a_{n'} \bar{c}_{n'}^{-\xi} \tau_{n'n}^{-\xi} \right)^{\frac{\alpha}{\xi}} \right]^{\sigma-1} \Gamma \left(1 - \frac{\alpha(\sigma-1)}{\xi} \right) \tag{52}$$

D.6 WELFARE ELASTICITY

Proof. Proposition 3. Rewrite the region-level welfare function as

$$V_n = L_n w_n^{\beta_w} \mathcal{T}_n^{\beta_\tau} C_n, \quad (53)$$

where $C_n = a_n^{(\sigma-1)} \Gamma\left(1 - \frac{\alpha(\sigma-1)}{\xi}\right)$, $\beta_w = 1 + (\alpha - 1)(\sigma - 1)$, and $\beta_\tau = \frac{\alpha}{\xi}(\sigma - 1)$ are constants. Recalling that $\pi_{n'n} = a_{n'} \bar{c}_{n'}^{-\xi} \tau_{n'n}^{-\xi} / \mathcal{T}_n$, log-differentiating yields:

$$\frac{\partial \log V_n}{\partial \log K_p} = \underbrace{\beta_w \frac{\partial \log w_n}{\partial \log K_p}}_{(1)} + \beta_\tau \sum_{n'} \pi_{n'n} \left[-\xi \underbrace{\frac{\partial \log \bar{c}_{n'}}{\partial \log K_p}}_{(2)} - \xi \underbrace{\frac{\partial \log \tau_{n'n}}{\partial \log K_p}}_{(3)} \right]. \quad (54)$$

(1) - *Wage elasticity* $\frac{\partial \log w_n}{\partial \log K_p}$. Recall the definition of the wage bill:

$$w_n L_n = \frac{1-\alpha}{\alpha} \sum_{n'} X_{nn'} \quad \text{with} \quad X_{nn'} = \alpha \pi_{nn'} \frac{w_{n'} L_{n'}}{1-\alpha}. \quad (55)$$

Log-differentiating with respect to $\log K_p$ yields:

$$w_n L_n \frac{\partial \log w_n}{\partial \log K_p} = \frac{1-\alpha}{\alpha} \sum_{n'} X_{nn'} \left[\frac{\partial \log \pi_{nn'}}{\partial \log K_p} + \frac{\partial \log w_{n'}}{\partial \log K_p} \right] \quad (56)$$

It remains to obtain the derivative of trade shares over $\log K_p$. Log-differentiating $\pi_{nn'}$

$$\frac{\partial \log \pi_{nn'}}{\partial \log K_p} = -\xi \left[\frac{\partial \log \bar{c}_n}{\partial \log K_p} + \frac{\partial \log \tau_{nn'}}{\partial \log K_p} \right] - \sum_{\tilde{n}} \pi_{\tilde{n}n'} \left[-\xi \frac{\partial \log \bar{c}_{\tilde{n}}}{\partial \log K_p} - \xi \frac{\partial \log \tau_{\tilde{n}n'}}{\partial \log K_p} \right] \quad (57)$$

Plugging into the wage derivative yields:

$$\frac{\partial \log w_n}{\partial \log K_p} = \frac{1-\alpha}{\alpha w_n L_n} \sum_{n'} X_{nn'} \left[-\xi \left[\frac{\partial \log \bar{c}_n}{\partial \log K_p} + \frac{\partial \log \tau_{nn'}}{\partial \log K_p} \right] + \xi \sum_{\tilde{n}} \pi_{\tilde{n}n'} \left[\frac{\partial \log \bar{c}_{\tilde{n}}}{\partial \log K_p} + \frac{\partial \log \tau_{\tilde{n}n'}}{\partial \log K_p} \right] + \frac{\partial \log w_{n'}}{\partial \log K_p} \right] \quad (58)$$

(2) - *Factory-gate cost elasticity* $\frac{\partial \log \bar{c}_{n'}^{-\xi}}{\partial \log K_p}$. Recall the definition of factory-gate costs:

$$\bar{c}_n^{-\xi} = a_n^\xi w_n^{(\alpha-1)\xi} \mathcal{T}_n^\alpha \Gamma(1-\alpha), \quad \text{where} \quad \mathcal{T}_n = \sum_{\tilde{n}} a_{\tilde{n}} \bar{c}_{\tilde{n}}^{-\xi} \tau_{\tilde{n}n}^{-\xi}. \quad (59)$$

Log-differentiating with respect to $\log K_p$ yields:

$$\begin{aligned} -\frac{\partial \log \bar{c}_n}{\partial \log K_p} &= (\alpha - 1) \frac{\partial \log w_n}{\partial \log K_p} + \frac{\alpha}{\xi} \frac{\partial \log T_n}{\partial \log K_p} \\ &= (\alpha - 1) \frac{\partial \log w_n}{\partial \log K_p} - \alpha \sum_{n'} \pi_{n'n} \left[\frac{\partial \log \bar{c}_{n'}}{\partial \log K_p} + \frac{\partial \log \tau_{n'n}}{\partial \log K_p} \right] \end{aligned} \quad (60)$$

(3) - *Bilateral transportation costs elasticity* $\frac{\partial \log \tau_{ll'}}{\partial \log K_p}$. Define $\mathbf{B} = (\mathbf{I} - \Delta)^{-1}$. By definition, $\log \tau_{ll'} = -\frac{1}{\xi} \log \mathbf{B}_{ll'}$, $\forall l \neq l'$ and $\log \tau_{ll'} = 0, \forall l = l'$. Differentiating \mathbf{B} with respect to $\log K_p$ yields:

$$\frac{\partial \mathbf{B}}{\partial \log K_p} = \mathbf{B} \left(\frac{\partial \Delta}{\partial \log K_p} \right) \mathbf{B}, \quad (61)$$

or, element-wise:

$$\frac{\partial \mathbf{B}_{ll'}}{\partial \log K_p} = \sum_i \sum_j \mathbf{B}_{li} \left(\frac{\partial \Delta_{ij}}{\partial \log K_p} \right) \mathbf{B}_{jl'}. \quad (62)$$

Realizing that $\partial \Delta_{ij} / \partial \log K_p = 0, \forall j \notin \mathcal{P}$, this yields:

$$\frac{\partial \log \mathbf{B}_{ll'}}{\partial \log K_p} = \frac{1}{\mathbf{B}_{ll'}} \sum_i \sum_{j \in \mathcal{P}} \mathbf{B}_{li} \left(\frac{\partial \delta_{ij}}{\partial \log K_p} \right) \mathbf{B}_{jl'}. \quad (63)$$

With the parametrization $\delta_{ll'} = d_{ll'}^{-\xi} \bar{t}_{l'}^{-\xi}$, and $\bar{t}_{l'}^{-\xi} = \Xi_{l'}^{\lambda_2} K_{l'}^{\lambda_3} \frac{\psi_{l'}}{\psi_{l'} + \xi}$ if $l' \in \mathcal{P}$, one obtains:

$$\frac{\partial \delta_{ij}}{\partial \log K_p} = \delta_{ij} \left(\lambda_3 \mathbf{1}_{j=p} + \lambda_2 \frac{\partial \log \Xi_j}{\partial \log K_p} \right). \quad (64)$$

Plugging this expression into $\partial \log \mathbf{B}_{ll'} / \partial \log K_p$ yields:

$$\begin{aligned} \frac{\partial \log \mathbf{B}_{ll'}}{\partial \log K_p} &= \left(\lambda_3 + \lambda_2 \frac{\partial \log \Xi_p}{\partial \log K_p} \right) \frac{1}{\mathbf{B}_{ll'}} \sum_i \mathbf{B}_{li} \delta_{ip} \mathbf{B}_{pl'} + \frac{1}{\mathbf{B}_{ll'}} \sum_{p' \in \mathcal{P}_{-p}} \left(\lambda_2 \frac{\partial \log \Xi_{p'}}{\partial \log K_p} \right) \sum_i \mathbf{B}_{li} \delta_{ip'} \mathbf{B}_{p'l'} \\ &= \left(\lambda_3 + \lambda_2 \frac{\partial \log \Xi_p}{\partial \log K_p} \right) \frac{1}{\mathbf{B}_{ll'}} (\mathbf{B}\Delta)_{lp} \mathbf{B}_{pl'} + \sum_{p' \in \mathcal{P}_{-p}} \left(\lambda_2 \frac{\partial \log \Xi_{p'}}{\partial \log K_p} \right) \frac{1}{\mathbf{B}_{ll'}} (\mathbf{B}\Delta)_{lp'} \mathbf{B}_{p'l'}. \end{aligned} \quad (65)$$

For all $l \neq p'$, $(\mathbf{B}\Delta)_{lp'} = \mathbf{B}_{lp'}$ since $\mathbf{B} = (\mathbf{I} - \Delta)^{-1}$, such that $(\mathbf{B}\Delta)_{lp'} = \mathbf{B} - \mathbf{I}$. Therefore,

$$\begin{aligned} \frac{\partial \log \tau_{ll'}}{\partial \log K_p} &= -\frac{1}{\xi} \frac{\partial \log \mathbf{B}_{ll'}}{\partial \log K_p} \\ &= -\frac{\lambda_3}{\xi} \frac{\mathbf{B}_{lp} \mathbf{B}_{pl'}}{\mathbf{B}_{ll'}} - \frac{\lambda_2}{\xi} \sum_{p' \in \mathcal{P}} \frac{\mathbf{B}_{lp'} \mathbf{B}_{p'l'}}{\mathbf{B}_{ll'}} \underbrace{\frac{\partial \log \Xi_{p'}}{\partial \log K_p}}_{(4)} \\ &= -\frac{\lambda_3}{\xi} \Theta_{p|ll'} - \frac{\lambda_2}{\xi} \sum_{p' \in \mathcal{P}} \Theta_{p'|ll'} \underbrace{\frac{\partial \log \Xi_{p'}}{\partial \log K_p}}_{(4)} \end{aligned} \quad (66)$$

where I use the identity $\Theta_{p|ll'} = \frac{\mathbf{B}_{lp} \mathbf{B}_{pl'}}{\mathbf{B}_{ll'}}$.

(4) - *Traffic elasticity* $\frac{\partial \log \Xi_{p'}}{\partial \log K_p}$. Traffic writes:

$$\Xi_{p'} = \sum_n \sum_{n'} \Theta_{p'|nn'} X_{nn'}, \quad \text{where } \Theta_{p'|nn'} = \left(\tau_{np'} \tau_{p'n'} \tau_{nn'}^{-1} \right)^{-\xi}. \quad (67)$$

Log-differentiating with respect to K_p yields:

$$\frac{\partial \log \Xi_{p'}}{\partial \log K_p} = \sum_n \sum_{n'} w_{nn'}^{(p')} \left[\frac{\partial \log \Theta_{p'|nn'}}{\partial \log K_p} + \frac{\partial \log X_{nn'}}{\partial \log K_p} \right]. \quad (68)$$

where $w_{nn'}^{(p')} = \Theta_{p'|nn'} X_{nn'} / \Xi_{p'}$. I first derive

$$\begin{aligned} \frac{\partial \log \Theta_{p'|nn'}}{\partial \log K_p} &= -\xi \frac{\partial \log \tau_{np'}}{\partial \log K_p} - \xi \frac{\partial \log \tau_{p'n'}}{\partial \log K_p} + \xi \frac{\partial \log \tau_{nn'}}{\partial \log K_p} \\ &= \lambda_3 \left[\Theta_{p|np'} + \Theta_{p|p'n'} - \Theta_{p|nn'} \right] + \sum_{\tilde{p} \in \mathcal{P}} \lambda_2 \left[\Theta_{\tilde{p}|np'} + \Theta_{\tilde{p}|p'n'} - \Theta_{\tilde{p}|nn'} \right] \frac{\partial \log \Xi_{\tilde{p}}}{\partial \log K_p}. \end{aligned} \quad (69)$$

The elasticity of trade volumes to port capacity is

$$\begin{aligned} \frac{\partial \log X_{nn'}}{\partial \log K_p} &= \frac{\partial \log \pi_{nn'}}{\partial \log K_p} + \frac{\partial \log w_{n'}}{\partial \log K_p} \\ &= -\xi \left[\frac{\partial \log \bar{c}_n}{\partial \log K_p} + \frac{\partial \log \tau_{nn'}}{\partial \log K_p} \right] - \sum_{\tilde{n}} \pi_{\tilde{n}n'} \left[-\xi \frac{\partial \log \bar{c}_{\tilde{n}}}{\partial \log K_p} - \xi \frac{\partial \log \tau_{\tilde{n}n'}}{\partial \log K_p} \right] + \frac{\partial \log w_{n'}}{\partial \log K_p} \end{aligned} \quad (70)$$

The first term writes:

$$-\xi \left[\frac{\partial \log \bar{c}_n}{\partial \log K_p} + \frac{\partial \log \tau_{nn'}}{\partial \log K_p} \right] = -\xi \frac{\partial \log \bar{c}_n}{\partial \log K_p} + \lambda_3 \Theta_{p|nn'} + \lambda_2 \sum_{\tilde{p} \in \mathcal{P}} \Theta_{\tilde{p}|nn'} \frac{\partial \log \Xi_{\tilde{p}}}{\partial \log K_p} \quad (71)$$

The second term writes:

$$\begin{aligned}
-\sum_{\tilde{n}} \pi_{\tilde{n}n'} \left[-\xi \frac{\partial \log \bar{c}_{\tilde{n}}}{\partial \log K_p} - \xi \frac{\partial \log \tau_{\tilde{n}n'}}{\partial \log K_p} \right] &= \xi \sum_{\tilde{n}} \pi_{\tilde{n}n'} \frac{\partial \log \bar{c}_{\tilde{n}}}{\partial \log K_p} + \xi \sum_{\tilde{n}} \pi_{\tilde{n}n'} \frac{\partial \log \tau_{\tilde{n}n'}}{\partial \log K_p} \\
&= \xi \sum_{\tilde{n}} \pi_{\tilde{n}n'} \frac{\partial \log \bar{c}_{\tilde{n}}}{\partial \log K_p} - \sum_{\tilde{n}} \pi_{\tilde{n}n'} \left[\lambda_3 \Theta_{p|\tilde{n}n'} + \lambda_2 \sum_{\tilde{p} \in \mathcal{P}} \Theta_{\tilde{p}|\tilde{n}n'} \frac{\partial \log \Xi_{\tilde{p}}}{\partial \log K_p} \right]
\end{aligned} \tag{72}$$

Therefore, the elasticity of trade volumes to port capacity writes:

$$\begin{aligned}
\frac{\partial \log X_{nn'}}{\partial \log K_p} &= -\xi \frac{\partial \log \bar{c}_n}{\partial \log K_p} + \lambda_3 \Theta_{p|nn'} + \lambda_2 \sum_{\tilde{p} \in \mathcal{P}} \Theta_{\tilde{p}|nn'} \frac{\partial \log \Xi_{\tilde{p}}}{\partial \log K_p} + \xi \sum_{\tilde{n}} \pi_{\tilde{n}n'} \frac{\partial \log \bar{c}_{\tilde{n}}}{\partial \log K_p} \\
&\quad - \sum_{\tilde{n}} \pi_{\tilde{n}n'} \left[\lambda_3 \Theta_{p|\tilde{n}n'} + \lambda_2 \sum_{\tilde{p} \in \mathcal{P}} \Theta_{\tilde{p}|\tilde{n}n'} \frac{\partial \log \Xi_{\tilde{p}}}{\partial \log K_p} \right] + \frac{\partial \log w_{n'}}{\partial \log K_p}
\end{aligned} \tag{73}$$

Using the previous expression in the elasticity of port traffic to port capacity therefore yields:

$$\begin{aligned}
\frac{\partial \log \Xi_{p'}}{\partial \log K_p} &= \sum_n \sum_{n'} w_{nn'}^{(p')} \left[\lambda_3 [\Theta_{p|np'} + \Theta_{p|p'n'} - \Theta_{p|nn'}] + \sum_{\tilde{p} \in \mathcal{P}} \lambda_2 [\Theta_{\tilde{p}|np'} + \Theta_{\tilde{p}|p'n'} - \Theta_{\tilde{p}|nn'}] \frac{\partial \log \Xi_{\tilde{p}}}{\partial \log K_p} \right] \\
&\quad + \sum_n \sum_{n'} w_{nn'}^{(p')} \left(-\xi \frac{\partial \log \bar{c}_n}{\partial \log K_p} + \lambda_3 \Theta_{p|nn'} + \lambda_2 \sum_{\tilde{p} \in \mathcal{P}} \Theta_{\tilde{p}|nn'} \frac{\partial \log \Xi_{\tilde{p}}}{\partial \log K_p} + \xi \sum_{\tilde{n}} \pi_{\tilde{n}n'} \frac{\partial \log \bar{c}_{\tilde{n}}}{\partial \log K_p} \right. \\
&\quad \left. - \sum_{\tilde{n}} \pi_{\tilde{n}n'} \left[\lambda_3 \Theta_{p|\tilde{n}n'} + \lambda_2 \sum_{\tilde{p} \in \mathcal{P}} \Theta_{\tilde{p}|\tilde{n}n'} \frac{\partial \log \Xi_{\tilde{p}}}{\partial \log K_p} \right] + \frac{\partial \log w_{n'}}{\partial \log K_p} \right)
\end{aligned} \tag{74}$$

or, in concise form:

$$\frac{\partial \log \Xi_{p'}}{\partial \log K_p} = \sum_n \sum_{n'} w_{nn'}^{(p')} \left[\lambda_3 \Delta_{np'n',p} + \lambda_2 \sum_{\tilde{p} \in \mathcal{P}} \Delta_{np'n',\tilde{p}} \frac{\partial \log \Xi_{\tilde{p}}}{\partial \log K_p} + \xi \left[\sum_{\tilde{n}} \pi_{\tilde{n}n'} \frac{\partial \log \bar{c}_{\tilde{n}}}{\partial \log K_p} - \frac{\partial \log \bar{c}_n}{\partial \log K_p} \right] + \frac{\partial \log w_{n'}}{\partial \log K_p} \right], \tag{75}$$

where

$$\Delta_{np'n',p} = \Theta_{p|np'} + \Theta_{p|p'n'} - \sum_{\tilde{n}} \pi_{\tilde{n}n'} \Theta_{p|\tilde{n}n'}, \quad \text{and} \quad w_{nn'}^{(p')} = \Theta_{p'|nn'} X_{nn'} / \Xi_{p'}. \tag{76}$$

Solving the system. Altogether, steps (1), (2), (3), and (4) form a system of $N \times N \times P$ equations

that reads:

$$w_n L_n \frac{\partial \log w_n}{\partial \log K_p} = \frac{1-\alpha}{\alpha} \sum_{n'} X_{nn'} \left[-\xi \left[\frac{\partial \log \bar{c}_n}{\partial \log K_p} - \frac{\lambda_3}{\xi} \Theta_{p|nn'} - \frac{\lambda_2}{\xi} \sum_{p' \in \mathcal{P}} \Theta_{p'|nn'} \frac{\partial \log \Xi_{p'}}{\partial \log K_p} \right] \right. \\ \left. + \frac{1-\alpha}{\alpha} \sum_{n'} X_{nn'} \left[\xi \sum_{\tilde{n}} \pi_{\tilde{n}n'} \left[\frac{\partial \log \bar{c}_{\tilde{n}}}{\partial \log K_p} - \frac{\lambda_3}{\xi} \Theta_{p|\tilde{n}n'} - \frac{\lambda_2}{\xi} \sum_{p' \in \mathcal{P}} \Theta_{p'|\tilde{n}n'} \frac{\partial \log \Xi_{p'}}{\partial \log K_p} \right] + \frac{\partial \log w_{n'}}{\partial \log K_p} \right] \right], \quad (77)$$

$$\frac{\partial \log \Xi_{p'}}{\partial \log K_p} = \sum_n \sum_{n'} w_{nn'}^{(p')} \left[\lambda_3 \Delta_{np'n',p} + \lambda_2 \sum_{\tilde{p} \in \mathcal{P}} \Delta_{np'n',\tilde{p}} \frac{\partial \log \Xi_{\tilde{p}}}{\partial \log K_p} + \xi \left[\sum_{\tilde{n}} \frac{\partial \log \bar{c}_{\tilde{n}}}{\partial \log K_p} - \frac{\partial \log \bar{c}_n}{\partial \log K_p} \right] + \frac{\partial \log w_{n'}}{\partial \log K_p} \right], \quad (78)$$

$$-\frac{\partial \log \bar{c}_n}{\partial \log K_p} = (\alpha - 1) \frac{\partial \log w_n}{\partial \log K_p} - \alpha \sum_{n'} \pi_{n'n} \left[\frac{\partial \log \bar{c}_{n'}}{\partial \log K_p} - \frac{\lambda_3}{\xi} \Theta_{p|n'n} - \frac{\lambda_2}{\xi} \sum_{p' \in \mathcal{P}} \Theta_{p'|n'n} \frac{\partial \log \Xi_{p'}}{\partial \log K_p} \right], \quad (79)$$

I represent the system in matrix form. Define the vector of unknown elasticities

$$x = [g_w \quad g_{\Xi} \quad g_c]^T$$

Starting from the factory cost block. The sub-system reads:

$$\mathbf{A}_{cw} g_w + \mathbf{A}_{c\Xi} g_{\Xi} + \mathbf{A}_{cc} g_c = b_c, \quad (80)$$

with

$$\mathbf{A}_{cw} = (\alpha - 1) \mathbb{I}_N, \quad \mathbf{A}_{c\Xi} = \frac{\alpha \lambda_2}{\xi} Z^{(1)}, \quad \mathbf{A}_{cc} = \mathbb{I}_N - \alpha \Pi^T,$$

and

$$b_c = \frac{\alpha \lambda_3}{\xi} Z_p^{(1)},$$

where I define

$$Z^{(1)} = [(\Pi \odot \Theta_1)^T \mathbf{1}_N \quad \dots \quad (\Pi \odot \Theta_P)^T \mathbf{1}_N], \quad \Theta \in \mathbb{R}^{N \times N \times P}, \quad \Theta_p \in \mathbb{R}^{N \times N}, \quad \Theta_{p|nn'} = \frac{\mathbf{B}_{np} \mathbf{B}_{pn'}}{\mathbf{B}_{nn'}},$$

and $Z_p^{(1)} = (\Pi \odot \Theta_p)^T \mathbf{1}_N$ denotes the p^{th} column of $Z^{(1)}$.

The wage block sub-system reads:

$$\mathbf{A}_{ww} g_w + \mathbf{A}_{w\Xi} g_{\Xi} + \mathbf{A}_{wc} g_c = b_w \quad (81)$$

with

$$\mathbf{A}_{ww} = \text{diag}(w \odot L) - \frac{1-\alpha}{\alpha} X, \quad \mathbf{A}_{w\Xi} = \lambda_2 \frac{1-\alpha}{\alpha} Z^{(2)}, \quad \mathbf{A}_{wc} = -\xi \frac{1-\alpha}{\alpha} [\text{diag}(X \mathbf{1}_N) - X \Pi^T],$$

and

$$b_c = \lambda_3 \frac{1-\alpha}{\alpha} Z_p^{(2)},$$

where I define

$$Z_p^{(2)} = (X \odot \Theta_p) \mathbf{1}_N - X \left[(\Pi^\top \odot \Theta_p) \mathbf{1}_N \right], \quad Z^{(2)} = \left[Z_1^{(2)} \cdots Z_p^{(2)} \right] \in \mathbb{R}^{N \times P}.$$

The traffic block sub-system reads:

$$\mathbf{A}_{\Xi w} g_w + \mathbf{A}_{\Xi \Xi} g_\Xi + \mathbf{A}_{\Xi c} g_c = b_w, \quad (82)$$

with

$$\mathbf{A}_{\Xi w} = -Z^{(3)}, \quad \mathbf{A}_{\Xi \Xi} = \mathbb{I}_P - \lambda_2 Z^{(4)}, \quad \mathbf{A}_{\Xi c} = \xi (Z^{(5)} - Z^{(6)}),$$

and

$$b_\Xi = \lambda_3 Z_p^{(3)},$$

where I define

$$\begin{aligned} Z^{(3)} &= \{Z_{p'n'}^{(3)}\}, \quad Z_{p'n'}^{(3)} = \sum_n w_{nn'}^{(p')}, \\ Z^{(4)} &= \{Z_{p'p}^{(4)}\}, \quad Z_{p'p}^{(4)} = \sum_{nn'} w_{nn'}^{(p')} \Delta_{np'n', p}, \quad \Delta_{np'n', p} = \Theta_{p|np'} + \Theta_{p|p'n'} - \sum_{\tilde{n}} \pi_{\tilde{n}n'} \Theta_{p|\tilde{n}n'}, \\ Z^{(5)} &= \{Z_{p'n}^{(5)}\}, \quad Z_{p'n}^{(5)} = \sum_{n'} w_{nn'}^{(p')} \pi_{nn'}, \end{aligned}$$

and

$$Z^{(6)} = \{Z_{p'n}^{(6)}\}, \quad Z_{p'n}^{(6)} = \sum_n w_{nn'}^{(p')}.$$

E QUANTIFICATION

E.1 ESTIMATING TRADE COSTS

In this section, I present the construction of the instruments for port traffic and port capacity used in the estimation of Equation (20). I need two orthogonal demand- and supply-side shifters to deliver consistent 2SLS estimates of the traffic and capacity elasticities embedded in transportation costs, discussed thereafter. Table E.1 demonstrate the first-stage relevance of the instruments for both exogenous regressors.

Endogeneity of port traffic. In the short run a port's throughput $\Xi_{p_o,t}$ is the equilibrium quantity where a downward-sloping demand curve for vessel traffic meets an upward-sloping supply curve of handling services. Unobserved shocks that shift either curve – e.g. a sudden surge in import demand from the port's hinterland – enter the regression error term but also move $\Xi_{p_o,t}$. As a result, $\Xi_{p_o,t}$ is mechanically correlated with the error term, biasing the estimated congestion elasticity. To break this simultaneity I employ a demand-side instrument that shifts the demand curve while leaving supply unchanged: global container traffic interacted with each port's share of coastal population in 1950. Historical population is predetermined with respect to contemporary trade shocks, and the interaction captures world-wide booms or slumps that raise demand proportionally across ports without affecting their marginal handling cost schedule. I construct the following instrument for port traffic:

$$z_{p_o,t}^1 = \sum_{p \in \mathcal{P}_{-c(p_o)}} \Xi_{p_o,t}^{TEU} \times SharePop_{\text{coastal}, p_o, 1950}. \quad (83)$$

The set $\mathcal{P}_{-c(p_o)}$ refers to the set of global ports, excluding ports in the same country as p_o . The share of coastal population $SharePop_{\text{coastal}, p_o, 1950}$ is constructed using the HYDE 3.3 data, providing estimates of inhabitants in 1950 at a 5-arc-minute resolution (Klein Goldewijk, 2024). I extract the total population in 1950 within a 20km buffer around the 621 ports used in the trade costs estimation, and construct the share of coastal population attributed to each port. Port traffic $\Xi_{p_o,t}^{TEU}$ is the same measure as in Section 5.1.

Endogeneity of port capacity. Port capacity K_{p_o} , is a long-run choice of the port operator and thus responds to the same latent forces that shape current trade flows. Forward-looking expansions link K_{p_o} positively to unobserved demand shocks, while congestion-induced upgrades or measurement noise in the 99th-percentile traffic proxy can violate exogeneity. I therefore

use a long-run supply-side instrument $z_{p_o}^2$ that shifts the marginal-cost curve independently of demand: the mean terrain ruggedness within 20 km of the port, constructed using the Terrain Ruggedness Index at a 30-arc-second resolution of [Amatulli et al. \(2018\)](#). Rugged hinterland topography raises the cost of transporting goods outside of the port area, leading port planners to install systematically lower capacity, yet it is fixed by geology and has no direct effect on route-specific demand.

Table E.1: Estimation of transportation costs: first stage

	Log Port Origin Traffic (1)	Log Port Origin Capacity (2)
$z_{p_o,t}^1$	0.59 (0.00)	0.47 (0.00)
$z_{p_o}^2$	-0.44 (0.00)	-0.39 (0.00)
Log Distance	1.14 (0.02)	0.95 (0.01)
Log Cyclone Risk	0.08 (0.01)	0.10 (0.00)
Observations	141,086	141,117
Adjusted R ²	0.69	0.69
n_d -week fixed effects	✓	✓
n_o -week fixed effects	✓	✓
p_d -week fixed effects	✓	✓

Notes: This table presents the results of regressing the two endogenous regressors in Equation 20 on exogenous instruments. The outcomes are Port Traffic, defined as weekly estimates of total TEU volumes transiting through ports of origin of shipments, and Port Capacity, defined as the 99th percentile of daily TEU volume at ports. Distance refers to the total route distance (land and sea). Cyclone Risk refers to the expected windspeed at ports, as reported in the STORM data. The instruments are described in Section E.1. Robust standard errors are clustered at the $\{n_o, n_d, p_o, p_d\}$ -week level.

E.2 QUANTIFYING FUNDAMENTALS

In this section, I describe the procedure to recover the region-level fundamental productivity shifters a_n . The procedure entails inverting the equilibrium conditions of the model to pin down fundamental productivity as a function of equilibrium objects, and solving the resulting fixed point system fundamental productivity a_n rationalize the data-driven GDP per capita $w_n^{data} \in \{w_n^{data}\}_{n \in \mathcal{N}} = \mathcal{W}^{data}$ obtained from [Rossi-Hansberg and Zhang \(2025\)](#). From the wage bill, bilateral trade shares and bilateral trade equilibrium conditions, I obtain the following

inversion of bilateral trade shares to recover fundamental productivity:

$$a_n = w_n L_n \left[\sum_{n'} \frac{\bar{c}_n^{-\xi} \tau_{nn'}^{-\xi}}{\sum_{\tilde{n}} a_{\tilde{n}} \bar{c}_{\tilde{n}}^{-\xi} \tau_{\tilde{n}n'}^{-\xi}} w_{n'} L_{n'} \right]^{-1}. \quad (84)$$

Given a modified geography $\mathcal{G} = \{\mathcal{N}, \mathcal{P}, \mathcal{L}, \mathcal{M}, \mathcal{D}, \mathcal{K}, \Psi, \mathcal{W}^{data}\}$ and a set of model parameters $\{\sigma, \alpha, \xi, \lambda_1, \lambda_2, \lambda_3\}$, the following algorithm recovers fundamental productivity shifters of the economy:

1. **Initialize** endogenous variables:

- (a) $\{a_n\}_{n \in \mathcal{N}}$ (productivity)
- (b) $\{\bar{c}_n\}_{n \in \mathcal{N}}$ (factory-gate cost indices)
- (c) $\{\Xi_p\}_{p \in \mathcal{P}}$ (port traffic)

2. **Outer-loop** – While $distance_{productivity} > tol$ or $distance_{traffic} > tol$:

- (a) Based on distances $\epsilon_{ll'}$, port capacity K_p and traffic Ξ_p , update Λ (*transportation network*)
- (b) Based on Λ , update transportation costs $\tau_{ll'}$ (*transportation costs*)
- (c) **Inner-loop (factory-gate costs)** – While $distance_{costs} > tol$:
 - i. Based on transportation costs $\tau_{nn'}$, region-level productivity a_n , factory-gate costs indices \bar{c}_n , and wages w_n^{data} , update \bar{c}_n (*factory-cost indices*)
 - ii. Compute $distance_{costs} = \sum_n [(\bar{c}_n)^{i_c} - (\bar{c}_n)^{i_c+1}]^2$, with i_c = iteration (inner-loop)
- (d) Based on transportation costs $\tau_{nn'}$, region-level productivity a_n , factory-gate costs indices \bar{c}_n , and wages w_n^{data} , update $\pi_{nn'}$ (*bilateral trade shares*)
- (e) Based on bilateral trade shares $\pi_{nn'}$ and wages bills $w_n^{data} L_n$, update $X_{nn'}$ (*bilateral trade*)
- (f) Based on the transportation network Λ and bilateral trade $X_{nn'}$, compute Ξ_p (*port-level traffic*)
- (g) Based on factory-gate costs indices \bar{c}_n , fundamental productivity a_n , transportation costs $\tau_{nn'}$, and wages wages bills $w_n^{data} L_n$, compute a_n (*productivity inversion*), up to a normalization $a_1 = 1$
- (h) Compute $distance_{productivity} = \sum_n [(a_n)^{i_{out}} - (a_n)^{i_{out}+1}]^2$ and $distance_{traffic} = \sum_p [(\Xi_p)^{i_{out}} - (\Xi_p)^{i_{out}+1}]^2$, with i_{out} = iteration (outer loop)

In practice, I dampen each productivity and traffic iteration using a dampening factor of 0.1, and use the 'daarem' R package to optimize the resolution of the fixed point.

E.3 GEOGRAPHY AND MODEL FIT

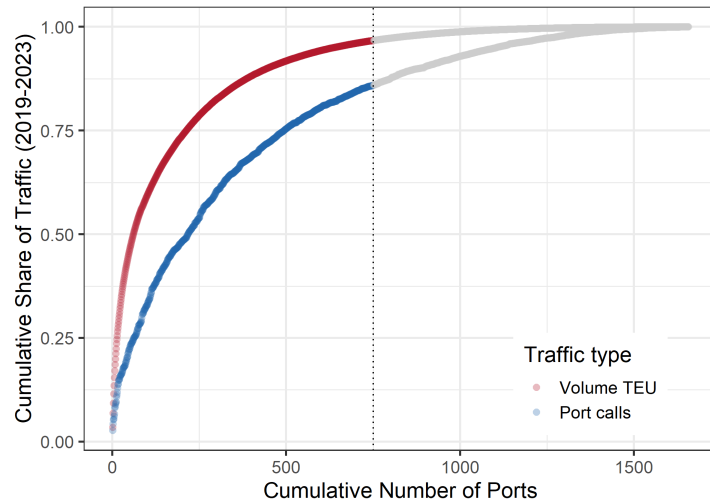


Figure E.1: Port selection for counterfactual

Notes: This figure plots the cumulative share of total TEU volume and vessel count by ports in the Port-Watch data (2019-2023). Grey dots are ports which are excluded from the sample in the counterfactual exercises.

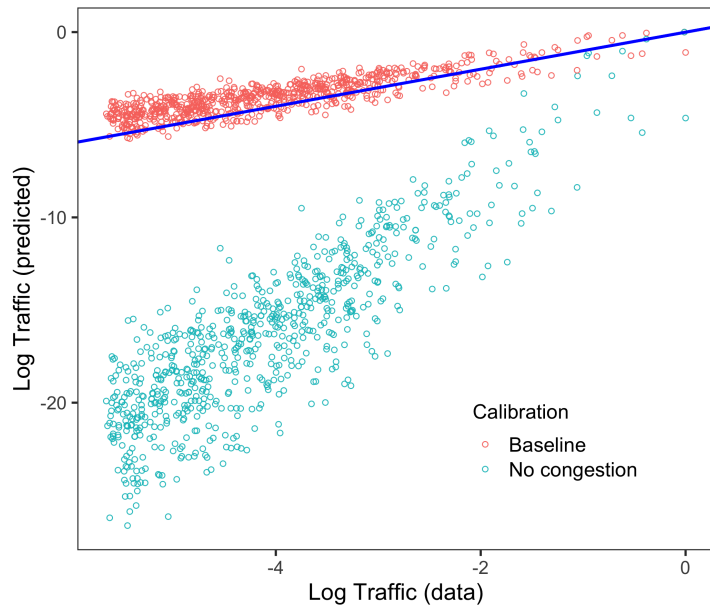


Figure E.2: Port congestion and model fit

Notes: This figure compares model-based port traffic to its (untargeted) counterpart in the data. I compare log-normalized port traffic in the data – measured as average yearly total TEU volume (x-axis) – to the log-normalized model-based estimates of port traffic (y-axis). I compare two calibrations: (i) with the estimated congestion elasticity (baseline), or (ii) with no congestion ($\lambda_2 = 0$). Model-based moments are computed using the model inversion described in Appendix E.2.

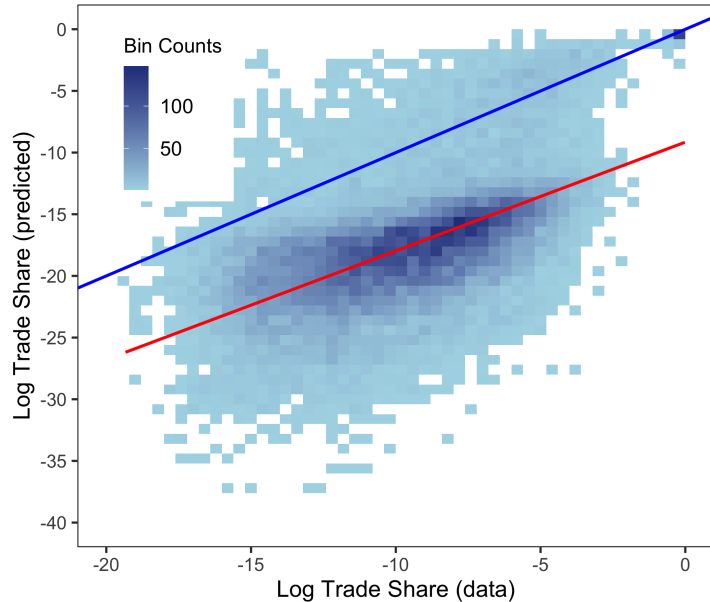


Figure E.3: Model fit – aggregate bilateral trade shares (untargeted)

Notes: This figure compares log country-level trade shares in the data – obtained from GLORIA input–output tables – (x-axis) to their model-based counterparts (y-axis). Model-based moments are computed using the model inversion described in Appendix E.2.

E.4 ADDITIONAL QUANTITATIVE RESULTS

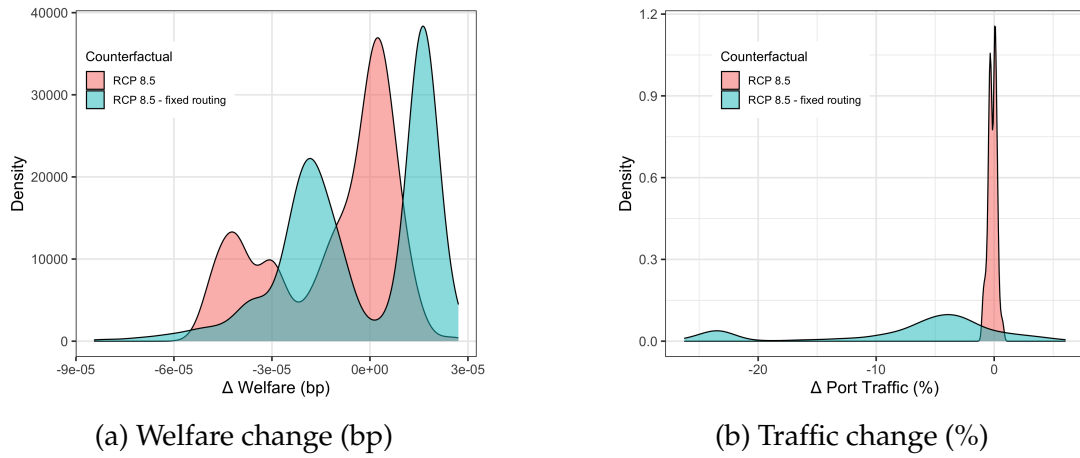


Figure E.4: RCP8.5 with rerouting vs. without rerouting

Notes: These Panels plot the density of the change in welfare (Panel a) and port traffic (Panel b), in both RCP8.5 counterfactuals with and without rerouting.

E.5 INFRASTRUCTURE POLICY

E.5.1 INVESTMENT AND PORT CAPACITY

Data. I combine World Bank PPI project data on port investments with IMF PortWatch outcomes at the port-year level. I use all *Ports* projects from the World Bank’s Private Participation in Infrastructure (PPI) database for 2019–2023 ([World Bank, 2025](#)). The data contain the port identifier, the investment year, and total committed investment for all port infrastructure projects in which the World Bank participated. For ports with multiple projects in the same year, I sum investment amounts to obtain a port \times year aggregate. I manually assign PortWatch IDs to recipient ports by port name.

I merge the investment data with PortWatch global traffic data, aggregated at the yearly level (2019–2024). The outcome of interest is yearly port capacity, defined as the 99th percentile of daily TEU over the calendar year. The main sample consists of all ports located in the same countries as the recipient ports of investments. The robustness sample consists of all ports in the PortWatch data. I also compute quartiles of annual total TEU traffic, $q_{p,t} \in \{1, \dots, 4\}$, used to flexibly control for heterogeneous time shocks.

Empirical strategy. I estimate a staggered difference-in-differences model with continuous treatment (amount of investment, in billion USD) to investigate how port capacity evolves around the investment year, allowing the dynamic effect to scale with the investment amount. Let $\tau_{p,t} \equiv t - t_p^{\text{treat}}$ denote event time (years relative to the investment year, with untreated ports assigned $\tau_{p,t} = 0$ and $I_p = 0$). I estimate the following model:

$$K_{p,t} = \sum_{\substack{k \in \mathcal{K} \\ k \neq -1}} \beta_k \mathbf{1}\{\tau_{p,t} = k\} I_p + \alpha_p + \gamma_{t \times q_{p,t}} + \varepsilon_{p,t}, \quad (85)$$

where $K_{p,t}$ is the 99th percentile of daily TEU traffic (capacity proxy) for port p in year t ; $\mathbf{1}\{\tau_{p,t} = k\}$ are event-time dummies; I_p is the port’s total investment amount (billions USD); α_p are port fixed effects; and $\gamma_{t \times q_{p,t}}$ are year-by-TEU-quartile fixed effects that absorb flexible global shocks with heterogeneous impacts across the traffic distribution. β_k measures the change in capacity at event time k per billion USD invested, relative to the pre-investment year. Standard errors are clustered at the country (ISO3) level.

Figure E.5a plots the results, suggesting that USD 1 billion of investment increases port capacity by 3,649 TEU-days for LMIC ports. This corresponds to a 27% increase in unconditional port capacity. I use this estimate to translate investment into port capacity increases in

the policy experiment of Section 7.3. Figure E.5b confirms that the result is robust to allowing comparisons with all global ports (within yearly traffic quartiles).

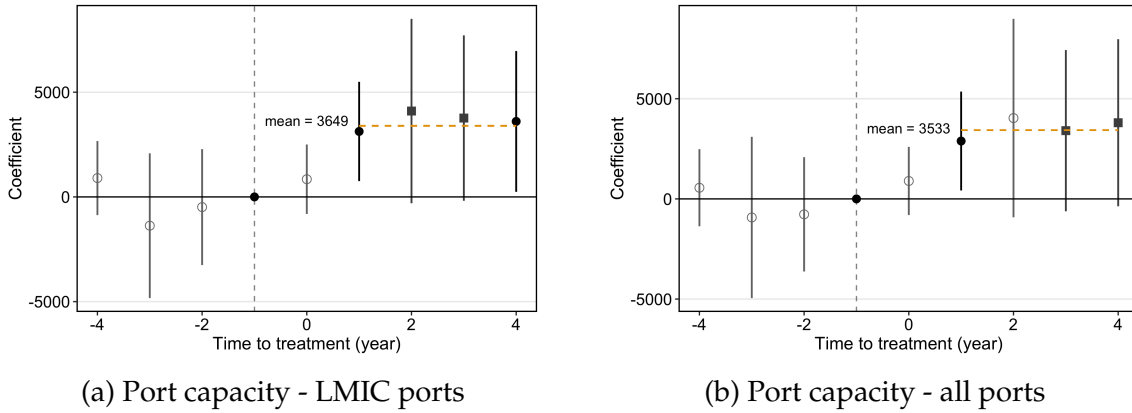


Figure E.5: The impact of port investment on port capacity

Notes: These Panels plot the effect of port investment on port capacity, as specified by Equation (85). The outcome of both Panels is the 99th percentile daily TEU traffic for port p in year t . The sample in Panel (a) consists of all ports in countries in which at least one port received a PPI investment. The sample of Panel (b) consists of all ports in the PortWatch data. The bars show 95% confidence intervals. Black dots indicate point estimates significant at the 5% level, gray squares at the 10% level, and empty dots denote non-significant estimates at the 10% level.

E.5.2 ADDITIONAL RESULTS: INFRASTRUCTURE POLICY

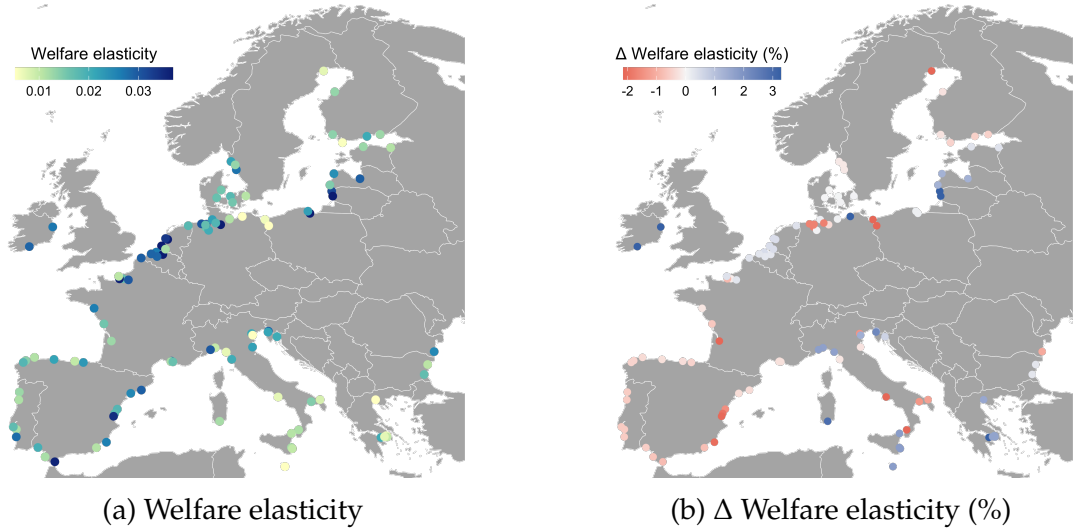


Figure E.6: EU27 welfare elasticity to port traffic

Notes: These Panels plot the social savings sufficient statistics of port capacity for EU27 welfare under a RCP8.5 scenario. In Panel (a), I plot the port-level elasticity of EU27 welfare to port capacity. In Panel (b), I plot the change in port-level EU27 welfare elasticities from the baseline scenario to the RCP8.5 one. EU27 welfare elasticities are computed from the counterfactual outputs of Section 6, using the solution method described in Appendix D.6. The color scales of both Panels are truncated at the 5th and 95th percentiles.